TAMPEREEN TEKNILLINEN YLIOPISTO
TAMPERE UNIVERSITY OF TECHNOLOGY

FAIZAN RAZZAQ SIDDIQUI

ANALOG BASEBAND BOARD DESIGN AND ARCHITECTURAL STUDIES FOR MILLIMETER WAVE BACKHAUL BEAMSTEERING RADIO IN 5G NETWORKS

Master of Science thesis

Examiners: Olli-Pekka Lunden
Prof. Mikko Valkama
Examiner and topic approved by the Faculty Council of the Faculty of Electrical Engineering
on 12.8.2015

ABSTRACT

Faizan Razzaq Siddiqui: Analog Baseband Board Design and Architectural Studies for Millimeter wave Backhaul Beam-steering radio in 5G networks.
Tampere University of Technology
Master of Science Thesis, 72 pages,
May 2016.
Master's Degree Program in Electrical Engineering.
Major: Wireless Communication.
Examiners: Olli-Pekka Lunden, Professor Mikko Valkama.
Supervisors in Nokia Bell Labs: Juha Nurmiharju, Pekka Wainio.

Keywords: 5G, millimeter wave, mmW Radios, Beam steering, Analog Baseband, Backhaul, Small cell

The mobile data rates and number of devices are constantly increasing, creating new challenges for the network operators to increase the cell and area capacities of the mobile networks. For LTE-A and future 5G networks, one well-known solution to improve the capacity and coverage is network densification i.e. introduction of more and smaller cells in the network. As these small cells are typically located in cities and other urban areas, adoption of unconventional installation sites such as lamp posts and building walls is needed. Thus, the provisioning of the conventional wired backhaul might not be feasible.

Potential solutions for the small cell wireless backhaul are technologies utilizing millimeter wave (mmW) frequencies, which can provide several gigahertz of spectrum. Typically, frequencies between 60 - 80 GHz are used for backhauling applications. The adoption of the mmW frequencies calls for narrow antenna beams, less than a few degrees, to compensate for the high path losses and other attenuation sources at these frequencies. Such narrow-beam radio links also need vibration compensation mechanisms to mitigate the effect of the sways and twists of the installation structures caused by wind. Therefore, electrical beam steering capability is needed to control the direction of the antenna beam quickly during link operation.

The main scope of this thesis work is related to architecture studies and hardware development for a proof of a concept for an mmW beam steerable backhaul radio for small cells, which can support multi-gigabit data rates. This work has been carried out as a part of Nokia Bell Labs 5G mmW Backhaul proof of concept (PoC) project. The author's contribution in the project includes system integration and system testing of the mmW radio PoC, whereas the other major thesis work and author contributions contain the specification, hardware design and testing of an analog baseband board and the associated satellite boards developed for the Nokia 5G mmW Backhaul PoC system.

The analog baseband board was designed to serve as a driver board for the integrated mmW transceiver and antenna module. All the supporting functions needed for mmW direct conversion transceiver like baseband amplifiers, microprocessor and reference oscillators, etc. were placed on this driver board. Based on the conducted module level tests, it was concluded that the analog baseband board was working up to the specifications of the system design. Moreover, during system integration testing with 500 MHz bandwidth modem, it was shown that the system is able to support up to 64-QAM and peak data rates of about 2 Gbit/s.

PREFACE

This Master's thesis has been done as a part of the 5G backhaul research project in Nokia Bell Labs, Espoo, Finland. This thesis work also completes of my studies at the Department of Electronics and Communications Engineering at Tampere University of Technology, Finland.

First of all, I would like to thank my examiners Olli-Pekka Lunden and Professor Mikko Valkama for reviewing and evaluating my thesis. I would also like to thank M.Sc. Pekka Wainio and Jorma Pallonen for giving me the opportunity to work in Nokia Bell Labs as a thesis worker. I wish to express my gratitude to M.Sc. Juha Nurmiharju, one of the supervisors of this thesis from Nokia, who deserves my sincere thanks for his first hand review and efficient guidance during this thesis work. I would like also to thank my work colleagues at Nokia, especially Bengt Björkvall, Jani Saarenpaa and Santtu Koskinen for always supporting and motivating me to improve my contribution to the system development.

Finally, my parents deserve my deepest thanks because without their support and motivation, I would never have finished my studies. Last but not the least, I want to thank my brother Shadman and my friends Usman Rashid and Ahsan Zia for supporting me during my university studies and my thesis work.

Espoo, May 2016

Faizan Siddiqui.

CONTENTS

LIST OF FIGURES

LIST OF SYMBOLS AND ABBREVIATIONS

2G	Second Generation Mobile Networks
3G	Third Generation Mobile Networks
3GPP	Third Generation Partnership Project
4G	Fourth Generation Mobile Networks
5G	Fifth Generation Mobile Networks
ABB	Analog Baseband Board
ADC	Analog to Digital Converter
AFE	Analog Front End
AGC	Automatic Gain Control
ATM	Asynchronous Transfer Mode
BER	Bit-Error Rate
BS	Base Station
BSP	Beam Steering Processor
BSS	Base Station Sub-System
BTS	Base Transceiver Station
CEPT	European Conference of Postal and Telecommunication
CDMA	Code Division Multiple Access
DAC	Digital to Analog Converter
DPST	Dual Pole Single Throw
EDGE	Enhanced Data rates for GSM Evolution
EIRP	Equivalent Isotopically Radiated Power
ETSI	European Telecommunications Standards Institute
FCC	Federal Communications Commission
FDMA	Frequency Division Multiple Access
FDD	Frequency Division Duplex
FEC	Forward Error Correction
FPGA	Field-Programmable Gate Array
GPRS	General Packer Radio Service
GSM	Global System for Mobile Communications
GUI	Graphical User Interface
HLP	Higher Layer Protocols
HSPA	High Speed Packet Access
IC	Integrated Circuit
IF	Intermediate Frequency
IIP3	Third order intercept point
ILA	Integrated Lens Antenna
ITU	International Telecommunication Union
LCD	Liquid-crystal-display
LNA	Low Noise Amplifier
LO	Local Oscillator
LOS	Line-Of-Sight
LTE	Long Term Evolution
LTE-A	Long Term Evolution Advanced
MBH	Mobile Backhaul
MER	Modulation Error Rate
MIMO	Multiple Input Multiple Output

MME	Mobile Management Entity
mmW	Millimeter wave
MIMO	Multiple Input Multiple Output
MSC	Mobile Switching Centre
NGMN	Next Generation Mobile Networks
nLOS	near Line-Of-Sight
NLOS	Non-Line-Of-Sight
OFDMA	Orthogonal Frequency Division Multiple Access
P1dB	1dB compression point
P2P	Point to Point
P2MP	Point to Multipoint
PA	Power Amplifier
PCB	Printed Circuit Board
PCRF	Policy and Charging Control Function
PCU	Packet Control Unit
PDH	Plesiochronous Digital Hierarchy
P-GW	PDN-Gateway
PLL	Phased Lock Loop
PoP	Point of Presence
PoC	Prove of Concept
QAM	Quadrature Amplitude Modulation
QoS	Quality of Service
QPSK	Quadrature Phase Shift Keying
RF	Radio Frequency
RNC	Radio Network Controller
RSSI	Received Signal Strength Indicator
RX	Receiver
S-GW	Serving Gateway
SP-GW	Serving and packet Gateway
SP2T	Single Pole Two Throw
SP4T	Single Pole Four Throw
SPDT	Single Pole Dual Throw
SON	Self-Organizing Network
SNR	Signal to Noise ratio
SWMN	Self-Optimizing Wireless Mesh
TDD	Time Division Duplexing
TDM	Time Division Multiplexing
TDMA	Time Division Multiple Access
TCO	Total Cost of Ownership
TRX	Transceiver
TX	Transmitter
UART	Universal Asynchronous Receiver Transmitter
VCO	Voltage Controlled Oscillator
VCTCXO	Voltage-controlled temperature-compensated crystal oscillator
VNA	Vector Network Analyser
WLAN	Wireless Local Arena Network
XPIC	Cross-Polarization Interference Cancelation

1. INTRODUCTION

In today's world, the number of smart phones and other communication devices are continuously increasing. As a consequence, high data rates and high network capacities are required to fulfill the demands of future networks. In order to keep pace with these ever-increasing demands, the industry needs to adopt new generations of mobile networks. The future 5G networks are anticipated to be complex heterogeneous systems that can provide more scalable and flexible services with a very low latency (< 1 ms) of gigabit experience [1]. The data rates can be increased by techniques such as massive multiple input multiple output (MIMO), while there are also issues that are difficult to overcome. In general, there is no limit to the number of cells in a network, which leads to the deployment of small cells with radii of a few hundred meters or less in urban environments. Typical installation sites for the small cell base stations are, for instance, building walls and light poles. The high number of small cells in unconventional locations sets new challenges for the backhaul [1] [2].

Due to the untypical installation structures and large number of cells, the extension of a conventional wired backhaul to a typical small cell site might become unreasonable. Therefore, wireless solutions play an important role when selecting the small cell backhaul solution. New problems arise when implementing reliable, low-cost and high-capacity backhaul. First, the high speed radio links require a great deal of spectra. Second, due to the high number of base stations, the total cost of ownership (TCO) should be kept at the minimum level; including expenses generated from the backhaul device, spectrum licensing, installation and maintenance. Third, the interference between the closely located devices should be kept at minimum level. The use of millimeter wave (mmW) frequencies in small cell technology can provide high capacity, reliable and low cost backhaul for a mobile network [3] [4].

Millimeter wave frequencies, such as E-band (71 to 76 GHz and 81 to 86 GHz) provide promising features to fulfill the requirements of the small cell backhaul due to huge available bandwidths at these frequencies. The transmission at millimeter wave frequencies suffers from high signal attenuations due to free space path loss, atmospheric absorption and rain. To overcome the attenuations, high gain is required. Such high gain decreases the antenna beam width to less than a few degrees. The high signal attenuation and the narrow beamwidth can decrease the co-channel interference for mmW radios [5] [6].

Despite of many promising features provided by the mmW technologies there are also some challenges that needs to be addressed. The narrow antenna beams get easily misaligned; especially if the devices are mounted on a structure like a lamp post that might

experience sways and twists due to wind [2]. Additionally, in future 5G networks, to keep the installation and maintenance costs low, the device should provide plug and play features connecting the narrow-beam radio links automatically when the power of the device is switched on. Afterwards, the small cell backhaul should automatically connect to devices that are brought within its reach. The automatic link alignment and vibration compensation require the ability of changing the direction of the antenna beam [5] [6].

This thesis work was done at Nokia Bell Labs as a part of a 5G backhaul proof of concept (PoC) system. The objective of making the PoC system is to have a mmW beam-steerable radio that can be used in small cell point to point backhaul applications. The project is conducted in a cooperation of VTT Technical Research Centre of Finland and Aalto University, who, respectively, designed the mmW transceiver module and the lens antenna for the system. The author's contribution to the project includes the architecture specification of the system and working with the team in Nokia to identify the possibilities, challenges and limitations of the beam-steering PoC system. The individual thesis work related parts of this overall PoC development activity contains the specification, hardware development and testing of the PoC system. The testing and measurements conducted by the author were divided into two parts. The first part included the module level testing of the hardware unit designed by the author as part of the system. The second part of the measurements include the system level integration and system level RF measurements for the complete integrated PoC system including the baseband modem, beam-steering software, mmW transceiver and antenna.

The PoC system functionality is designed using a modular structure, where the key functions are divided into smaller working units or boards rather than using a single main board. This helps in debugging and testing of several working blocks of a radio and understanding of the problem related to mmW radio transmissions. The supported modular structure also makes it possible to exchange individual modules easily to evaluate alternative technologies and implementation options. Since the mmW module board contains most of the high frequency components, the target was to keep the module design as simple and robust as possible. Thus all the supporting functions like amplifiers, microprocessor and reference oscillators, etc. were placed on a separate driver board referred to in this thesis as an analog baseband board.

The testing of system operation was conducted in two phases: the first phase included the analog baseband board testing as an individual module i.e. frequency response, gain and phase response testing for both TX and RX chains. The second part of the testing includes the system-level testing of the mmW transceivers. That includes the phase noise testing, frequency response of the system and the modem and data throughput of the system. The system testing results included in this thesis will be for 500 MHz of RF bandwidth support due to modem limitations, but the RF part will support bandwidths up to 2 GHz.

The organization of the rest of the thesis is as follows: Chapter 2 provides basic theory about mobile backhaul system and current topologies and limitation of backhaul networks. This chapter is mainly divided into two parts, where first part includes a brief introduction about LTE and 5G backhaul and small cell backhaul system. In the second part of the chapter the main focus will be millimeter wave frequencies, which are gaining great attention for small cell backhaul applications. Chapter 3 will give a theory of application and technologies that are used in designing the mmW system architecture. The theory will focus on the system requirements of self-aligning and self-organizing wireless mesh backhaul. The system description and architecture details of proof of a concept beam steerable millimeter wave backhaul radio that is developed at Nokia Bell Labs are discussed in chapter 4. Furthermore, chapter 5 concentrates on the main task of the thesis work that is the design of the hardware module of Analog Baseband Board (ABB). This chapter will explain the construction blocks of the analog baseband board like the PCB layer stack-up, interface design between several working modules and mechanic's design of the board. The measurement results and analysis of the analog baseband board and the system integration results of the system are all reported and discussed in chapter 6. Finally, a summary of the results and a discussion of the future prospects are provided. In general, one additional purpose of the written thesis is to provide a good and comprehensive overview of the mmW wireless backhaul technologies and the associated hardware and system level challenges.

2. MOBILE BACKHAUL AND MILLIMETER WAVE TECHNOLOGIES

In mobile communication networks, backhaul links provide connectivity between the cell site and the Mobile Switching Center (MSC). Copper wires, fiber optics and over the air (mostly through microwave frequencies) are used as a medium of transferring data.

A mobile communication system requires a network with high capacity, low latency and a robust backbone for transmitting the data gathered from numerous Base Stations (BS) to the MSC. As the number of users increases, the amount of data also increases in the base station. This data has to be accumulated and then hauled to one medium to be carried over a long distance towards MSC.

Conventionally the Mobile Backhaul (MBH) uses fiber optics, copper line or microwave links to carry the data, depending on the geographical terrain and accessibility to the cell site location. This kind of technologies were dominating during the days of voice centric mobile devices but in the current days with the increase in data centric traffic the cells need to be smaller and of higher capacity to fulfill the demands.

2.1 Backhaul Networks

Current backhaul connections are usually fixed bandwidth, but they can be changed with newer equipment or with node reconfigurations locally. The capacity of Second Generation (2G) network is 1.5 to 6 Mbit/s. The upper level of the backhaul network can reach up to 155 Mbit/s and its multiples [7].

Third Generation (3G) mobile networks contain Asynchronous Transfer Mode (ATM) equipment. Such equipment improves capacity efficiency compared to TDM, but the drawback for this is that it adds one more network layer to be managed and maintained, which increases network operative costs. ATM equipment has similar interfaces as Plesiochronous Digital Hierarchy (PDH) and Synchronous Digital Hierarchy (SDH) equipment with similar data rate [7].

Considering 2G and 3G mobile networks, there are no direct logical interconnections between the base stations, as the backhaul is in a pure star shaped configuration, so the traffic flow is directly from the BS to its controller [7].

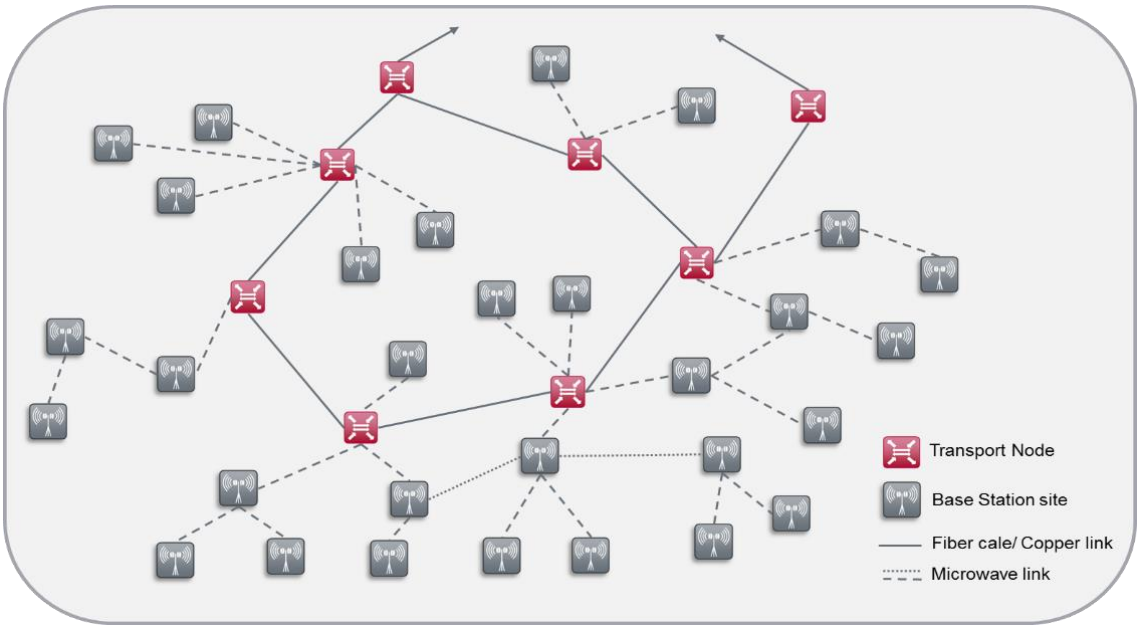

Figure 1. MBH physical topology consideration. Adapted from [7].

The physical topology of backhaul is, however, quite different based on economic optimization of transport links and nodes while on the upper layer of the network it needs to have resilience. It also depends on the network's history and the evolution of the network as more BS sites will get added to the network. Usually, the topology near the nodes are tree or chain shaped, but as it moves to the higher network tiers, the physical topology is more rings based [7]. The physical topology of MBH can be observed in Figure 1.

The current backhaul networks need a dramatic change in their architecture because of the growing number of users, increased coverage area and higher data rates. These factors are discussed in detail in the following paragraphs.

Higher data rates are the primary reason for the development of new generation of mobile networks. Most of mobile traffic load in 2G mobile networks are based on low bit rate formats, such as voice data. For example, for each user, GSM uses only 16 Kbit/s per voice channel. So the capacity required for these base stations is not high. Therefore, in some rural areas often a fraction of 2 Mbit/s link is used. It can carry all the traffic generated by many BSs in that area [7].

Nevertheless, the backhaul needs some change in terms of capacity because the mobile data is growing fast as many new applications are introduced in 3G and 4G mobile networks. The mobile data will continue increasing according to the latest surveys of Statista as illustrated in Figure 2. Increasing use of data intensive applications such as high-quality video stream, and also by the increasing number of laptops, tablets and new types of terminals in the system are causing a rise in average traffic volume [7].

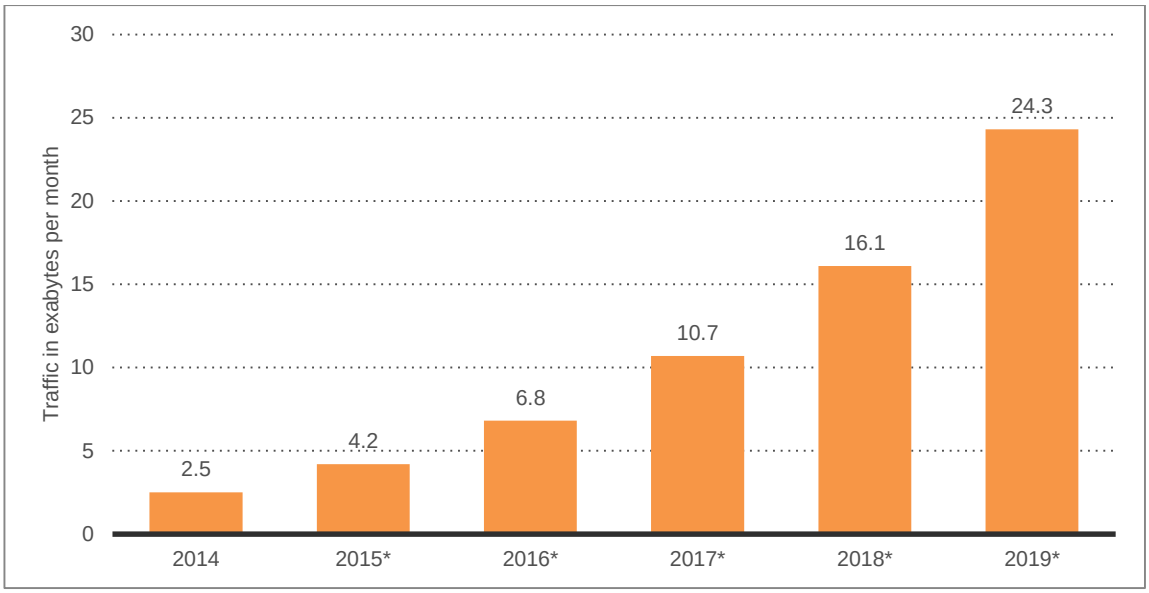

Figure 2. Global mobile data traffic from 2014 to 2019 (in Exabyte per month) [8].

Previous reasoning implies that all of this mobile traffic will also be present in the backhaul links. Substantially higher MBH throughputs will be needed for providing the desired mobile services for users. This kind of situation can create a bottleneck in MBH if it is not dimensioned properly for expansion of bandwidth in the user services [7].

More cell sites are also needed with the increasing capacity of the cell, to accommodate the growing number of mobile terminals. The size of the cell should be smaller, and the capacity should be increased in highly dense urban areas with a high flexibility in the network. The cost of MBH should be lower than that of current bigger backhaul links, because with the increase in the number of backhaul links the cost of the network infrastructure will increase [7].

2.2 Long Term Evolution (LTE) Backhaul

With the introduction of LTE and LTE-Advanced (LTE-A) there is a need to slowly retire the traditional 2G and 3G backhaul architecture, because LTE is based on packet technology, which includes Ethernet physical interface for interconnection between different network elements. Fourth generation (4G) throws away the traditional hierarchical architecture of 2G/3G networks, being replaced by cost-effective and high capacity numerous small cell backhaul scenarios. When early LTE-ready backhaul was deployed, it was considered future proof to target 100-200 Mbps of capacity, but now 4G necessitates of 300 Mbps to 1 Gbps of backhaul throughput [8] [9].

In LTE, backhaul system will be shifted more towards the core network. In 2G the backhaul link was made of access part and in maximum cases, one level of aggregation was

needed until the base station controller is reached. The 3G network had more Radio Network Controller (RNC) sites; so additional aggregation layer was not needed [8].

Now in LTE network architecture, the RNC is not needed anymore, which leads to the more concentration on the Mobility Management Entity (MME) and Serving Gateways (S-GW) and Packet Data Gateway (P-GW)- which are usually joined together to form Serving and Packet Data Gateway (SP-GW) [8].

2.3 Small cell Backhaul

The increase in demand of mobile data traffic is putting enormous pressure on mobile networks to provide more capacity, especially in urban areas. Making a denser cell topology by deploying small cells could be a great solution for the future need and the capacity problems [8] [5]. The small cells and the technologies related to them are the solution for providing a secure future in terms on capacity for the present generation (4G) networks and the future generation (5G) mobile networks.

A small cell should be cheaper compared to the macro base station, so the first challenge is the cost of the small cell backhaul. For the traditional macro cell backhaul networks, there is a fixed cost for the deployment of the transfer media like fiber cable or copper cable deployment. This kind of approach cannot be used for the small cells backhaul. So new technologies and new planning and installation methods are needed to overcome these issues [8].

For a Line of Sight (LOS) wideband backhaul connection, automatic antenna steering technologies may be a good candidate. In planning perspective, the backhaul will enjoy a higher priority over the radio access aspects. In the future, it could be that in some scenarios, a site will be chosen because a cheaper backhaul link is feasible, instead of the radio access requirements [8]. In LTE small cell backhaul requirements, the two most crucial aspects would be ‘cost’ and ‘physical design and planning [8] [4].

One study looks urban area macro cell heterogeneous network to determine the number of small cells needed in a macro cell. The study finds that between six and seven small cells would need to be deployed per macro cell by 2019. Figure 3 shows the evolution of the increase of small cells capacity compared to the hop length. It is important to note that the number of small cells required is sensitive to factors such as subscriber traffic demand and available spectrum [4].

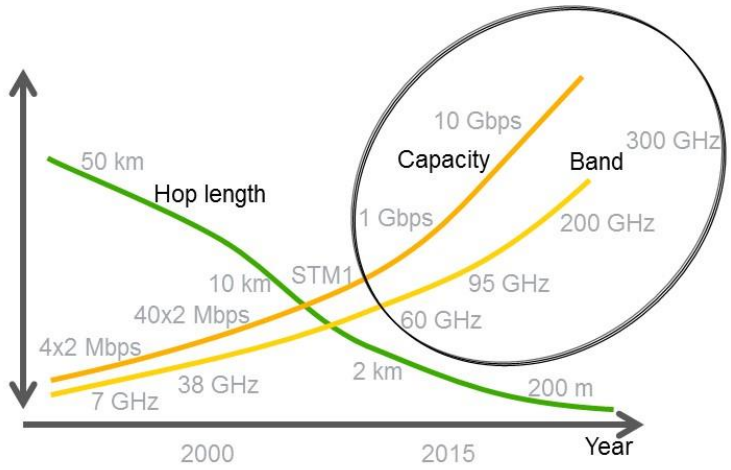

Figure 3. Evolution of small BH in capacity, band and hop length [3].

2.4 Wireless Backhaul Technologies

In this section, some technologies related to backhaul networks for future mobile system will be discussed. This thesis is related to wireless backhaul radios so the discussion will be concentrating more on wireless technologies and solutions for backhaul. Figure 4 gives an overview of backhaul technologies available today.

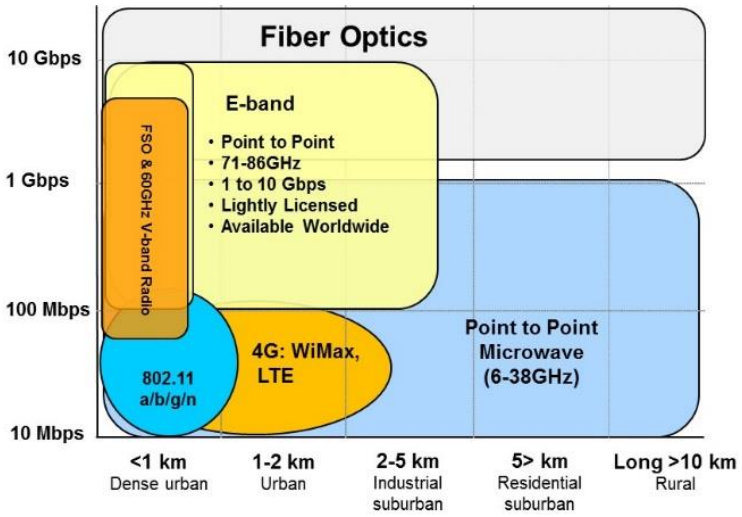

Figure 4. Backhaul technology choices [3].

A great number of alternative wireless solutions have been proposed for the small cell backhaul. These solutions can be grouped into some wider categories which are governed by several key design choices. They include:

- Connectivity and topology (point-to-point, point-to-multipoint, ring or mesh).
- Line-of-sight and non-line-of-sight and near-line-of-sight propagation.
- Carrier frequency from ~600MHz to 80 GHz.
- Spectrum licensing arrangement and dynamic allocation.

Table 1 shows a comparison between the wireless backhaul solutions depending on the connectivity, bandwidth, spectrum licencing, and carrier frequency. From the table it can be clearly estimated that to meet the need of future network capacities, one should concentrate on frequencies that have higher bandwidth availability so that system complexity and cost could be reduced, because as the size of the cell will keep on getting smaller these factors will start counting more and more, compared to other factors.

Table 1. *Summary of wireless backhaul solution technologies [4]*

Category Name	Carrier Frequency	LOS or NLO	Spectrum Licensing	Connectivity
mmW 70-80 GHz	71-76 GHz 80-85 GHz	LOS	Light licensed	Point-to-point
mmW 60 GHz	56 – 64 GHz	LOS	Unlicensed	Point-to-point
Microwave P2P	6 – 56 GHz	LOS	Link licensed	Point-to-point
Microwave P2MP	6 – 56 GHz	LOS	Area licensed	Point-to-multipoint
Sub 6GHz unlicensed	800 MHz – 6 GHz	NLOS	Unlicensed	Point-to-multipoint
Sub 6GHz licensed	800 MHz – 6 GHz	NLOS	Area licensed	Point-to-multipoint

2.5 Millimeter Wave Frequencies

The millimeter wave spectrum is located between 30 to 300 GHz. In general, mobile communication industry is starting to move the focus on all frequencies that is above 10 GHz because of the higher bandwidth availability. Nokia is also looking for deployment and technology development in several mmW frequency bands, but in this thesis E-band frequencies that include 70-80 GHz are focused on. With the growing demand of higher data rates and cell densification, the operators are looking for higher bandwidth which can provide much higher data rates. Propagation aspects of V-band and E-band frequencies favour the evolution of backhaul links due to high capacity and shorter hop lengths [4].

For achieving higher data rates at lower frequencies below 6 GHz, complex RF techniques like carrier aggregation, spatial multiplexing and multipath propagation are studied and developed. Contrary to these, mmW technology utilizes wide RF bandwidths to deliver higher data rates with simple single channel configuration. This can also reduce the cost per bit as of potentially smaller size and more simple hardware configuration can be adapted for a high-capacity backhaul link instead of heavy MIMO hardware configurations [4].

2.5.1 Frequency Bands

Some of the frequency bands available for mobile communication developments are V-band, which ranges from 57-66 GHz and E-band that corresponds to 71-76 GHz, 81-86 GHz and 92-95 GHz frequency regions as shown in Figure 5. As we go higher in the frequency, the electromagnetic energy absorption in the medium also gets higher while the V-band has particularly high medium absorption, compared to other mmW frequencies like 40 GHz or 90 GHz, which makes it only suitable for a short range, Point-to-Point (P2P) and Point-to-Multipoint (PMP) scenarios.

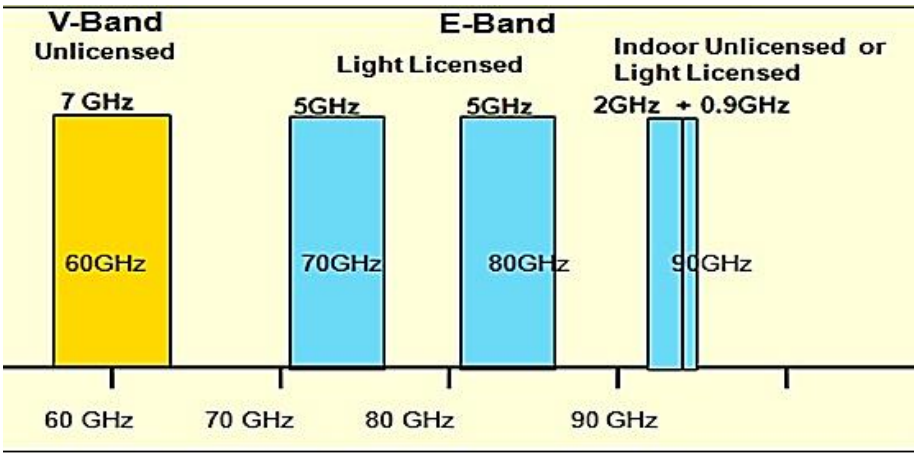

Figure 5. Selected millimeter wave frequency spectrums.

E-band frequencies at 71-76 GHz and 81-86 GHz bands, being lightly licensed form a good candidate for P2P mobile backhaul applications. With a bandwidth of 5 GHz at each frequency band, it offers the widest bandwidth available within all licenced carrier frequencies available for mobile communication. The 94 GHz band is mostly unlicensed for indoor applications but may also be used outdoor point to point communication with light licencing. With a simple modulation technique like BPSK, data rates up to a few Gbps can be achieved, using wide bandwidth of these channels. These simple modulation schemes enable simple system architecture for mmW technologies that have a distinct advantage of spectrum cost and availability [6].

2.5.2 Propagation Characteristics

As the radio signal propagates through the air, atmosphere adds some attenuation to the signal. It affects the radio wave in form of scattering or absorption of radio signals. Atmospheric loss is normally defined in decibels loss per kilometre of propagation. The loss in signal power is dependent on the hop-length of the link, so it should be noted that the signal loss in an mmW link due to atmospheric effect is exponentially dependent on the length of the link [6].

The mmW propagation characteristics are primarily depending on atmospheric oxygen, fog, rain and humidity. As it can be seen in Figure 8, the atmospheric attenuation at sea level pressure is around 0.2dB per km in 70-80 GHz band. The effect of humidity and water vapour is limiting the propagation between 0 to 50% losses per km, i.e. 3dB/km. Though 50% loss may occur through atmospheric effects, they are still lower compared to rain losses, which are important for long distance deployment [4] [6].

The amount of rainfall also defines the attenuation of the signal. Table 2 provides the signal attenuation per kilometer with different rain rates for E-band frequencies. These results show that extra path loss is added to the link budget due to heavy rainfall in mmW radio link. Thus, these frequencies are not very well suited for the areas which experience heavy rain. But still the performance of the mmW link depends on several factors, which include the actual distance between the radios, the link margin, antenna gain, modulation scheme and the receiver sensitivity [6].

Table 1. *Signal power loss due to rain at E-band [6].*

Description	Rainfall rate	Additional Signal Loss (dB) per km
Light Rain	1 mm/hr	0.9
Moderate Rain	4 mm/hr	2.6
Heavy Rain	25 mm/hr	10.7
Intense Rain	50 mm/hr	18.4

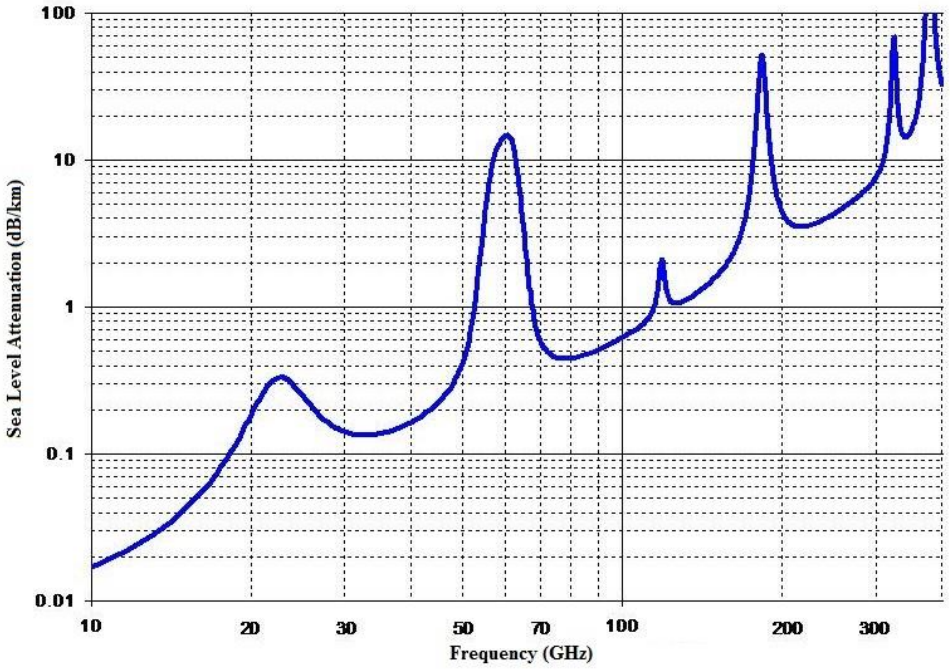

Figure 6. Radio signals atmospheric attenuation in dB/km [10].

2.5.3 Performance and Availability

The performance of a communication system can be quantified in terms of percentage availability of a system or its services. It identifies the average percentage of time the system is providing the services or expected to operate according to specifications.

As was already discussed earlier, there are several factors that affect the mmW link performance. Heavy rain is also a significant cause of attenuation in the signal level, but it does not cause any outage of mmW links if there is sufficient link margin. The availability of the system also depends on the probability of occurrence of such heavy rain. The availability percentage of mmW link is naturally bound to rainfall characteristics of the location where the link is deployed and also the path length of the hop [6].

The rainfall characteristics throughout the world are well studied and based on such studies international telecommunication union (ITU) has developed a model for computing the probability of the rain at various locations of the world. Table 3 provides a comparison of the expected performance of mmW radio links in large metropolitan areas based on ITU model [11]. In the table, first column shows the location of study, the second column describes the maximum length of the link that can achieve 99.99% availability and the third column shows the availability of the link at 2 km of distance.

Table 2. *Availability of Typical mmW link [6].*

Location	**Link Range (km, at 99.999%)**	**Availability of 2 km link**
Los Angeles	1.75	99.998%
New York	1.25	99.991%
London	1.65	99.998%
Milan	1.35	99.994%
Sydney	1.2	99.99%
Riyadh	2.85	>99.999%

2.5.4 Beamwidth

Millimeter wave frequencies allows for adopting narrower beamwidth as compared to the microwaves, with the same kind of antenna configuration as shown in Figure 7. This characteristic of mmW link allows several independent link deployments closer to each other. The beamwidth is dependent on the wavelength and aperture size of the antenna, which can be described mathematically as [11]:

$$BW = 70\lambda / D, \quad (1)$$

where BW denotes antenna beamwidth, λ means wavelength and D means the diameter of the antenna aperture. So, for example, with this rule of thumb an 18 GHz link will

have 4 times wider beamwidth than a 70 GHz link with the same size antenna aperture, which enables 16 times higher cell density for an E-band link in one given area [6].

Scalability is one key benefit of a highly narrow-beam of mmW links. Other wireless technologies have limited scalability because of cross interference with their neighbouring radio links and cannot be realized to their full potential. So mmW radios can be deployed in several topologies like point-to-point mesh, or a ring [6].

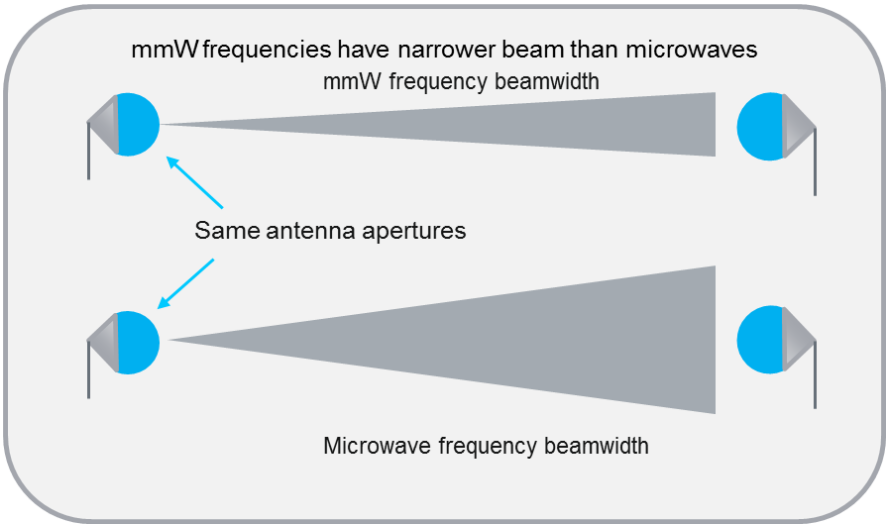

Figure 7. Microwave and mmW beamwidth comparison. Adapted from [6].

2.6 Challenges in mmW Link Deployment

A narrow-beam line of sight radio installation is more complex compared to non-line of sight deployments. The transmitter and receiver need to be aligned precisely with each other on installation. As discussed previously that while narrow-beam has advantages like lower level of interferences in mmW links, it also implies the problem of correct alignment of the link and line of sight link disturbance due to pole sway [4] [6].

Pole sway also causes loss of link if there is a change in degree angle greater than half of the beam width of radiation pattern. There could be noticeable effect on user experience if the mounting pole keeps on shaking substantially for longer period of time. This kind of aspect need to be resolved in small cell environment [4].

The huge path loss is a critical problem in outdoor mmW link, if compared with microwave frequencies. Outdoor mmW systems have much longer hops as compared to indoor, so higher gain through advanced antenna system are required for these links [12]. Table 3 shows the link budget for the additional gain that is need to deploy mmW frequencies in the system.

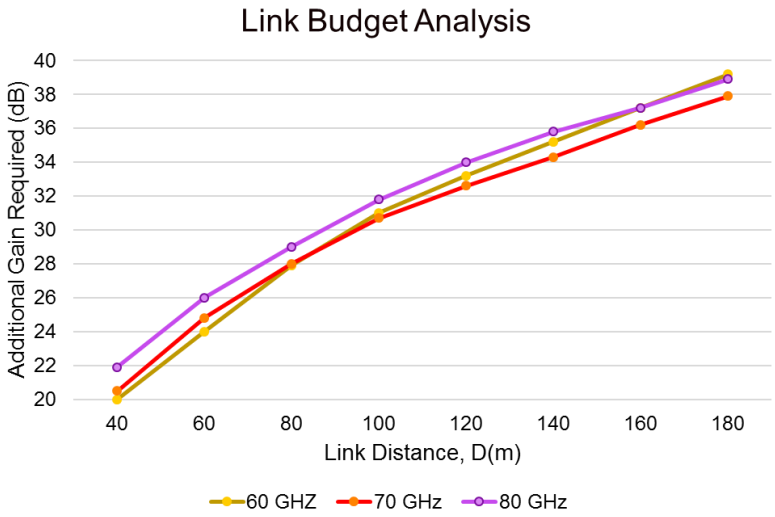

Figure 8. Additional gain required by mmW link. Adapted [12].

Table 3. *Link budget for additional gain of mmW link*

Parameters	**Values**
Transmit Power, P_t	15 dBm
Noise Figure, NF	6 dB
Thermal noise, T	-174 dBm/Hz
Bandwidth, *B*	2 GHz
Required SNR (QPSK)	5 dB
Path Loss exponent, a	2.2 for LOS path [13]
Additional Path loss for O_2 and rain, Ai	20 to 36 dB/km [14]
Path loss model, *PL (D)*	$32.5 + 20\ \log_{10}(fc) + 10.a.\log_{10}\left(\frac{D}{1000}\right) + Ai.\frac{D}{1000}\ dB$

In the above table, fc is the centre frequency and D shows the distance or the hop length. In Figure 8, through link budget analysis, total required gain for mmW frequencies can be calculated. For example, for the same amount of distance, an additional 20 to 36 dB of additional gain is needed as compared to microwave radio link. The graph shows the path loss model for three frequency bands of mmW frequencies [12]. The 60 GHz band has a bit steeper path loss curve than 70 GHz and 80 GHz. This is because of the higher O_2 absorption at 60 GHz band than the other two bands as described in [13] [14]. This is why 60 GHz frequency band allows for smaller hop lengths than any other frequencies.

3. ARCHITECTURE STUDIES FOR MILLIMETER WAVE BACKHAUL RADIOS

This chapter will provide some fundamentals related to the application and technologies that are going to be used in building the system architecture. The theory will focus on the system requirements of self-aligning and self-organizing wireless mesh backhaul. In the further discussions, several architecture specifications such as duplexing scheme, capacity requirements and beamforming techniques will be discussed. In addition, mmW beam steering antennas, that are important for deployment of the new small cell backhaul, will also be discussed.

3.1 Self-Optimizing Wireless Mesh (SWMN) Backhaul for 5G

In densely populated metropolitan areas, the operators are looking for deployment of 5G small cell networks which are cost effective and easier to deploy. In such scenarios operators have to deploy nodes in non-traditional places such as building, billboards and lamp-posts, where there is no easy access of fibre cables. The only solution left for the connectivity of such nodes is wireless link that should be self-organizing, self-optimizing, can achieve high capacity, are easy to deploy and resistant to network impairments [15] [16].

The self-aligning and beam steerable radio technology cannot be very helpful until and unless the network has some intelligence for self-organization and dynamic routing. This kind of intelligence is provided by SWMN. SWMN is a smart backhaul solution that is link layer status sensitive and can react to link failures and capacity reductions in real time. SWMN topology supports a directional partial mesh backhaul implementation with a narrow-beam P2P mmW links [16].

The detailed work required for planning and designing of a wireless transport network can be reduced through SWMN. It also reduces the optimization efforts by independently deploying the wireless transport layer for small cells. It offers self-optimization feature, flexible Quality of Service (QoS), congestion control and management, extensive load balancing and traffic management features. Further details about SWMN backhauling can be found in [15] [16]. Figure 9 shows small cell self-organizing mesh network architecture. Furthermore, Figure 10 shows a simple mesh system containing three mmW backhaul nodes architecture where each node has the capability of time divisional point to multipoint connectivity.

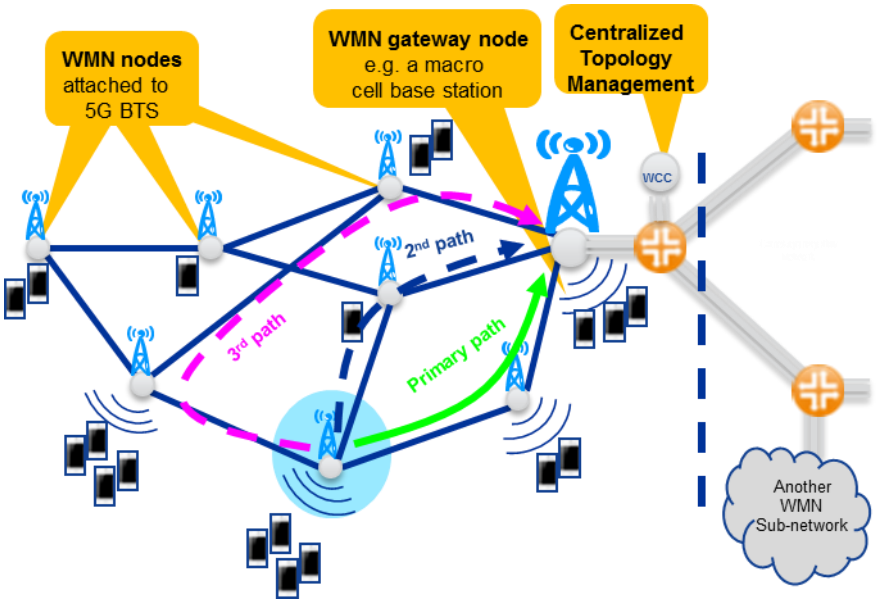

Figure 9. Typical SWMN topology for small cell networks [17].

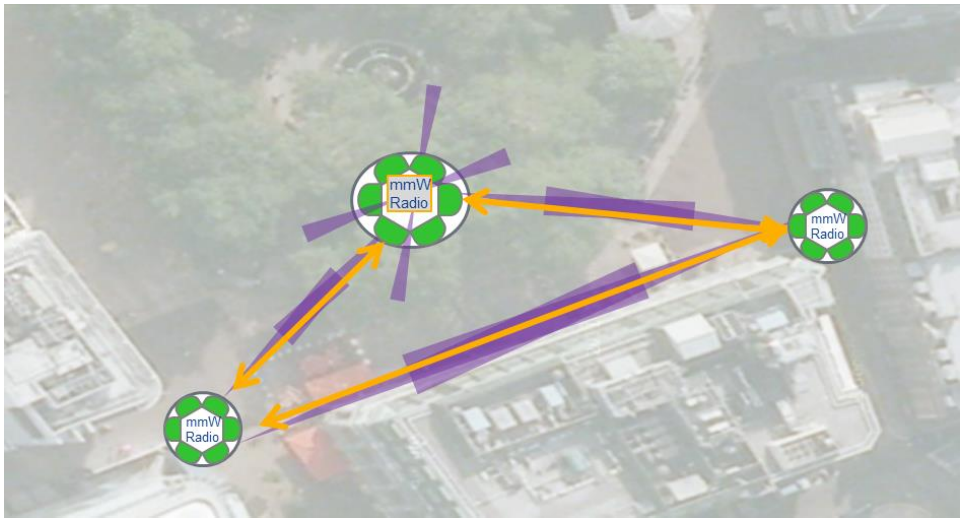

Figure 10. PMP architecture for mmW LOS radios.

3.2 Self-Aligning Radios

For a low-cost self-organizing small cell mesh system, an important aspect of mmW radios is electrical beam steering. Due to narrow beamwidth of mmW links it is hard to align them on time of deployment or making continuous repairs for the link in case of some miss alignments. These kind of issues can be easily coped-with by using electrical beam steering in mmW radio. The electrical beam steering enables the self-alignment of the radio nodes and can provide several advantages in making of self-organizing mesh networks. Some advantages for the links are discussed below.

Easier Deployment of the Radio Node

The mmW backhaul radio can have a narrow antenna beam up to 3 degrees of beamwidth, which will be hard to deploy if there is no electrical beam steering available. By adopting electrical beam-steering, the manual work is considerably reduced in case of deployment. Figure 11 shows the deployment scenario of mmW beam steering link to a pole [17].

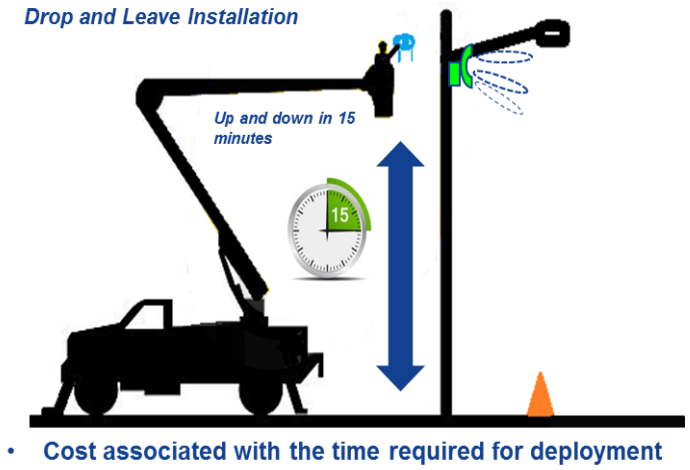

Figure 11. Millimeter wave node deployment scenario.

Automated Neighbour Discovery and Network flexibility

The beam steering enables the possibility of autonomous self-build up network. The node can keep on searching for some neighbouring nodes to connect to. With the addition of new node, it can automatically be added to the network. Figure 12 shows an example of addition of new node to the network through beam steering capabilities [17].

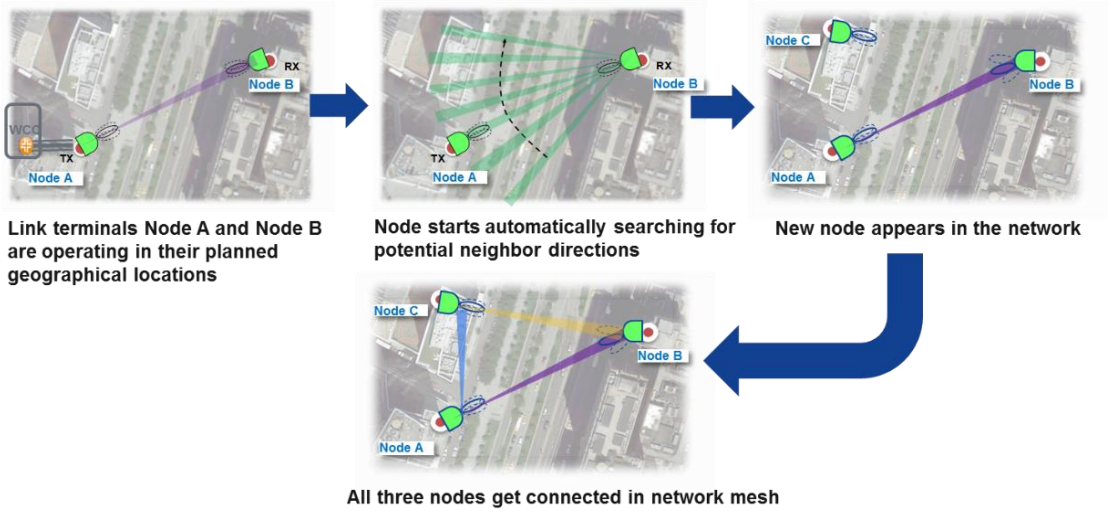

Figure 12. Automated neighbour discovery and self-building network.

Twist and Sway Misalignment Compensation

The electric beam steering also provides compensation for twist and sway of the mmW nodes during operation. As the beamwidth of the mmW radios are narrow, even a small disturbance in the alignment of the node can cause outage of the link. Beam-steering can effectively cope with such situations. Figure 13 shows a demonstration for vibration compensation between two nodes [17].

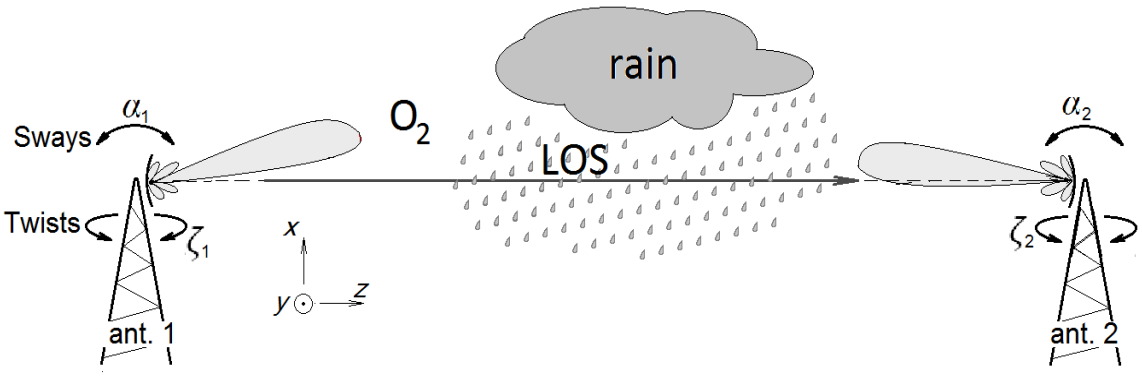

Figure 13. Vibration compensation though beam steering.

3.3 Beam Steerable Antennas

The challenges that are faced in the deployment of the narrow-beam radio links can be solved though few technologies, like electrically steerable antennas can be used to change the direction of the beam for alignment. There are two methods of implementing electrical beam steering: distributed phased antenna array or switched beam method with traditional collimator such as parabolic dish or lens that has selectable feed point. There could also be mechanical steerable methods for alignment of the mmW radios but the mechanical movements are always not as fast as the electrical steering and it is also expensive to maintain, thus compensation of the pole sway could not be achieved [18].

Array of antennas whose gain and phase can be adjusted individually are used in beamforming technology. By changing phase of each antenna element, the signals are added constructively or destructively, so the beam is shifted to a desired direction. The signals add constructively when the sine waves are in phase and add destructively when the sine waves are out of phase, so the point of maximum gain changes when the signal phase is changed. The maximum gain of the antenna depends upon the number of antenna elements and number of phase shift points. Generally, for higher gain or for achieving higher scanning ranges of the antenna, more antenna elements are required with higher points of phase change, which will increase the system complexity. The beamforming techniques through phase shifters will not be discussed further because there are no mature phase shifting devices available for E-band but they are under development. This technology works well for lower frequency bands [18].

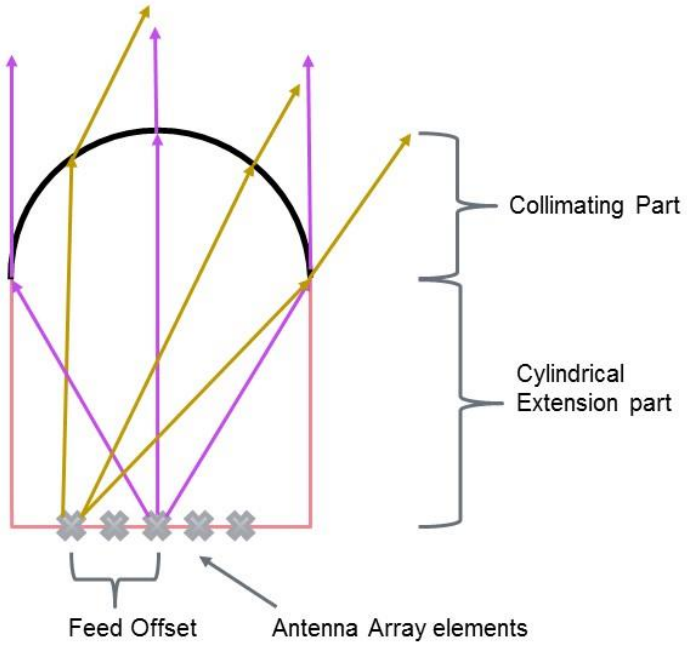

Figure 14. Integrated lens antenna with feed array. Adapted from [19].

Integrated Lens Antenna (ILA) is the second option that can be used for the beam steering. ILA consist of two parts: the feed array antenna elements and the dielectric lens. The principle of ILA is described in Figure 14. For switching between the antenna elements an electric switching network is needed consisting of Single Pole Four Throw (SP4T) and Single Pole Two Throw (SP2T) RF switches. The array of antenna elements is placed at the back of the surface of lens. The lens is a hemispherical or elliptical shaped that accumulates radiations from the antenna array. The beam steering is achieved by the changing position of the active antenna patch. Only one element is active at one time. The directivity and the gain of the lens depend upon the extension part length and the lens material. Different combinations of material and lens lengths can be used for specific beam width and directivity [18] [19] [20]. Beamwidth of 2 to 2.5 degree and gain of around 28 dBi were achieved for 77GHz by using extension part length of 85mm and lens radius of about 100mm [18]. In another design study ILA was designed for the operating frequency of 73 -94 GHz with the gain of 16 to 120 dBi [19], with the lens diameter of 15 to 25 mm and an extension part of 5.5 and 9mm respectively [21]. In another study an antenna with 37 to 43 dBi of gain was achieved with the beam width less than two and one degree. The diameter of the lens antenna was 120 and 246 mm [22].

Beam steering through ILA shows promising results, as can be seen through the studies above, so it has high potential to be used in mmW small cell backhaul. This beam steering technique can provide different beam widths at different directions. ILA is a complex system but it provides efficient beam steering with a low cost implementation [18] [19].

3.4 Millimeter wave Radio Design Specifications

The radio design needed for constructing a SWMN system should be able to support the capacity requirements and beam steering capabilities. In this section, features and technologies for making a beam steerable mmW radio will be discussed. The main features and requirements that need to be considered for the mmW radios are listed below.

- Duplex schemes
- Beamforming and beam steering capabilities
- Capacity requirement
- RF transceiver architecture
- Multiple beam requirements
- Regulation and power requirement for E-band cases

These points will be discussed in details below, to find an optimal solution with the available resources to make an efficient mmW radio.

3.5 Duplex Schemes

Frequency Division Duplex (FDD)

In FDD the TX and RX chains are operated simultaneously on separate carrier frequency and can have different bandwidths for uplink and downlink [5]. FDD system can be more complex for a beam steerable radio because one needs to have two different kind of systems in the mesh network i.e. if the TX of one node is at the lower band, then the RX of the other node should be in the lower band and vice versa. This will make the network planning difficult and if there is any change in the network structure then it will be hard to redesign the network configurations. Moreover, FDD needs duplex filter which is always the most expensive part especially for E-band.

Time Division Duplex (TDD)

In TDD scheme the TX and RX chains operate on same carrier frequency but in different time slots. This means that only TX or RX is operating at a given time slot. The amount of RF hardware needed for TDD system is comparatively lower than FDD so cost of the system will be lower. Planning and optimizing of TDD system in mesh network is easier than those of FDD system. The downlink and uplink capacity can also be dynamically adjusted in TDD system by changing the time share of TX and RX, which makes TDD perfect candidate for this project [5].

The discussion on duplexing scheme concludes that for an E-band backhaul radio, TDD system is a better duplexing technique for dense mesh networks because of easier network planning through symmetric nodes. Because of availability of huge amount to frequency spectrum one can utilize it more efficiently for getting highest capacity achievable wirelessly.

3.6 Beamforming and Beam Steering Capabilities

In this project, the need of beam forming is compulsory, and the ETSI requirement of high gain antenna make it very difficult to have a sufficient size of beamwidth. Beam forming and electrical beam steering of antennas at E-band is discussed in detail in chapter 3.3. Integrated Lens Antenna (ILA) gives promising results in terms of narrow beam width, steering range and gain.

Regarding the specifications for ILA, the number of elements and the lens antenna gain is also debatable. The amount of antenna elements is limited, because with the increase of antenna elements the number of RF switches will also increase. The problem with the E-band RF switches is that they have higher insertion loss. There is a trade-off between number of antenna elements and power loss. According to [18] [19] more dynamic horizontal sway compensation is needed than the vertical sway. So the scanning elements can be arranged in 4x16 or 2x8 configurations, depending on the amount of losses that are applicable for the system link budget. Figure 15 shows an example of the ILA lens and antenna elements selection. Same configuration is considered for the final demo system radio. Further discussions on compensation of loses in the switching matrix will be done in architecture designs and link budget analysis section.

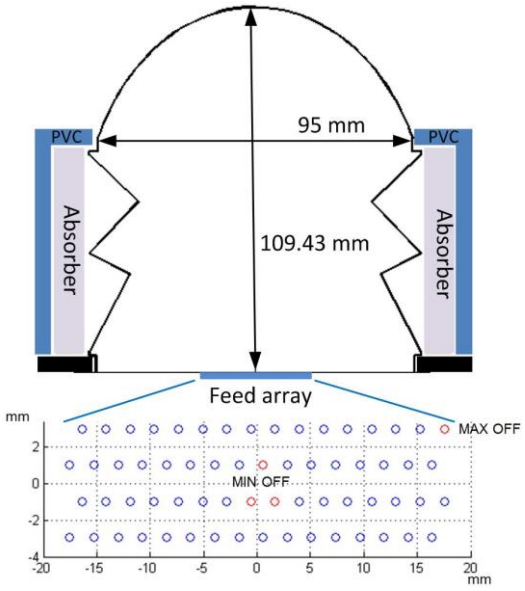

Figure 15. ILA with 64 antenna elements.

3.7 Capacity Requirements

The new target for 5G networks is to achieve the capacity of 10 Gbps over the air, to meet the future backhaul capacity requirements. This kind of high throughput is only possible to achieve in E-band because of the availability of wide bandwidth and lower interferences. There can be more than one approach for achieving such capacity. In this section some options for achieving 10 Gbps will be discussed.

1. **Applying High Level QAM in Convention System (< 42 GHz):**

If it is assumed that baseband bandwidth is 56 MHz in a conventional system with dual polarization to achieve 10 Gbps of data rate, 2^{100} QAM is required, as calculated in Table 4. This kind of modulation schemes are not possible to be used in practice. Even if the bandwidth of the baseband is doubled to 112MHz the capacity is only doubled, thus requiring the adoption of 2^{50} QAM. So a lower bandwidth is not the solution to the capacity requirements. Only a huge array of MIMO can achieve such a high capacity at lower frequency bands which is not possible because going substantially beyond 2x2 MIMO configuration is technologically and hardware-wise challenging. For much higher MIMO matrix the number of radios needs to be increased which will cause huge amount of hardware requirements.

Table 4. *Modulation scheme calculations.*

System Parameter	Calculation	Value
Bandwidth, BW	56 MHz x 2 (Dual Polarization)	112 MHz
Baud-rate	12% of modulator inefficiency	100 MBaud
Required throughput		10 Gbit/s
Bits Per Symbol	Throughput/ Baud-rate	100 bits/symbol
Unique Symbols		2^{100} symbols

2. **Wide Bandwidth in E-band:**

System capacity is not limited only by RF bandwidth but also by baseband processing capability: size of Field-Programmable Gate Arrays (FPGA) and speed of data converters. There is 10 GHz of bandwidth available at E-band frequencies. For achieving 10 Gbit/s speed, a bandwidth of 2 GHz with 1600 Mbaud symbol rate can be adopted. It is possible with the current data converters and FPGAs to achieve 2 GHz of channel bandwidth. This could be one simple approach for reaching the goal of 10 Gbit/s.

3. **Dual Polarization (XPIC) in E-band:**

The requirement for high speed converters can be reduced to half if the radio is able to support dual polarization so the capacity could be doubled and only 1GHz of bandwidth will be required for achieving 10 Gbit/s goal. So this recommendation for achieving the 10 Gbit/s radio can also be considered.

4. **LOS space divisional MIMO and XPIC in E-band:**

Another option is to introduce 4x4 LOS-MIMO, which will further decrease the bandwidth requirement to half. So with MIMO only 500 MHz of baseband bandwidth will be

required with 400 Mbaud rate. But this system architecture will considerably increase the complexity of the system and the SDMA concept requires that the angle between parallel antennas is larger than antenna beamwidth. Figure 16 shows the spatial division MIMO with XPIC for achieving higher capacity.

So option 2 and option 3 have a high potential for achieving the desired data rate within desired cost effectiveness, therefore the demo system should be able to support both of the proposed recommendations for achieving 10 GB/s.

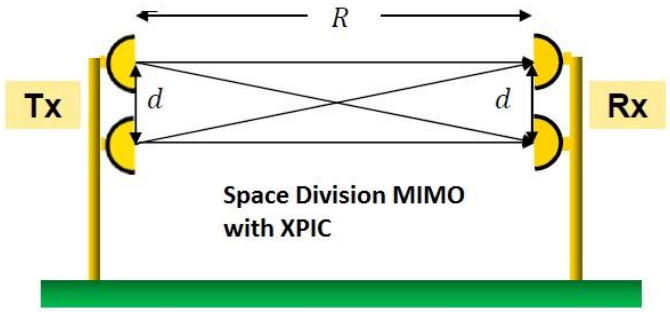

Figure 16. LOS space divisional MIMO and XPIC in E-band.

3.8 RF Transceiver Architecture

There are many transceiver architectures proposed in the literature, but most popular among them are heterodyne and homodyne receivers which will be compared in this section. There are also other transceiver architectures available such as Wideband-IF and Low-IF receivers but they will not be discussed here.

Heterodyne Architecture

This kind of architecture is most extensively used architecture in wireless transceivers, especially on base-station side. In this dual conversion architecture, RF is down converted first to Intermediate Frequency (IF) and then it is further down converted from IF to base-band signal [23] [24] [25]. Figure 17 shows the block diagram of heterodyne receiver architecture.

The benefits that a heterodyne architecture provides are: good sensitivity, good signal isolation by arithmetic selectivity, and feasibility to adopt high quality fixed IF frequency band components [23]. Beside these advantages this architecture has some drawbacks as well, such as, it needs to have high performance oscillator or LO and LNA output impedance matching is challenging because of the integration of image reject filter. There are number of LO and IF signals harmonics that leak to different places and may cause problems for signal to noise ratio. Because of its high power consumption and complicated structure, there is substantial interest to develop and adopt a simpler and easy to integrate architecture [24].

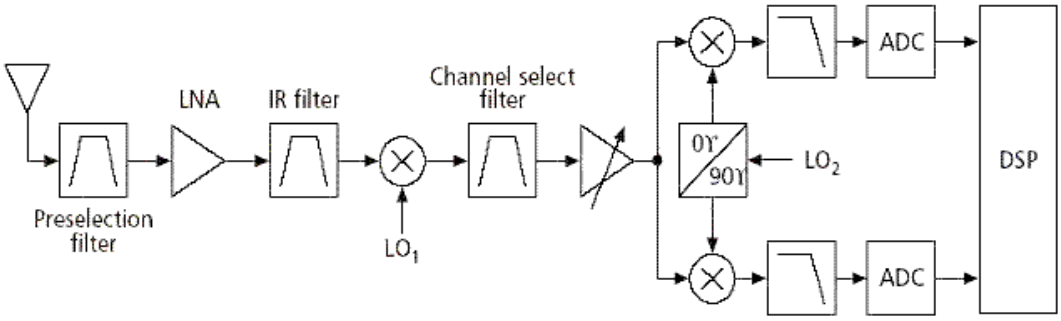

Figure 17. Heterodyne architecture [26].

Homodyne Architecture

Homodyne architecture works on a principle of Zero-IF which means it converts the RF frequencies directly to baseband in a single stage conversion. In the direct conversion process the converter should provide quadrature outputs, that will help to avoid the loss of information in case of frequency and phase modulated signals [23] [24] [25]. Figure 18 shows the block diagram of a homodyne architecture.

The homodyne architecture has several benefits over heterodyne architecture. The biggest benefit is that it needs smaller amount of hardware to operate because it does not include several expensive blocks that are needed by heterodyne architecture such as high image and harmonics cancelation filters because of no IF stage is used. Furthermore, just a LPF is sufficient and gain is only needed at baseband stage offering potential for reduced power consumption. In the integrated circuit the LNA needs no matching to 50Ω impedance because no image reject filter is present between mixer and LNA [23] [24]. Apart from benefits this architecture also has some challenges that needs to be under considerations when working with this transceiver.

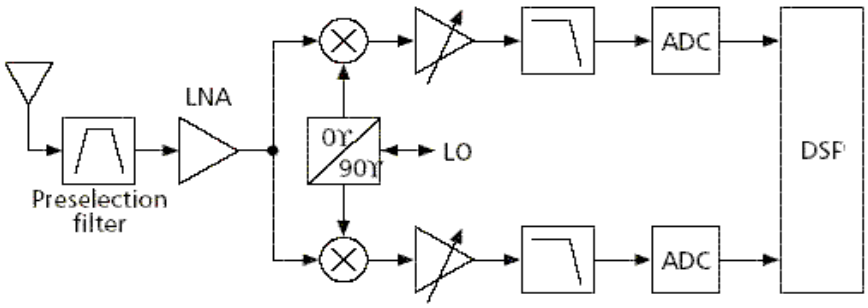

Figure 18. Homodyne architecture [26].

The main challenge is DC-offset in direct-conversion receivers which mainly appears due to LO leakage though this can be reduced by calibrating the receiver without any input signal and then subtracting the LO leakage power in reception. 1/f type noise may also create some problem in this architecture. Signal leakage from antenna to surrounding can also take place more easily than in heterodyne receivers. I/Q mismatch is also a problem

if the length of I/Q traces or the amplification are not identical, so the processing of base-band I/Q signals should be precise in order to tackle this error [25].

3.9 Beam-steering and Multiple Beam Requirements

While using the integrated lens antenna for mmW communication, the number of elements define the scanning range for the mmW radio beams. By increasing the number of feeding elements the scanning range and coverage area of the system will increase but because of inclusion of bigger switching matrix behind the feeding elements, the insertion loss will also increase which will increase the noise figure of the system and degrade the system performance.

Another issue that can be faced in deployment of SWMN system is that it has a mesh topology so just point-to-point link is not useful for the network. Point to multipoint and multipoint to multipoint connectivity among the mmW nodes is highly important for the mesh network. A multi beam system which can provide connectivity with more than one node at the same time without loss of capacity is beneficial. In this section some architecture details of beam-steering and multiple beams that are feasible for a proof of concept demo will be discussed.

The highly directive nature of mmW communication enables reduced level of interference with multiple coexisting RF beams [26] [27]. By the possibility of using multiple beams one can think of using more than one RF chains which can provide connectivity to more than one node simultaneously. But even in mmW frequencies there are some limitations for number of simultaneous users because of the limited hardware resources and also the adjacent channels can still interfere with each other if the beams are situated close to each other. The side lobes of the antenna can also be another reason for the interference.

Single beam-steerable radio architecture

This architecture includes a single chain TRX that is feeding an antenna switching matrix. The mmW RF switches have high insertion loss, so with the addition of each layer of switching matrix, the insertion loss increases. Figure 19 shows the architecture details.

In general, each kind of architecture has its own benefits and challenges involved. In case of this architecture, it has minimal power consumption and simplest transceiver chain design. It can have codebook based beam switching through electrically switching RF chain. But it just provides support for single beam so multiple users cannot be supported by this system. Another huge drawback is that the insertion loss of mmW RF switches is high, and with the addition of more layers of switches this loss will keep on increasing, which can depreciate the performance of the system.

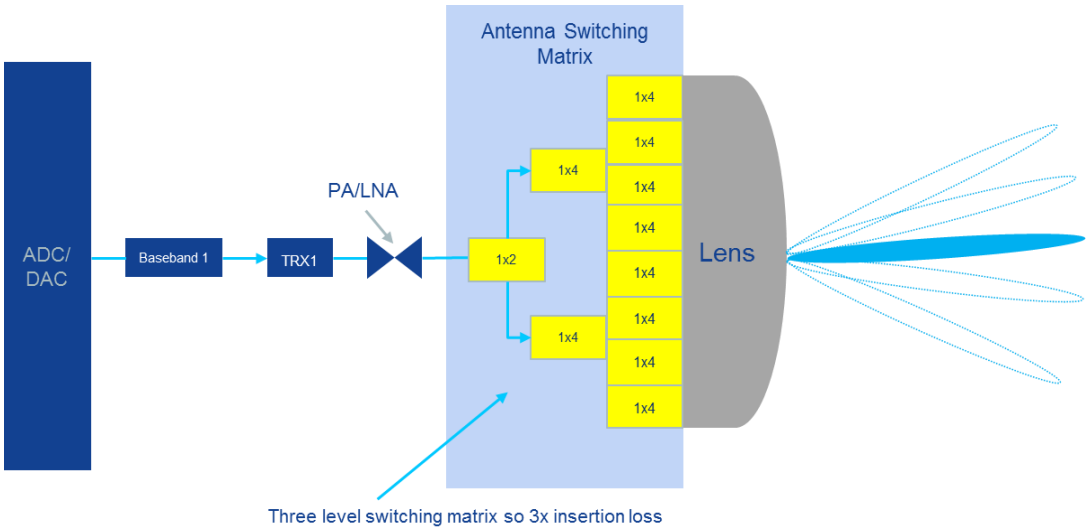

Figure 19. Single beam steerable mmW radio architecture.

Multiple beam-steerable radio architecture

For the support of multiple users, the number of RF chains should be increased. Each RF chain includes two to four antennas and have the limited ability for beam steering. Multiple beams and beam forming is beneficial for multiple node connectivity. Figure 20 shows the architecture details for the multiple beam-steerable antenna.

This kind of architecture provides higher flexibility in terms of transmission modes, number of antennas, and beams. Each RF chain can have smaller antenna matrix which means lower losses in RF switching matrix. But the overall cost and power consumption on a system level becomes high if larger antenna arrays are considered. Since most of the power is consumed by ADC/DAC's in each RF chain, there is a tradeoff between number of RF chains and antenna matrix size [27]. The main problem in such architecture is the co-channel interference. Higher frequencies like mmW can be used in dual beams but the side lobes interference of adjacent antennas can disrupt the communication. The spacing of both of the communication beams should be calculated before deployment in any scenario [28].

Dual beam-steerable radio architecture

Dual beam steerable radio includes at least two RF chains. This architecture is an interim form of the two architectures discussed above. With this architecture the two beams can considerably be apart from each other with considerably larger antenna arrays, so larger scanning range and the number of switch matrix level is also decreased by one. And the number of PA's and LNA's for each RF chains is increased which can provide more output power to antenna patches. Figure 20 shows the architecture details for the dual beam-steerable antenna. This kind of architecture can also be used for transmissions in dual polarization, which can be used for increasing the capacity of the system instead of support for two different users [28].

With a limited amount of RF chains, one can provide dual connectivity with two nodes. The lower amount of levels of switching matrix at the front end of the transceiver reduces the insertion loss. The architecture provides lower complexity version of shared array architecture by reducing number of TRX chains, while also implying reduced amount of interference from co-channel transmissions because of wider channel spacing. The overall cost and power consumption are also reduced even with considerably larger antenna arrays.

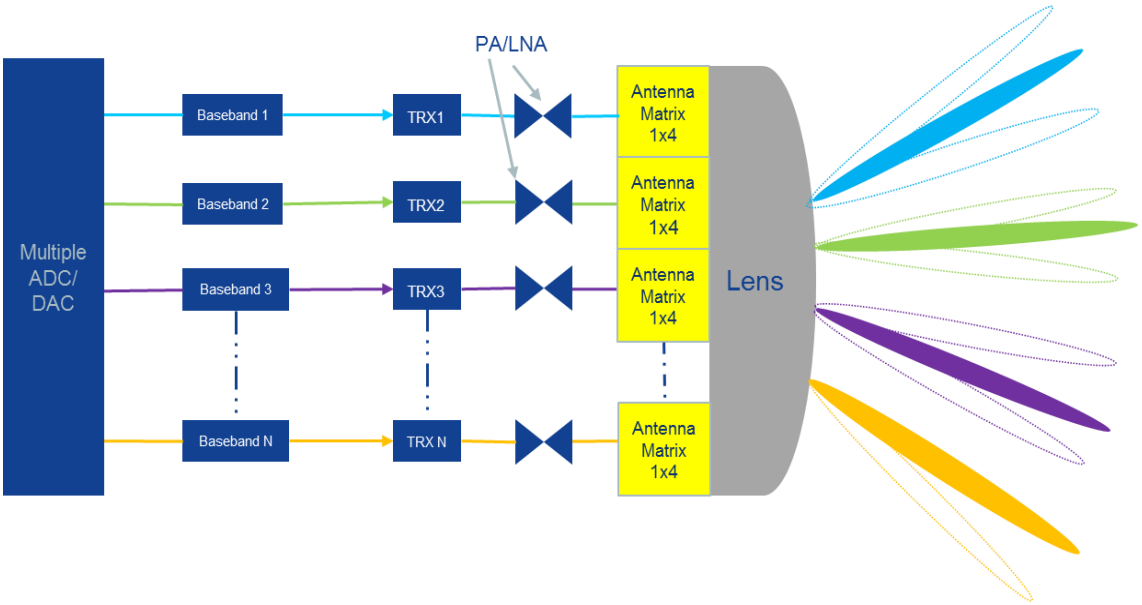

Figure 20. Multi-beam steerable mmW radio architecture.

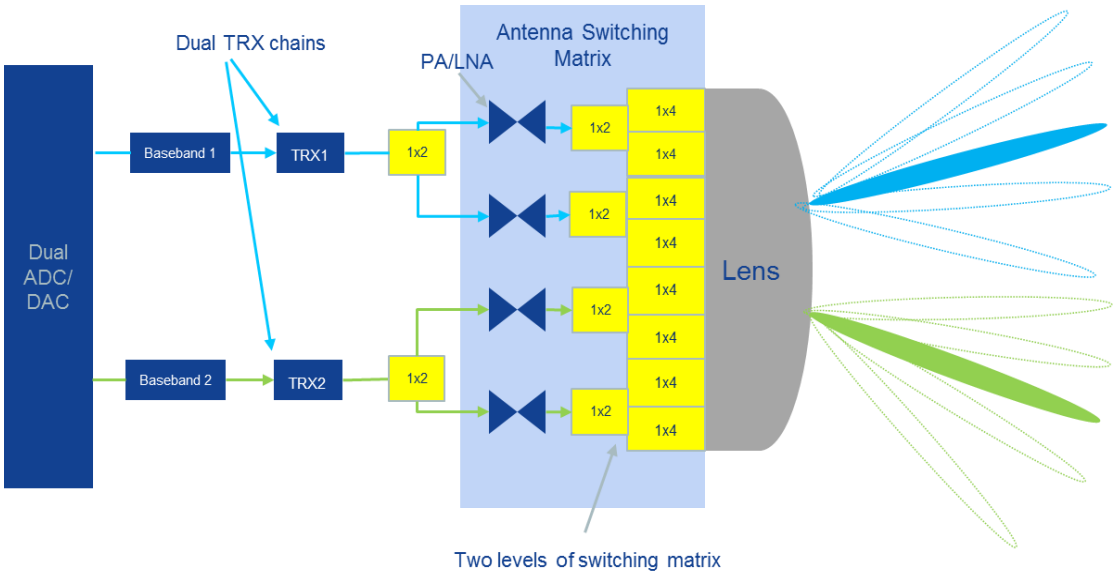

Figure 21. Dual beam steerable radio architecture.

3.10 Regulations and Power Requirements for E-Band Cases

There are certain requirements and regulations for radiating at any frequencies in the air. The transmit power antenna gains and licencing requirements are regulated by several regulatory bodies like ITU, ETSI, CEPT/ECC and FCC. These regulations are covering most of the regions, however, other national regulations could also be present [29].

FCC commission in 2003 approved a report and order (modified by Memorandum Opinion and Order on reconsideration [30]) in which service rules were established to support non-federal use of mmW spectrum at 71-76 GHz, 81-86 GHz and 92-95 GHz bands [29]. E-band use regulations were first produced by FCC [29]. The channel size and channel arrangements are not restricted in these frequency bands. Both kinds of duplex schemes TDD and FDD are allowed. The duplex separation in FDD applications should be 10GHz. Minimum antenna gain was set to 43 dBi but in future can become 38 dBi. Table 5 shows the summary of FCC technical specifications for operation in E-Band.

Table 5. *FCC technical specifications for E-Band [29].*

Maximum power limit	5 dBW
Maximum equivalent isotopically radiated power (EIRP)	55 dBW
Transmitter maximum power spectral density (PSD)	150 mW/100 MHz
Minimum antenna gain	43dBi (can be 38dBi)
Provision for reduced EIRP	Max EIRP reduced by 2 dB per 1 dB reduction in antenna gain respect 50dBi
Minimum spectral efficiency	0.125 bits/s/Hz

CEPT/ECC in 2009, for high density deployment in 3G/4G mobile backhaul, increasing the importance of E-band, specific channel arrangements for channel sizes ranging from 250 to 4750 MHz were introduced in a revision of *ECC/REC(05)07*. Both TDD and FDD applications were allowed with 10 GHz and 2.5 GHz duplex separation. Link-by-link coordination will be more efficient in these arrangements, which was observed by most of the CEPT administration [29]. The summary of technical specifications for E-Band proposed by ETSI are shown in the Table 6.

Table 6. *CEPT/ECC technical specifications for E-band [29].*

Maximum power limit	30 dBm
Maximum equivalent isotopically radiated power (EIRP)	85 dBm = 55dBW
Minimum antenna gain	Pout (dBm) + 15; or 38 (whichever is the greater).
Maximum antenna gain	85 – Pout (dBm)
Minimum spectral efficiency	According to ETSI Radio Interface capacity [RIC]

4. MILLIMETER WAVE RADIO SYSTEM DESCRIPTION

This chapter provides the system description and architecture details of Proof of Concept (PoC) beam steerable millimeter wave backhaul radio that was developed at Nokia Bell Labs. In addition, the discussion on several system modules such as the baseband modem, mmW transceiver module and beam switching control card will be presented. The PoC system data control flow and beam switching architecture along with link budget analysis will also be discussed.

4.1 System Architecture Overview

A proof of concept system is designed for demonstration of mmW beam steering radio for backhaul and access applications for 5G. The radio has integrated lens antenna with total of 64 antenna elements, which provide a scanning range of 34 degrees in azimuth and 8 degrees in elevation. The radio operates at 71-76 GHz band and is designed to support TDD duplexing scheme. The analog part of the radio has the ability to support 2 GHz of bandwidth with up to 64-QAM of modulation scheme.

The radio has dual beam capabilities so it can support the connectivity with two other nodes at the same time. The architectural details of the radio system will be discussed in detail in this chapter along with the link budget and phase noise calculations. Figure 22 shows the architectural block diagram of the radio including all of the logical blocks of the system. Explanations and descriptions of each working modules are given below. The architecture of the radio consists of the following modules.

- Wideband modem and Analog Front End (AFE) card.
- Analog baseband board.
- Millimeter wave transceiver module.
- Beam switching control card.

4.2 Wideband Modem and AFE Card

A single carrier wideband modem which is located inside the Field-Programmable Gate Array (FPGA) provided by Xilinx is used in this PoC system. This wideband modem provides solution for point to point and point to multipoint applications and can support bandwidth from 20 MHz to 500 MHz. It also includes integrated automatic digital pre distortion and other signal processing compensation algorithms to counter measure various signal distortion and impairments. Summary of the modem features is given below.

- Support for both FDD and TDD operation.
- Support for US and ETSI standard channel allocations.
- Modulation support: QPSK, QAM8, QAM16, QAM32, QAM64, QAM128, QAM256.
- Automatic adaptive modulation and coding.
- RX analog gain control.
- Automatic signal impairments correction in demodulator.
- Automatic carrier frequency recovery
- I&Q frequency dependent imbalance compensation

The Analog Front End (AFE) card contains analog signal conditioning circuitry (amplifiers and filters), IF transceiver and Digital to Analog (DA) and Analog to Digital (AD) converter module. This card can also provide IF stage outputs that can support up to 500 MHz of bandwidth. In this PoC system the AFE card mainly used as an ADC convertor module because IF stage is not needed in the direct conversion architecture. The TX chain has 12-bit interface with 450MHz bandwidth and AD-converter sample rate of 900MSPS. Whereas, the RX chains is 16bit interface with 312.5MHz bandwidth and DA-converter sample rate of 625MSPS.

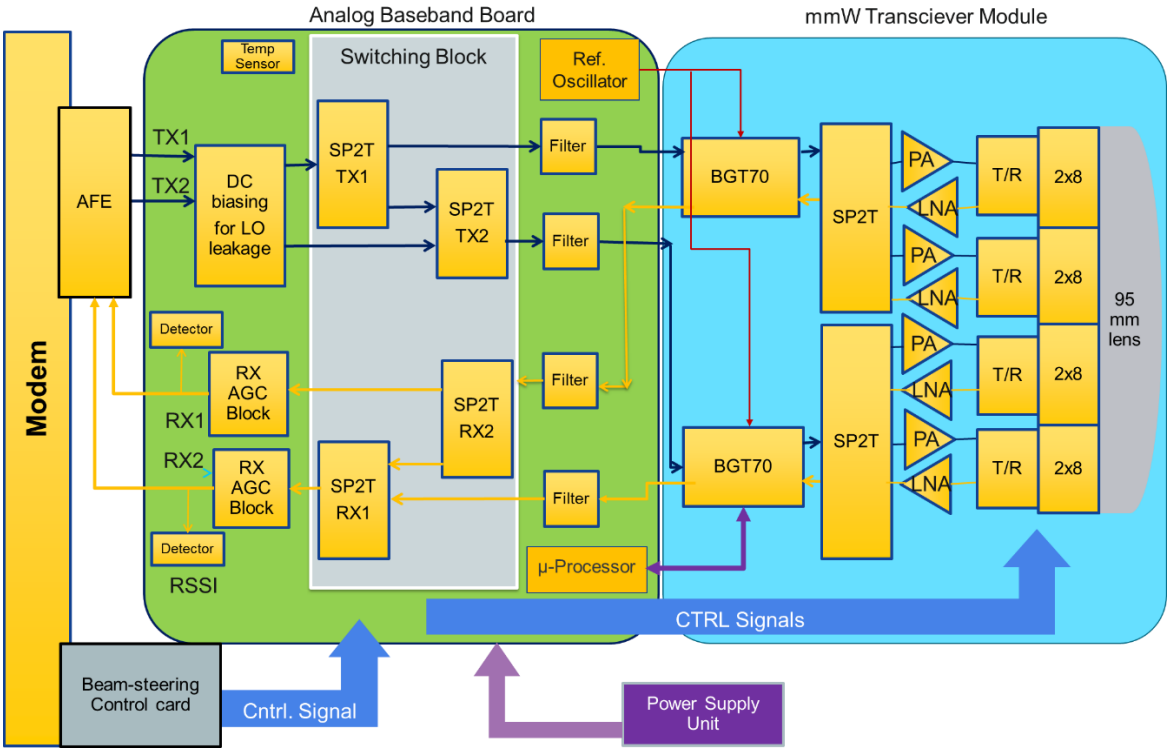

Figure 22. Architecture block diagram for mmW beam-steering radio.

4.3 Analog Baseband Board

Analog baseband board (ABB) acts as an interface board for the mmW module. The PoC demonstrator is designed in modular form, each module for special task so that trouble-shooting for each step can be made easier. This board is called analog baseband board because it widely contains baseband signal conditioning blocks, such as filters, Automated Gain Control (AGC) amplifiers, ADC driver amplifiers and RSSI detectors etc. This board also provides baseband switching between the two transceivers on mmW module. Further details about switching architecture will be discussed in the following sections.

Beside baseband conditioning and switching blocks, ABB also contains some supporting modules for the mmW board such as a microprocessor that is needed to configure the transceiver chips on the mmW board. Reference oscillator for the transceiver Phase Lock Loop (PLL) is also placed on the baseband board to reduce the circuitry of mmW module. The analog baseband board and its submodules will be discussed in Chapter 5 in detail.

4.4 Millimeter Wave Transceiver Module

A single-chip transceiver BGT70 developed by Infineon is used in this module, and is operating at the lower E-band from 71-76 GHz. Furthermore, the mmW module also contains Power Amplifiers (PA), Low Noise Amplifiers (LNA) and switching matrix for antenna selection. Figure 23 shows the block diagram of the mmW module which can be divided into three sub-modules, namely:

- Transceiver sub-module, which contains transceiver chips, LNA's and PA's
- Beam selection sub-module, which contains T/R selection switch (for TDD switching between TX and RX chain) and antenna selection switching matrix.
- Antenna feed array patches for lens antenna.

As can be observed from Figure 23, the module is divided into two identical Halves. Each Halve is the mirror image of one another and contains one BGT70 chip. Both of the Halves are further divided into two quadrants, so with this arrangement the whole mmW module contains four quadrants in total. Each quadrant has its own PA and LNA chain, which are further connected to the T/R switch that selects the TX and RX mode in TDD switching scheme. Each quadrant has 2x8 antenna matrix, so in total the mmW transceiver module has 64 antenna feeding elements, which can provide 34 degrees of azimuthal scanning range and 8 degrees of elevation scanning range. In single beam mode only one antenna element is active at a time and in the dual beam mode two antenna elements can be active at the same time. Millimeter wave module is connected to a dielectric lens antenna, which concentrates the radiated energy from the patch antenna into a narrow beam in transmitting mode, and vice versa in receiving mode. The lens antenna provides a gain of 27 dBi to 30 dBi depending on beam direction, with a beamwidth of 3 degrees.

BGT70 uses fully differential direct conversion or homodyne architecture for the transceiver. At higher frequencies, unwanted effects like common-mode interference, even-order harmonics and RF grounding issues become very critical. These issues can be diminished by using a fully differential architecture. Bulky and expensive off-chip filtering components are reduced and frequency up/down processes is also simplified by using the direct conversion architecture for the transceiver [31].

This transceiver chip can provide saturated output power up to 14 dBm. The receiver noise figure of the chip is 8 dB and the VCO phase noise is in between -77 to -83 dBc/Hz at 100 kHz offset [31]. The chip can also support the bandwidth of almost 2 GHz at RF which can be used to achieve the data rates up to 10 Gbit/s. More details about the link budget and link performance will be discussed in the further chapters.

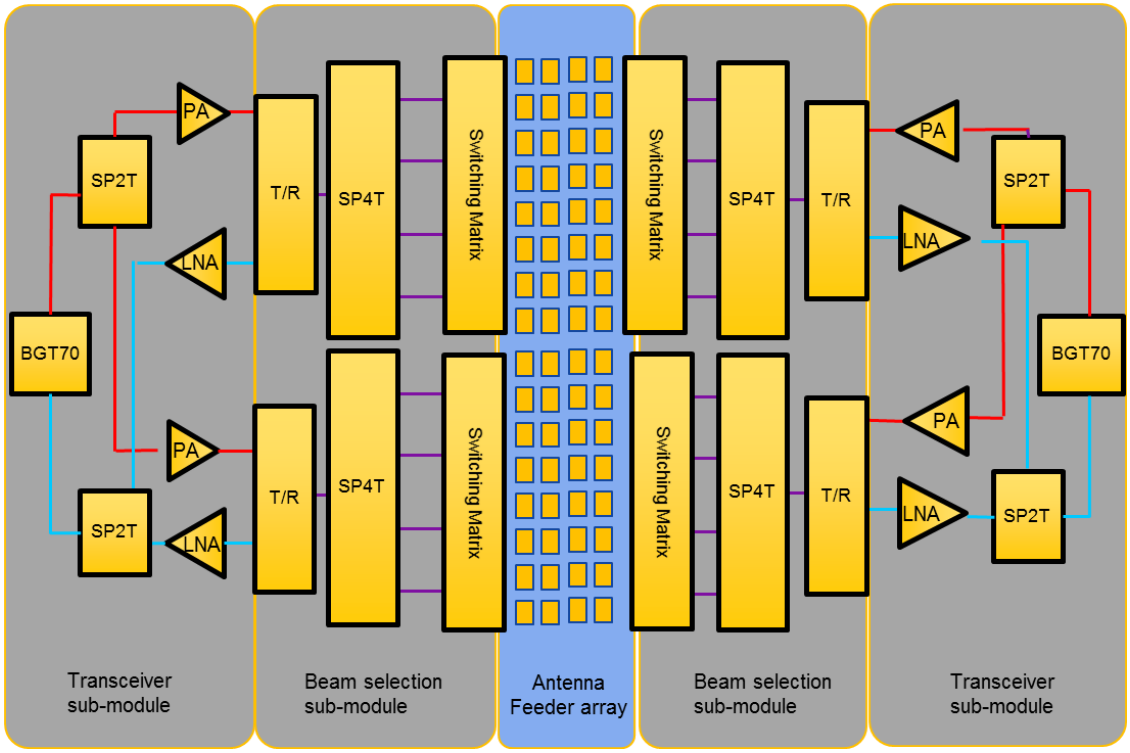

Figure 23. mmW transceiver module block diagram.

4.5 Beam-switching Architecture

The beam switching architecture can be divided into four main layers of switching.

- Baseband switching
- Quadrant selection switching
- TX and RX chain selection switching
- Antenna selection switching

Figure 24 shows the architecture of the mmW beam-switching antennas. The whole module can be divided in two Halves each with one BGT70 transceiver. Both of the BGT70

transceiver are called TRX 1 and TRX2 which are placed in Halve 1 and Halve 2, respectively. Both of the Halves or mmW transceiver module are symmetrical to each other. Each Halve can further be divided in two quadrants. Each Quadrant contains its own PA and LNA, so in total the module has four quadrants. Each Quadrant then contains antenna selection matrix of 2x8 antenna elements. All the RF switches are controlled through the beam control card. The baseband switching has two layers of switching, the TRX selection, which is used to switch between two halves i.e. TRX1 and TRX2 and the other is channel selection switch by which the system operation can change from single beam to dual beam by switching TRX2 to the second baseband channel into the system. In dual beam mode both of the transceivers will be operating. Quadrant selection switch is used to switch between the two Quadrants of each Halve. Both of the Halves have independent control for the quadrant selection. TX/RX selection switch is used to select between TX chain and RX chain in TDD operation. The final level of switching is for the antenna element selection. There are two layers of SP4T switches in each Quadrant, so each Quadrant has total of 16 antenna elements. Both of the Halves have independent controls for the beam selection but the two Quadrants in each halve share the controls for this switching level.

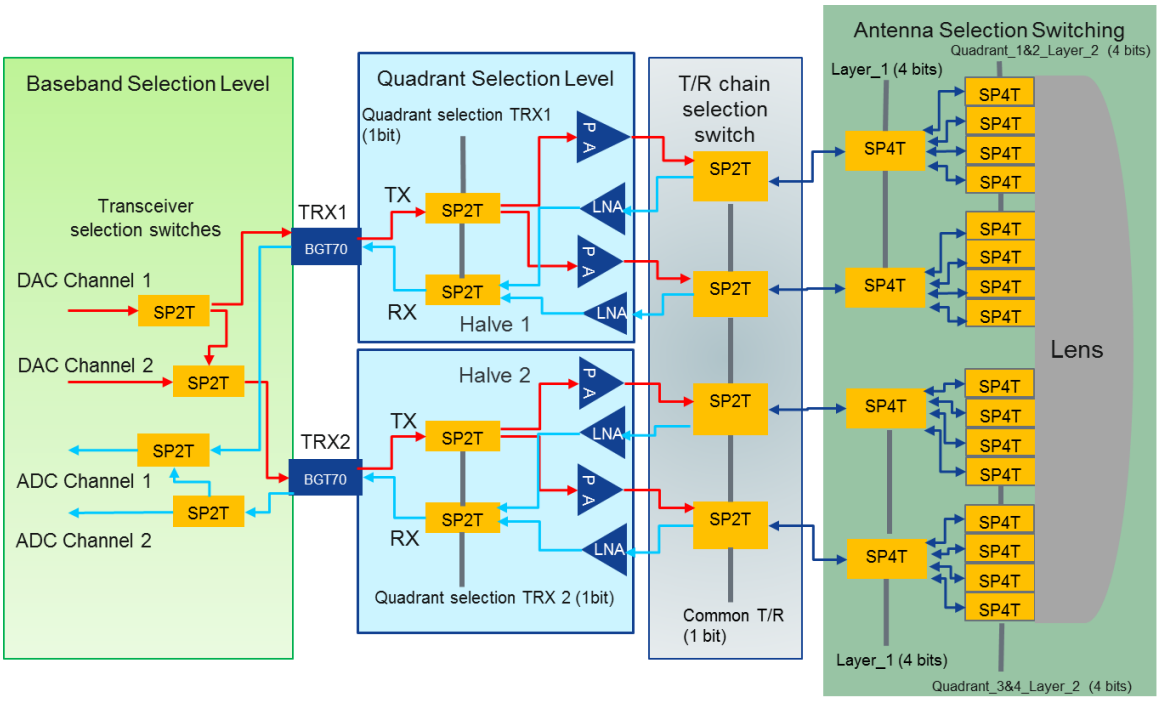

Figure 24. Beam switching architecture.

4.6 Beam-switching Control Card

The beam selection is controlled by beam-steering processor which is located in the soft-core inside FPGA. The vibration compensation and beam alignments are done on basis of RSSI readings, orientation sensor data and information from the modem. Beam switching control card has the responsibility to translate the control signals from FPGA digital

I/O to currents for pin diode control for beam selection switches. Beam switching card also provides TDD switching signal to the TX/RX chain selection switch. Beam switching card also provides controlled gate biasing voltages for PAs and LNAs to be switched on and off during each TX or RX chain. Several other peripherals are also connected with the control card as they provide an interface for the manual settings and beam-steering for the integrated system.

4.7 Data Control Flows and Interfaces

Figures 25 and 26 show the signal flow architecture of the system. The architecture can be divided into two mains parts, digital control signals and I/Q data signals. The digital control signal flows from the modem core to beam-steering control card where pin diode switches are biased to analog bias voltages which is then transferred to mmW module through analog baseband board.

There are two high speed connectors between mmW module and analog baseband board, each with 32 differential pins to transfer both analog and digital data. An analog baseband board acts as a driver for mmW module as it provides all the power supplies, control and analog signal interfaces. The data I/Q signals are also transferred through same high speed connectors between analog baseband board and mmW module. The I/Q signals pass through the amplifiers in RX chain and connected with the AFE card through a high speed ribbon cables. The TX chain, on the other hand, contains only baseband filters and baseband switches.

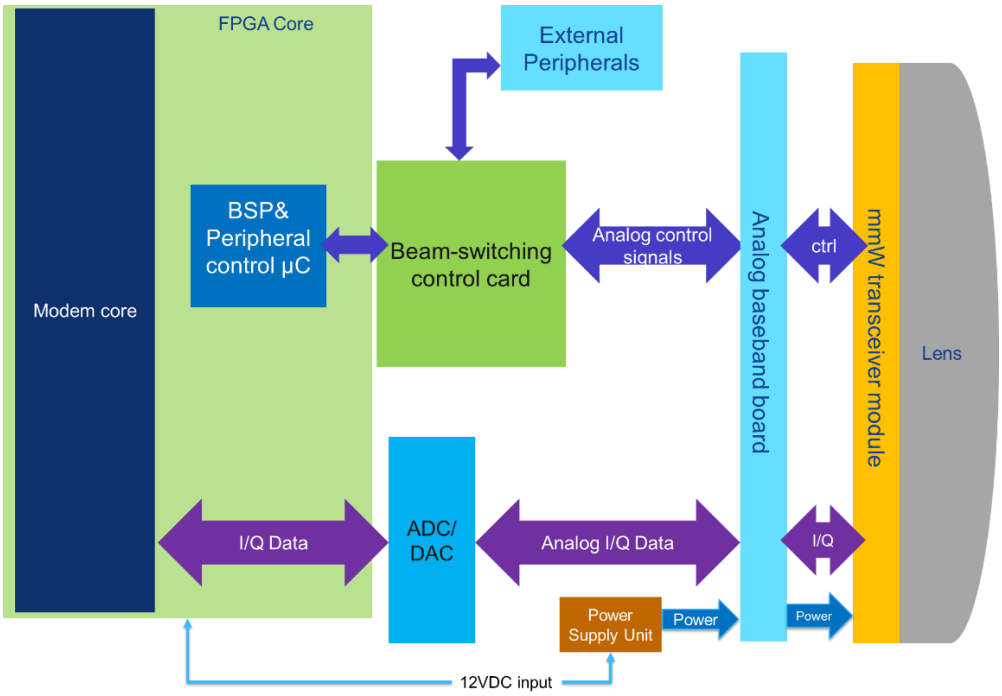

Figure 25. Signal flow Architecture.

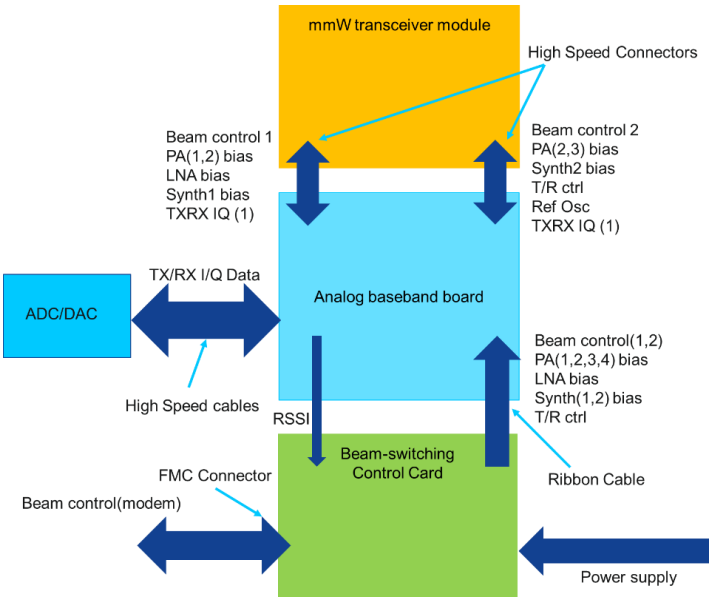

Figure 26. Signal flow interface design.

4.8 Link Budget Analysis

A transmission system's gains and losses are accounted through the link budget analysis. The link budget analysis is a necessary ingredient of any radio communication system development because it enables any pass fail criteria for the system. The link budget is also able to predict the hop lengths if the considerations are taken properly [32].

The Equivalent Isotropic Radiated Power (EIRP) of the transmitter is one of the key parameter for the link budget calculations. The EIRP of the transmitter depends mainly on three factors, transmitter power, line loss and antenna gain. In this kind of integrated PoC system, the saturated power of the power amplifier in the TX line-up determines the transmitter output power as shown in Figure 27. The line losses that appear after the transmitter output stage affect the EIRP of the system. So, an important consideration in this link budget analysis will be that the mmW feeder loss and the lens gain in this system are combined to consider as antenna gain which is 17 dBi on both TX and RX directions. Table 7 below shows the EIRP calculations for the transmitter of this system.

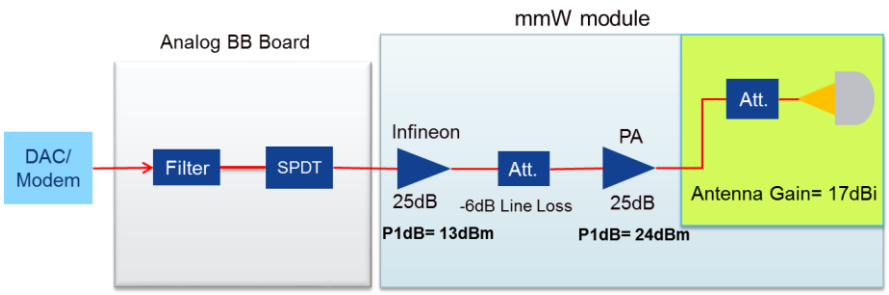

Figure 27. TX line-up analysis.

Table 7. *Transmitter parameters.*

Parameter	**Value**
Frequency, f	73 GHz
Bandwidth, BW	500 MHz
Infineon transceiver 1dB compressed output, P_1	13 dBm
Line loss, L_1	6 dB
Power amplifier gain, G_2	25 dB
Power amplifier 1dB compression point, P_2	24 dBm
Back-off margin from compression point, B	6 dB
TX antenna gain, TG_A	17 dB
$EIRP = P2 - B + TG_A$	35 dBm

Noise Factor is the measure of how much additional noise is contributed to input signal by the components of the receiver, whereas noise figure is the dB scale of the of noise factor. The noise factor of the system can be calculated by the following formula [5].

$$F = F1 + \frac{F2-1}{G1} + \frac{F3-1}{G1*G2} + \frac{F4-1}{G1*G2*G3} + \cdots \frac{Fn-1}{G1*G2*G3 \ldots . Gn}, \quad (2)$$

$$Noise\ Figure, NF = 10 \log_{10}(F) \quad (3)$$

where F denotes noise factor of the system, G_N is the gain of a component, F_n means the noise factor of a component and NF means noise figure of the system. Table 8 shows the calculation of the noise figure for the receiver.

Table 8. *Noise Figure Analysis*

Components	**Gain (dB)**	**Noise Figure (dB)**
LNA	20	3.5
Line Loss	-6	6
Infineon TRX	20	9
Baseband Switch Losses	-3	3
Baseband Amp	10 (typical)	7

The overall noise figure of the system can be calculated through equation (2) and equation (3), by using the system component values given in Table 8. The total noise figure for the system is calculated to be 4.1 dB, which is good enough for the system, considering the noise figure given for the LNA.

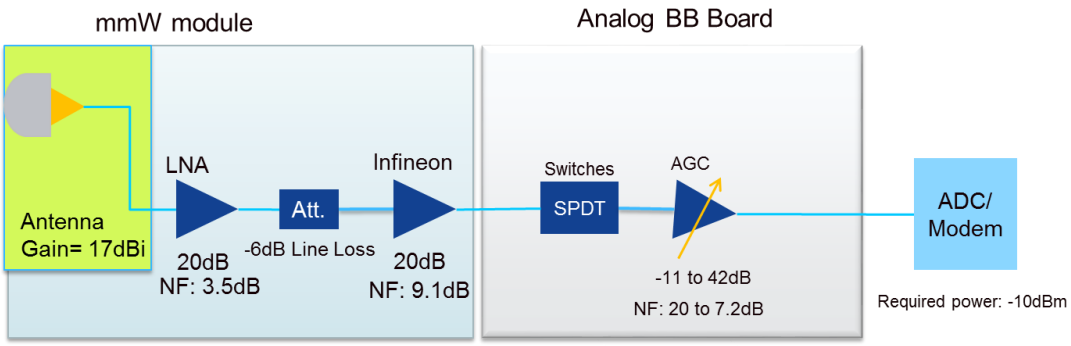

Figure 28. RX line-up analysis.

Table 9. *Receiver Gain and Other Key Parameters.*

Parameter	**Equation**	**Value**
Frequency, f		73 GHz
Bandwidth, BW		500 MHz
Noise Power/Hz, N_P	$k.T.BW$	-174.00 dBm/Hz
RX antenna gain, RG_A		17 dBi
LNA gain, G_L		20 dB
Line loss, L_1		7 dB
Infineon transceiver gain, G_I		20 dB
Infineon noise figure, N_I		9 dB
ABB gain, G_{BB}	-11dB to 42 dB (AGC range more than 50dB)	10 dB
Total RX gain, RXG	$G_A + G_L + L_1 + G_I + G_{BB}$	**60 dB**

Tables 9 and 10 show the receiver gain and sensitivity calculations. The receiver sensitivity determines the capability of the system to detect the signal from a required noise level. The receiver gain is also necessary for determining the system performance because the received signal should be amplified to a certain level so that it can be processed by the ADC block of the modem. The PoC system receiver sensitivity is calculated for a 16-QAM modulation scheme as shown in Table 10. The receiver sensitivity will be used to calculate the system fade margin and hop length.

Table 10. *Receiver Sensitivity.*

Parameters	**Equation**	**Value**
Noise power, N_P	$-174 + 10log\ (BW) + NF.$	-83 dBm
Required SNR @16QAM		15 dB
Receiver sensitivity, *RXS*	$P_N + SNR.$	-68 dBm

Table 11. *Allowable Free Space Loss and Fade Margin data*

Link budget variables	**Value**
Free space loss at 73GHz, P_L	70 dB @ 1m
Free space loss at 73GHz, P_L	110 dB @ 100m
EIRP	35 dBm
RX antenna Gain, RG_A	17 dBi
RX sensitivity, *RXS*	-68 dBm
Other losses, *Po*	10 dB

The allowable free space loss and fade margin of the system can be calculated through the following formulas [5] [32].

$$AFSL = EIRP + RG_A - RXS, \quad (4)$$

$$FM = SG - P_L - P_O, \quad (5)$$

where *AFSL* is the total allowable free space loss for the system, *EIRP* means the equivalent isotropic radiated power of transmitter, RG_A denotes the receiver antenna gain, *RXS* means the receiver sensitivity, P_L is the path loss and *Po* denotes the other losses in the system. We can calculate the maximum allowable free space loss for the system from equation (4) to be 120 dB. With equation (5) the system fade margin at different hop lengths can be calculated. The system requirement for the minimum fade margin is nearly 10 dB, so the system should not exceed the hop length of 50 meter. Other losses in the calculation include the rain losses and some multipath fading losses. Because, the link hop is short and therefore atmospheric losses and rain losses will not be higher than few dBs even in heavy rain, but it is still safe to add 10 dB to the fade margin considering other losses. The targeted hop length for the actual product phase is set to be longer than this prototype design. The hop length can be increased by reducing the losses in the feeder networks and by increasing the lens antenna gain.

5. ANALOG BASEBAND BOARD DESIGN

In this chapter, the analog baseband board (ABB) design simulation details will be presented. This hardware design is one of the author's major contribution to the thesis work. This chapter is structured such that first the specification details for the analog baseband module will be presented, then the design details for the board such as PCB layer stack up and several construction blocks will be discussed. In addition, the simulations and hardware prototyping for analog baseband board and the interface connectors used, will be presented in this chapter.

The analog baseband board is designed to work as a driver board for the mmW module. The mmW module is designed to contain mostly higher frequency components. The other supporting components like microprocessor, reference oscillator and the baseband switching unit were placed on a separate board to keep the mmW module design simple and easier to troubleshoot. Analog baseband board provides an interim interface between the modem unit and the mmW transceiver.

Figure 29 shows a general block diagram of the analog baseband board including major components in the module. ABB module can be divided into four blocks for better describing the functionalities of the module. These functional blocks will be discussed in detail later in this chapter:

- Analog baseband TX chain block
- Analog baseband RX chain block
- Microprocessor and A/D converter block
- Reference oscillator block

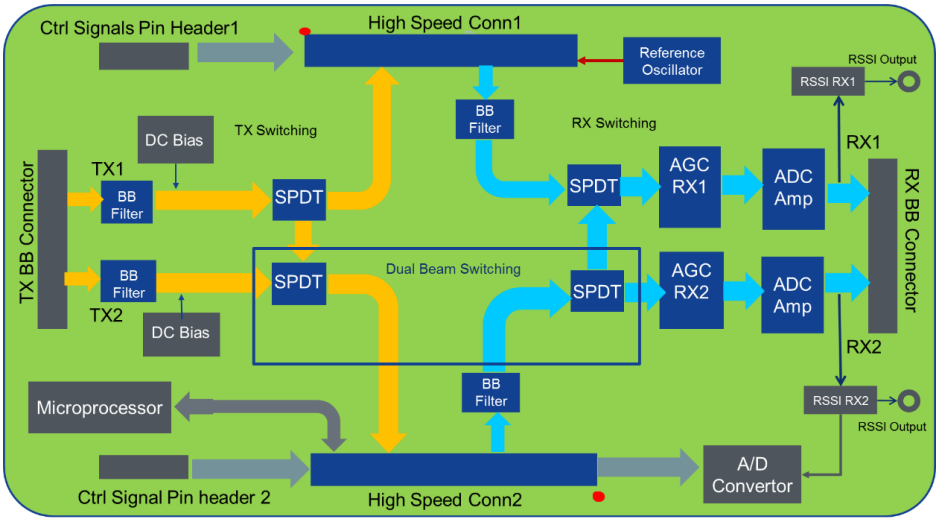

Figure 29. Analog baseband board block diagram.

5.1 Analog Baseband Board Specifications

The ABB is designed to provide support for different baseband modems with different bandwidths. The current modem can only support 500 MHz of bandwidth so for this system the baseband board should have low pass cut-off filters for 250 MHz on baseband. The current modem design can compensate the I/Q phase error up to 10 degrees and amplitude imbalance of up to 3dB.

The modem can also support up to 6-7 dB of frequency response ripples in the baseband signal. The baseband board however can support bandwidth up to 2 GHz at RF. In the baseband frequencies it should be able to support above 800 MHz of bandwidth. A set of specifications were designed for analog baseband board which are described in Table 12 to Table 16 in the following:

Table 12. *General Specifications.*

Parameter	**Value**
System bandwidth	2 GHz
TRX switching	From ADC channel 1 to TRX1 or TRX2
Dual beam operation	Support for two active ADC channels at same time
Baseband switching time	<500 ns

Table 13. *Transmitter Chain Specifications.*

Parameter	**Value**
Baseband output and input interfaces	Differential I/Q with 100Ω impedance
Baseband 3dB low pass cut-off frequency	> 800 MHz
Baseband 3dB high pass cut-off frequency	DC coupled
TX baseband gain	Not required
TX power P1dB	> 0 dBm

Table 14. *Receiver Chain Specifications.*

Parameter	**Value**
Baseband output and input interfaces	Differential I/Q with 100Ω impedance
Baseband 3dB low pass cut-off frequency	> 800 MHz
Baseband 3dB high pass cut-off frequency	DC coupled
RX baseband gain	> 40 dB
AGC dynamic requirement	> 45 dB of dynamic range
RX power output P1dB	> 10 dBm

Table 15. *Reference Oscillator Block Specifications.*

Parameter	**Value**
Phase noise	<-144 dBc/Hz @ 100 kHz
Frequency	100 MHz

Table 16. *Power Consumption Specifications.*

Power supply	**Voltage [V]**	**Current per unit [mA]**	**Units in one module**	**Total Current [mA]**	**Total power [mW]**
RX AGC	5	100	4	400	2000
RX Gain Block	5	170	2	340	1700
SPDT Switches	3.3	0.02	8	0.16	0.533
RSSI Detector	5	70	2	140	700
u-Processor	3.3	300	1	300	1000
A/D convertor	3.3	130	1	130	450
Ref Oscillator	3.3	12	1	12	39.6
Reference divider	5	194	1	194	970
Reference Splitter	3.3	35	1	35	116
Peak Power					**7000 mW**

5.2 Design and Implementation

One of the major task in this master's thesis project was the hardware design and testing of Analog Baseband board. The board was designed on PADS software which is used in many professional PCB design tasks and projects. The board stack-up consisted of 8 layers in total. The outer-most two layers i.e. top and bottom were Rogers RO4350 dielectric because of the impedance controlled RF traces on these layers and the internal layers were FR4. This mixed layer stack-up with FR4, allows a cheaper manufacturing of the board. The inner layers mostly included digital control signals and power signals which were

not needed to be impedance controlled lines. To guarantee the simplest routing topology and to minimise net lengths, component placements were designed and optimized carefully, and were eventually located on the bottom side because the board is assembled so that only bottom side is accessible for testing equipment connections.

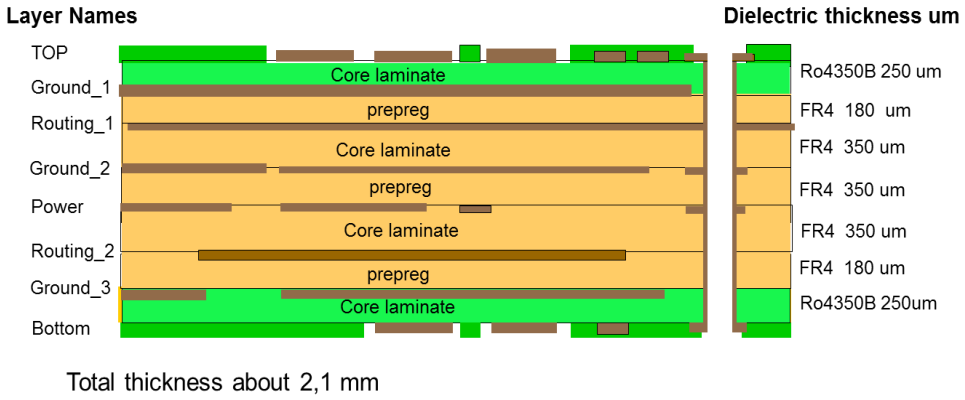

Figure 30. Analog baseband board stack-up.

Most of the IC's were placed on the top side of the PCB, while connectors, headers and test points Decoupling capacitors were placed as close as possible to IC's to reduce power supply transients. Efforts were made to isolate high speed signals from lower speed signals to reduce cross-talk. In addition, analogue signals were isolated from digital signals wherever possible. The ground planes were also separated into three groups i.e. RF ground plane, digital ground plane and reference oscillator ground plane. All the grounds were connected with each other on just one point through an inductor to isolate the coupling of digital signals into RF signal ground planes. Figures 31 and 32 show the complete analog baseband board with all the components on both top and bottom side assembled. The figures are marked with identifying each area separately.

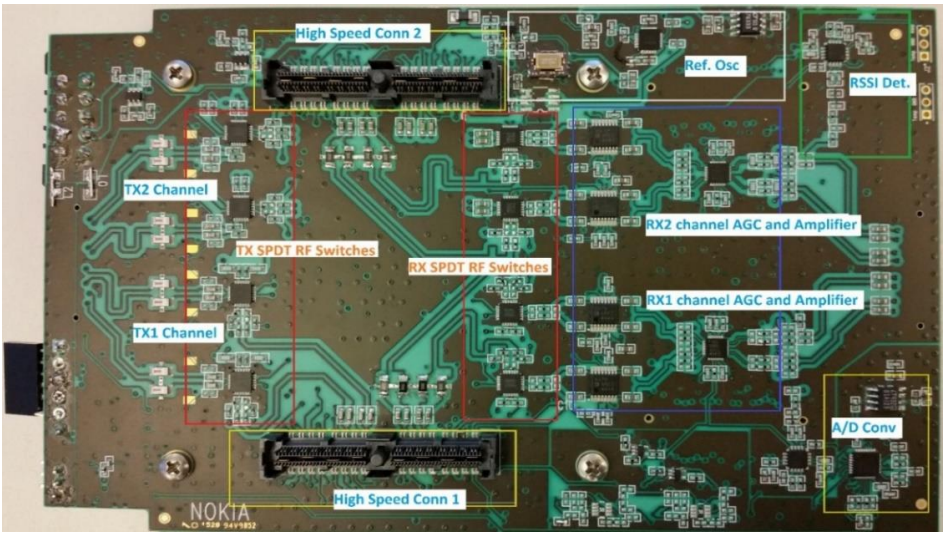

Figure 31. Assembled ABB top/inner side.

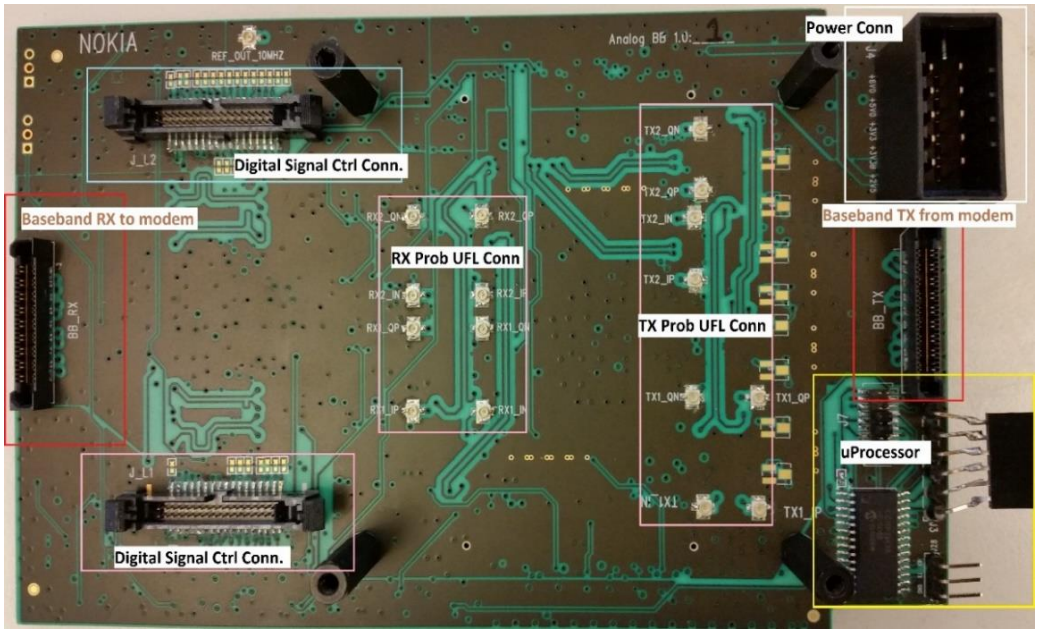

Figure 32. Assembled ABB bottom/outer Side.

5.2.1 Analog baseband TX chain block

The TX chain supports two baseband channels, both having fully differential I/Q interfaces. The TX chain in analog baseband board includes baseband filters, TRX switching network and DC biasing circuit for LO leakage cancelation at TRX output. Figure 33 depicts complete block diagram of the TX chain where all of the components of TX chains are presented.

The baseband filters are added as the first stage in the chain and can be variably selected based on the requirements of the bandwidth. The DC biasing circuit is capable of adding a DC offset to an RF signal, which can be used for LO rejection techniques. The DC bias circuit is implemented in ABB as a backup circuit for LO cancelation. If the internal calibration routine of the Infineon transceiver is not sufficient then the LO cancelation can be performed manually through adding DC voltage to the baseband I&Q channels. The test points are added to the circuit as UFL RF connectors to get a direct connection with the transceiver chips bypassing the baseband switching and filter circuits for testing purposes. The test points are not always connected and can only be switched by moving jumper resistors on the baseband board. The switching circuit includes two stages of switching. The first switch is single pole dual throw (SPDT) switch which takes in channel 1 and switch it between TRX1 and TRX2 while the second switch decides that either the TRX 2 should be operated through channel 1 in case of single beam mode or through channel 2 for dual beam mode. This switch is dual pole and single throw (DPST) and is reverse of the previous switching stage.

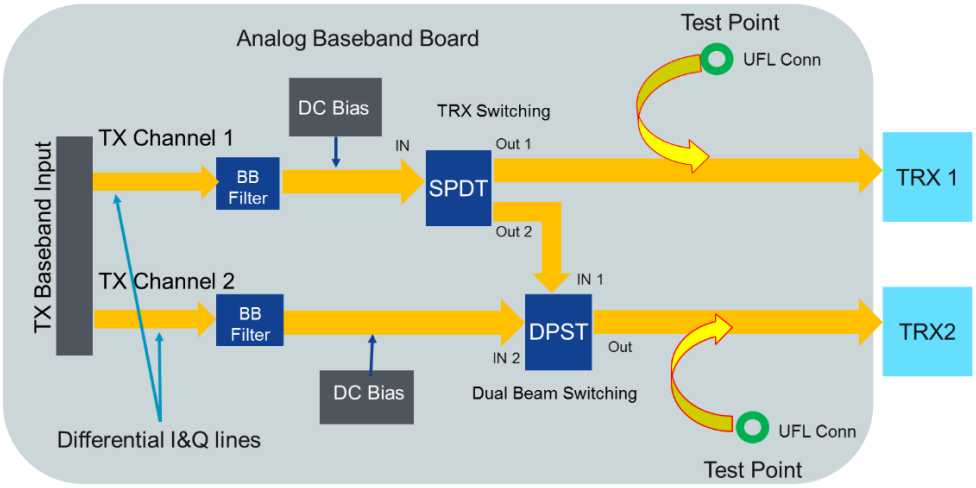

Figure 33. ABB TX block diagram.

5.2.2 Analog baseband RX chain block

The RX chain also supports two baseband channels which have fully differential I/Q interfaces. The RX chain in analog baseband board includes baseband filters, TRX switching network, automated gain control stage, ADC amplifier stage and RSSI detectors. Figure 34 includes complete block diagram of the RX chain where all of the components of RX chains are presented.

The UFL connectors are placed as a test point to get direct connectivity with the transceivers for testing purposes. The passive baseband filters can be selected according to the bandwidth requirements. The SPDT and DPST switches perform the switching between the transceiver and baseband channels similarly as the TX chain baseband switches. Attenuation pads are added before and after AGC and ADC amplifiers to have a controlled gain and use the AGC more efficiently in case of excessive gain. The AGC is capable of providing the variable gain range from -22 dB to 34 dB, which is 52 dB of dynamic range. The ADC amplifier is added in the circuit to provide extra gain in case of different baseband ADC requirements and it can be bypassed with alternate RF lines that do not involve the ADC amplifier stage.

The RSSI detectors are also added at the end of the chain to determine the received signal level. The RSSI detector is connected to the A/D converter and microprocessor on ABB and also the A/D connector for RSSI is connected with the softcore of FPGA where beamsteering protocol is located to identify beam with the best RSSI value. RSSI chip also includes integrated temperature sensor, which can identify the temperature rating of ABB. The temperature reading is also connected with on-board microprocessor.

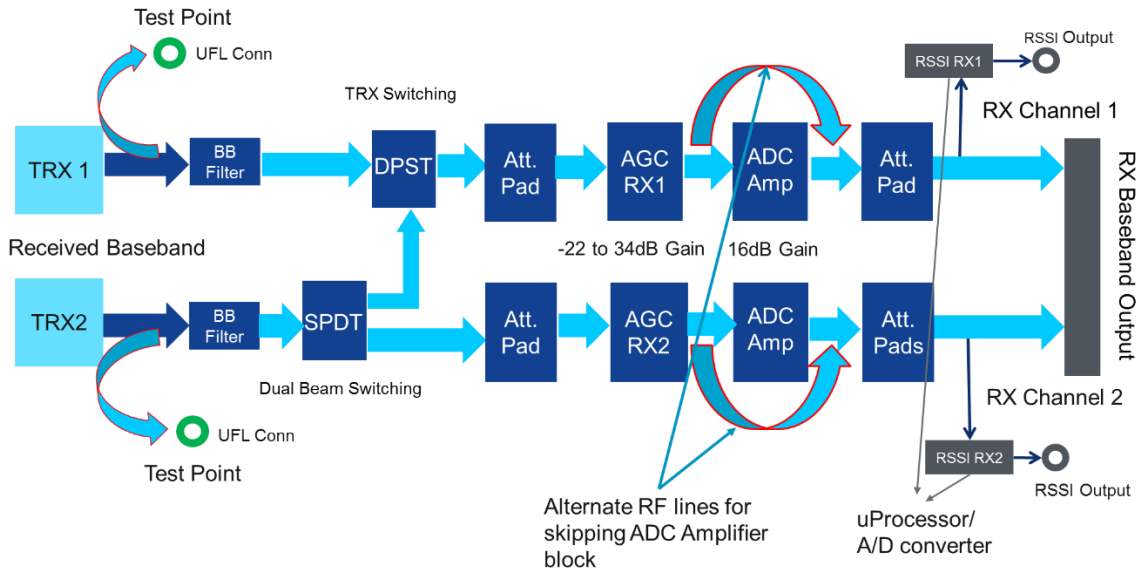

Figure 34. ABB RX block diagram.

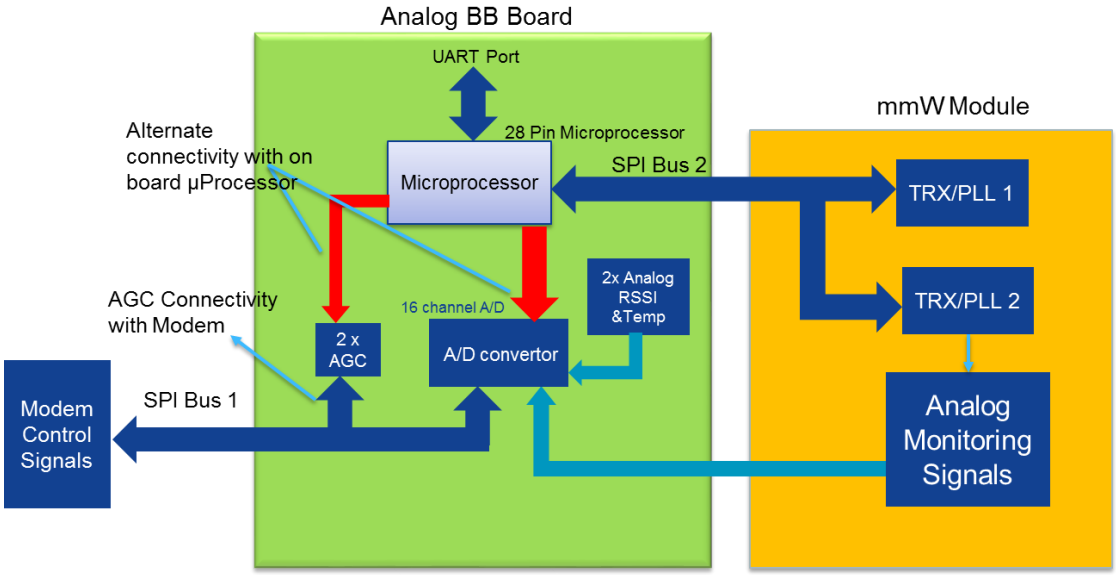

Figure 35. Microprocessor and A/D converter block diagram.

5.2.3 Microprocessor and A/D converter block

A 16-bit microprocessor is placed on ABB to control and program the Infineon transceiver chips and perform the LO cancellation routine in these transceiver chips. Figure 35 shows the connectivity of the microcontroller and A/D converter chip.

A separate A/D converter chip was added to the system to convert all analog RF power monitoring signals to digital domain and connected to the microcontroller on ABB or alternatively to softcore microprocessor of FPGA where these signals are needed for the RX gain control through AGC. The RX AGC block on ABB can also be controlled either

through on-board microprocessor or the control can directly come from the FPGA core. There is no direct connection between the microprocessor and FPGA core.

5.2.4 Reference Oscillator block

The reference oscillator block is added to ABB to provide clocking to Phase Locked Loop (PLL). A 100 MHz crystal oscillator is used to provide clock signal to the transceiver PLL on mmW module. The oscillator is Voltage-Controlled Temperature-Compensated Crystal Oscillator (VCTCXO). The frequency can be fine-tuned few Part-per Millions (PPM). The frequency control signal is varying voltage either through variable resistor or through a single channel DAC chip so that frequency can be tuned through microprocessor digitally. A buffer stage is added after the oscillator to provide enough power to fulfil the PLL power requirements. A separate 10MHz output is also created by adding a frequency divider after the buffer stage which can be used for synchronizing of the nodes and some other possibilities.

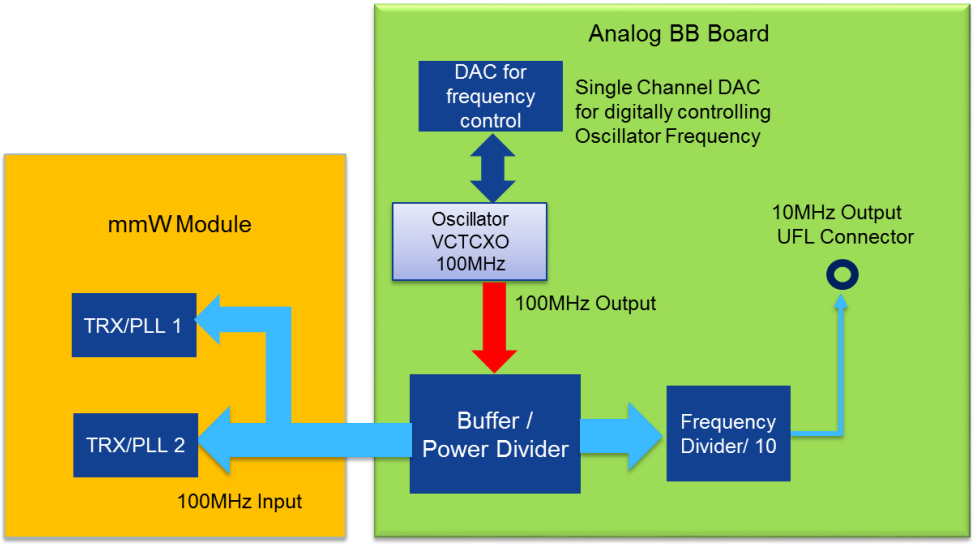

Figure 36. Reference oscillator block diagram.

The specification for the reference oscillator can be calculated as below [38]:

$$N_{add} = 20 * log(\frac{73\ Ghz}{100MHz}) \quad , \tag{6}$$

$$PN - N_{add} >> \mathcal{L}_f , \tag{7}$$

where PN denotes the phase noise of transceiver, N_{add} means the phase noise degradation due to multiplication and $\mathcal{L}_f$ is the reference oscillator phase noise. The reference oscillator should not affect the phase noise of the transceiver after the multiplication so the phase noise of the reference oscillator should be considerably better than the phase noise of TRX VCO plus the phase noise degradation. The phase noise degradation calculated by equation (6) is 57.22 dB. Whereas, the maximum phase noise of the transceiver is given

to be -77dBc/Hz. Now from equation (7) the specification for the reference oscillator phase noise can be calculated. The reference oscillator should have significantly better phase noise than -134.2 dBc/Hz. If a 10 dB headroom is required, then the oscillator phase noise should be -144 dBc/Hz at 100 KHz offset. Phase noise better than this is required for the reference oscillator so that it will not increase the phase noise of the transceiver VCO.

5.3 Simulations and Prototyping

After finalising the specifications and understanding the nature of different working blocks of ABB board, the next step was to evaluate and simulate several components that will be used in the board design. One of the major challenges in this process was the RX chain design, because most of the working modules were placed in this chain. So the hardware prototyping was mainly focusing on the design and layout challenges of RX block in ABB module.

Attenuator stage was placed at the end of RX chain to control the maximum output power from the analog baseband board. The resistive values for unbalanced pi attenuator are first calculated, but this time the values of series resistor R2 is divided by 2 placing half in each line as shown in Figure 37. The value calculated for two parallel shunt resistors remains the same [33].

The RSSI detector that is used in the baseband board has a single ended input. The RSSI detector will be connected to the system through an unequal resistive power divider. So from both differential I and Q channels of RX chain only one line from them will be probed for RSSI detector input. For these calculations balanced attenuator is simulated in ADS software with the addition of single ended RSSI detector with the differential lines. In this case the balanced attenuator will not be completely balanced because of extra loss in one of the differential lines because of resistive divider. Figure 38 shows the schematics from ADS for differential attenuator and unequal resistive power divider. It can be seen that R1 and R6 are not equal, which is because the overall loss of both differential line should be kept same. So the overall loss for both of the differential lines will remain the same.

Marker ‘Output’ in Figure 39 shows the insertion loss from the differential input to the differential output which is 3.35 dB, which is close to the desired attenuation. Marker ‘RSSI’ shows the power delivery to the RSSI detector which has -22.4 dB of insertion loss. This insertion loss toward RSSI detector will be taken into account when calculating the actual power level from the detector value. The resistor values used in the simulations usually do not match the exact values found in any standard series (E12, E24, E96 etc.). Closest match to simulated values are used in the real system. Because of this reason the resistors from E24 and E96 series were used which provided the nearest possible values for the resistors.

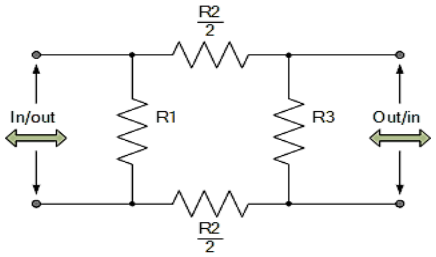

Figure 37. Balanced pi-attenuator [33].

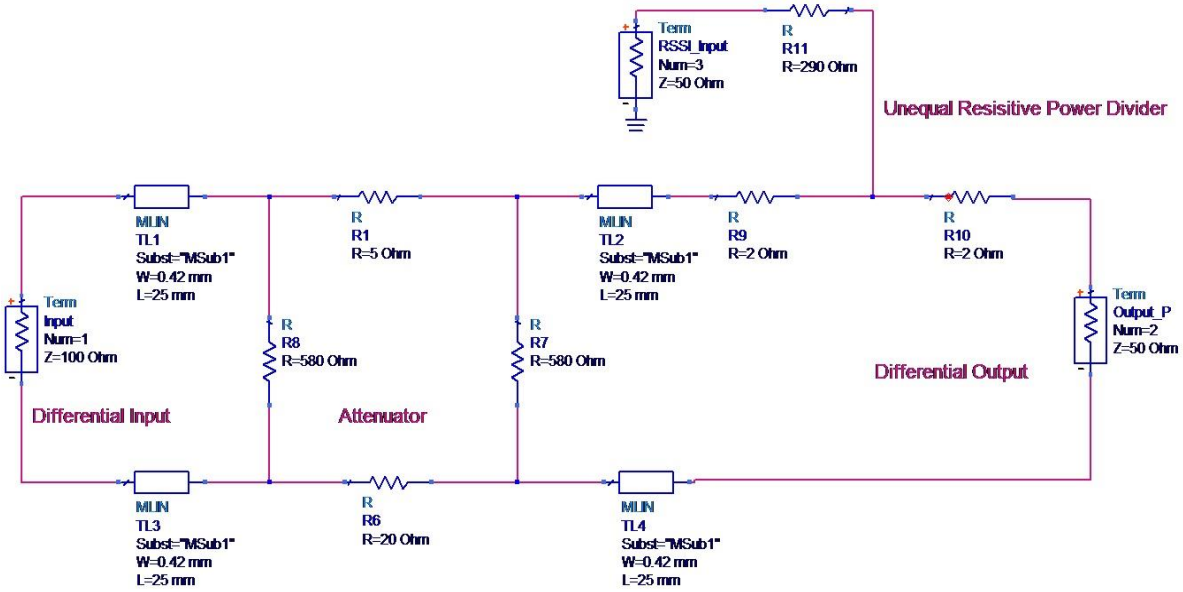

Figure 38. Schematics of attenuator and resistive power divider.

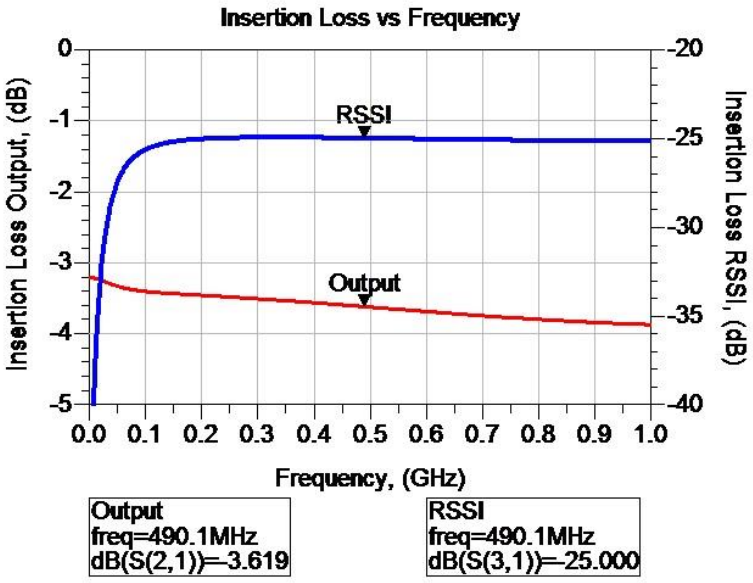

Figure 39. Insertion loss for output and RSSI detector input.

Differential Impedance Calculation:

Both TX and RX chains have to support fully differential I and Q inputs and outputs. Each differential pair impedances and lengths need to be maintained along entire signal path. It is important to have same kind of losses and nearly same lengths along the entire signal path because of phase or amplitude differences between I and Q signals can cause poor performance of the system. The differential impedances can be calculated though following equation [39].

$$Z_d = \frac{174}{\sqrt{\varepsilon_r + 1.41}} \ln\left(\frac{5.98h}{(0.8w+t)}\right)\left(1 - 0.48\exp\left(-0.96\frac{d}{h}\right)\right), \quad (8)$$

where Z_d is the differential impedance, d is the trace separation, w is the trace width, t denotes the trace thickness, h means the dielectric thickness and ε_r means the relative dielectric constant. This equation is used to calculate the differential impedance of a co-planar micro-strip, which is the structure adopted for all the differential signals in this project. The main advantage of differential signalling schemes is their common-mode noise rejection. In order to maximise this property, the lines were kept to equal length and impedance values. First the single ended micro-strip trace width can be found by the following formula [39].

$$w = \frac{7.48h}{e^{\left[Z0\sqrt{\frac{\varepsilon r+1.41}{87}}\right]}} - 1.25t, \quad (9)$$

From equation (9) w is calculated to be 0.42 mm which is the trace width of single ended micro-strip trace. Next, the values can be inserted to the differential impedance equation to find the differential trace separation for 100Ω differential impedance. Through the calculations the trace separation of the differential pair is 0.4 mm. With this amount of separations between the traces they will have near to 100Ω differential impedance.

Hardware Prototype:

Before making a final version of the analog baseband board first an evaluation board of integrated RX amplifiers chain was made in the lab using Printed Circuit Board (PCB) milling machine LPKF ProtoMat S63. One additional reason for this stage of prototype design was to get familiar with the PADS software and run through the process of PCB design. Figure 40 shows the block diagram of prototype hardware design and test environment.

The hardware was tested using Agilent 4-port Vector Network Analyser (VNA) which was needed because of differential input and output. The testing results from the prototype design are presented in Figure 41. The test results are plotted in Agilent ADS software. The markers ‘m1’ and ‘m2’ on the plot shows the maximum gain value and 3 dB

bandwidth, respectively. The maximum gain achieved in this prototype phase was 46.2 dB and the 3 dB bandwidth of the amplifier was measured to be 920 MHz.

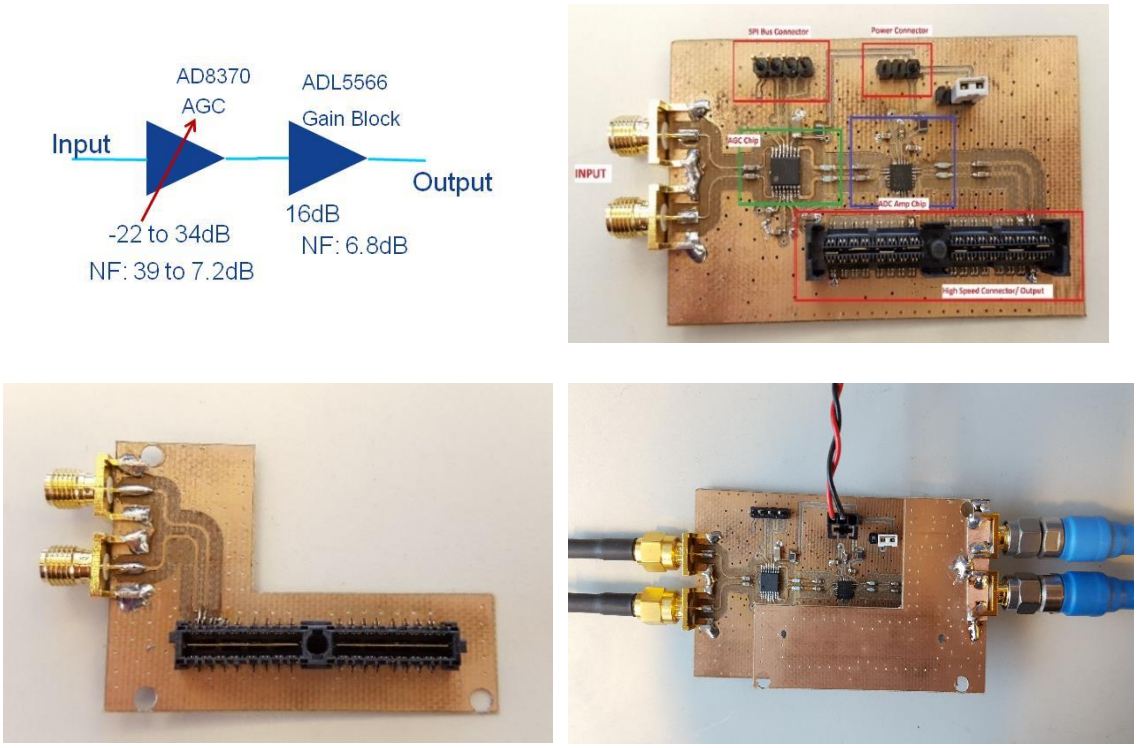

Figure 40. RX chain amplifier chain evaluation board.

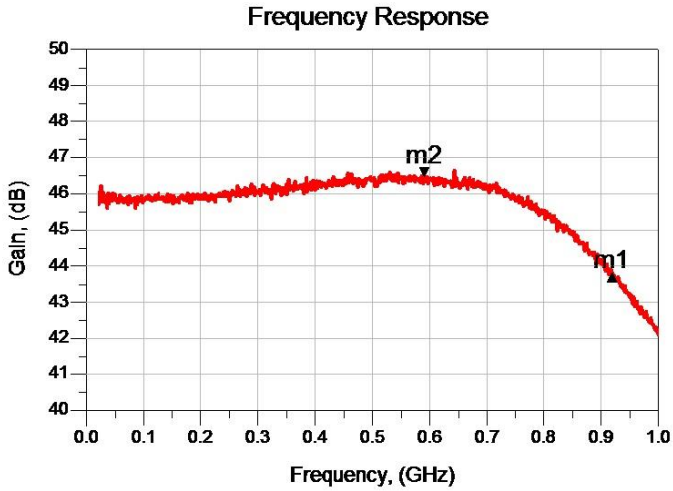

Figure 41. Frequency response of evaluation board.

5.4 Interface Connectors

Connection between Baseband Board and Feeder:

All analog, control, and power supply signals between baseband board and feeder were routed through 32 differential pin high speed connector made by Samtec. These connectors were chosen because the pitch of the connector was very narrow as compared to the

number of pins of these connectors. The connectors come in pair and they are non-symmetrical so the connectors of one gender were placed on analog baseband board and the connectors on the other gender were placed on mmW n module. Figure 42 shows the connectors places on ABB and mmW module.

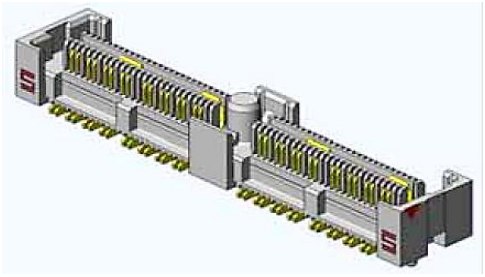

Samtec QFS-032 connector on ABB

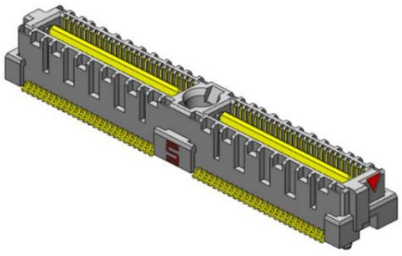

Samtec QMS-032 connector on mmW module

Figure 42. High speed connectors for ABB and mmW module connectivity.

Connection between Baseband Board and Modem AFE:

The analog baseband signals between baseband board and modem AFE are routed through two Samtec *QRF8* connectors which pair with Samtec *EQRP* high speed cable. Each connector and cable carries TX and RX channels separately to modem AFE. This high speed cable was soft in terms of material that allows freedom to bend them at any angle and they can carry up to 9 GHz of frequency and data rate up to 18 Gbit/s [34]. Figure 43 shows the Samtec high speed connector and cable connecting between ABB and modem AFE.

Samtec QRF8 connector on ABB

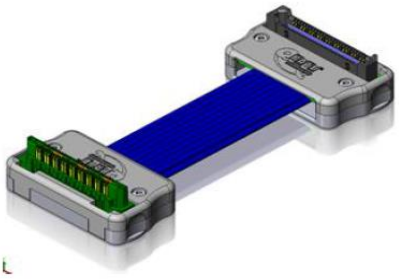

Samtec EQRP high speed cable

Figure 43. High speed connectors for ABB and AFE connectivity [34].

Connection between Baseband Board and Beam switching Control Card:

The control signals from beam switching control cards are carried to ABB through flat ribbon cables which are connected to pin headers on ABB and beam switching control card. Each connector has 2x17 pin and there are two connectors connecting ABB and control card. This connector has a mechanism to prevent connection wrong way around, which could cause damage to the circuits in mmW module. Figure 44 shows the connector and flat ribbon cable.

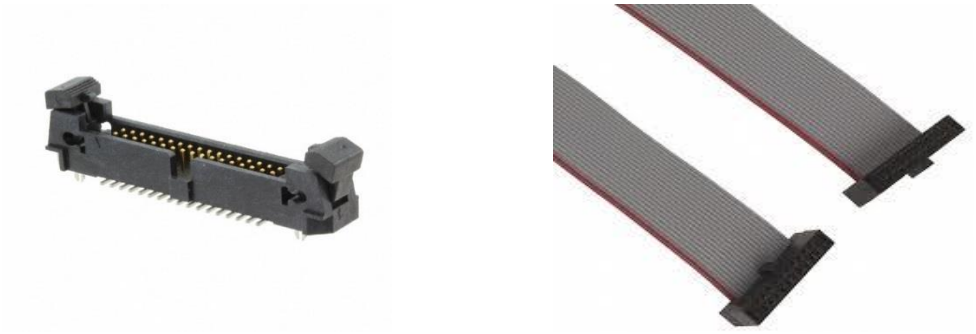

Pin header on ABB *Ribbon cable between ABB and control card*

Figure 44. Connectors between ABB and control card [34].

6. RESULTS AND DISCUSSION

This chapter includes the testing and measurements of the analog baseband board and also system integration testing results. The measurements done for the baseband board includes the frequency response, compression point and phase response of both TX and RX chains. The testing results from the complete system integration includes the phase noise testing, frequency response of the system and the modem and data throughput of the system.

6.1 Measurement Equipment and Test setup

The hardware designed in the project that is analog baseband board was also tested to check the performance of the board according to the requirements that were set before manufacturing. The input and output interfaces of the analog baseband board are differential high speed connectors as shown in Figure 46. For testing purposes, interface boards were designed to route the connections from the high speed connectors to SMA or UFL connectors. Figures 45 and 47 show the interface board connectivity and the test setup. The testing has been conducted mostly using Agilent 4-port Vector Network Analyser (VNA). Because of the differential inputs and outputs of the ABB the VNA was used in balanced signal mode, where port 1 and port 2 were used as balanced input and port 3 and 4 were used as balanced output ports.

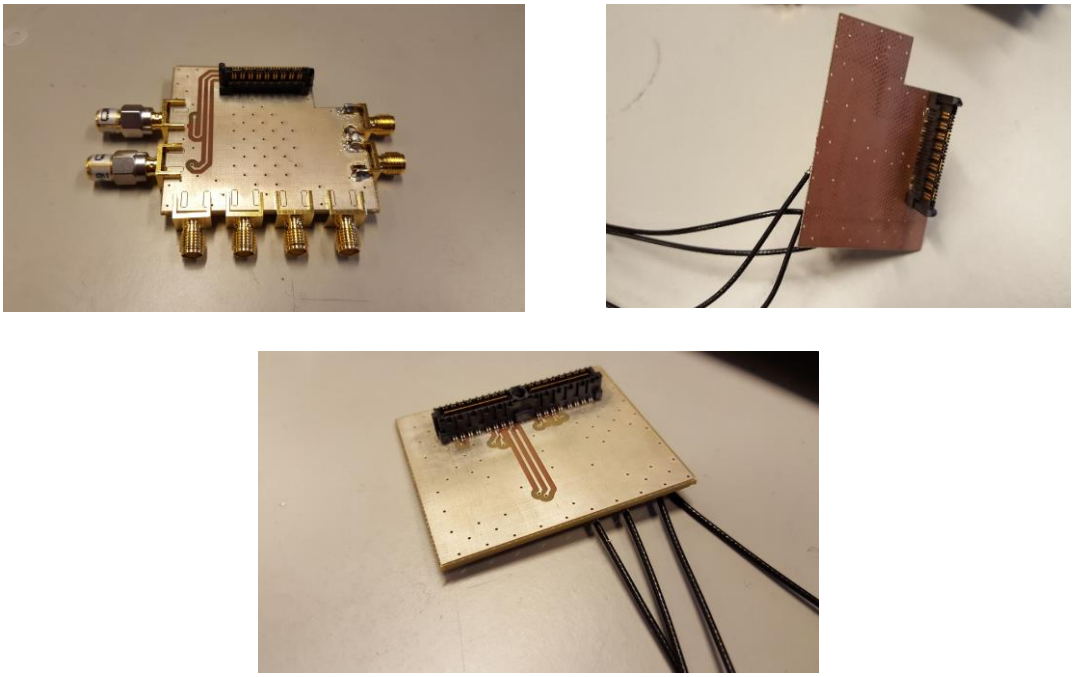

Figure 45. Interface boards for ABB testing.

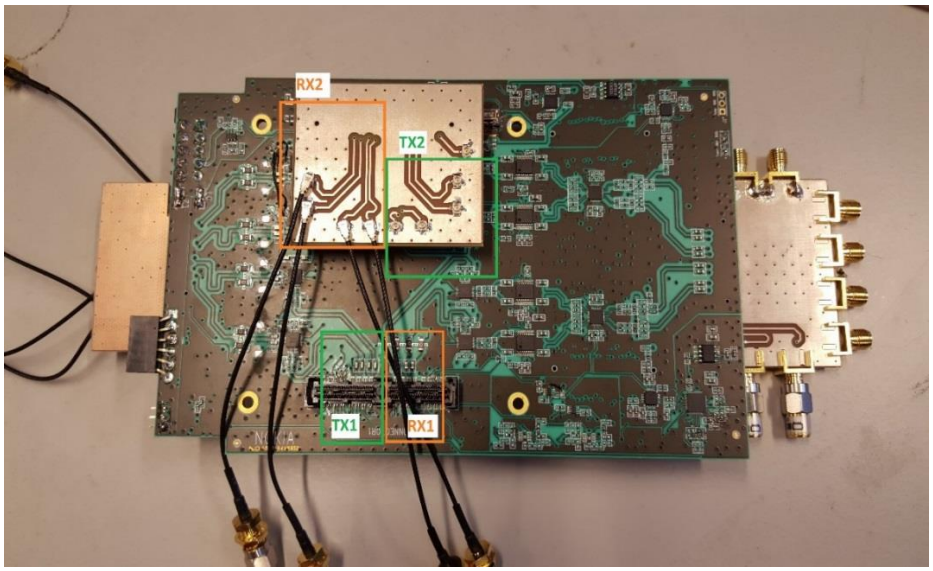

Figure 46. ABB with interface boards attached mmW module side.

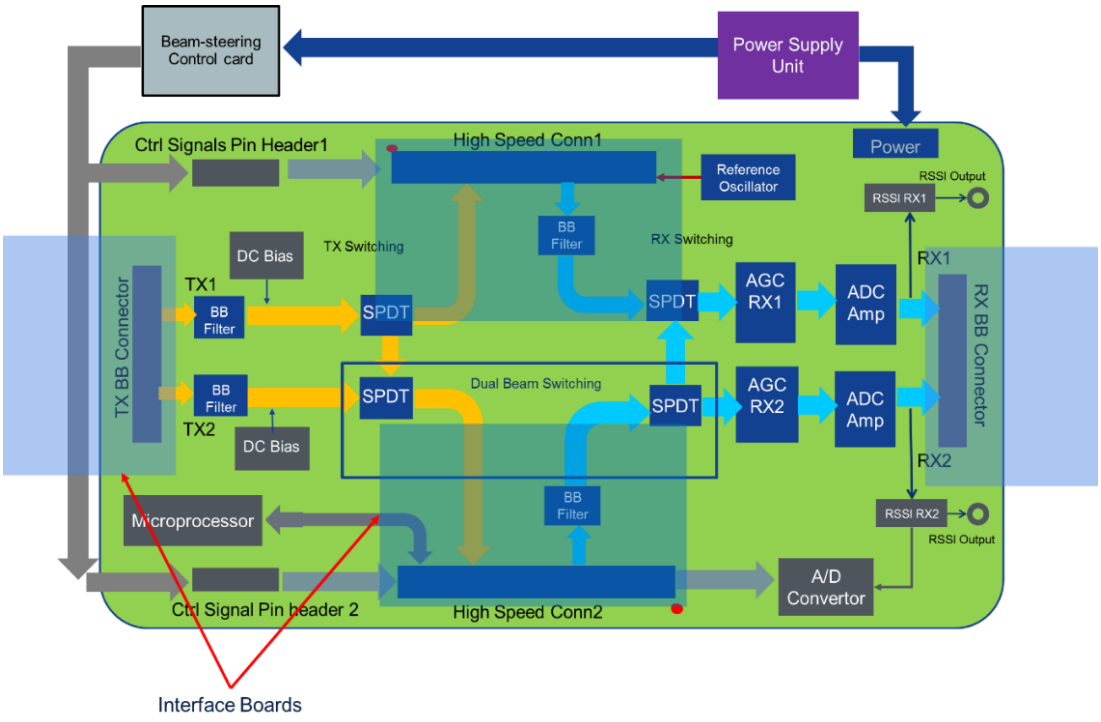

Figure 47. ABB with testing setup block diagram.

6.2 RX Channel Testing

The RX side of ABB has two separate channels to be tested for their frequency response and phase difference in I and Q channels separately. For testing purposes, in place of mmW module, interface boards are placed on the high speed connectors to provide proper interface for test equipment to be connected. One interface board is connected to the mmW high speed connector to give the input to the RX chain and the output high speed connector is attached to another interface board to receive the signal from the RX chains.

6.2.1 RX Channel 1 Response

In this testing scenario the interface board is connected to high speed connector which simulates the connection from Infineon TRX1 and the output is taken from baseband RX channel 1. This configuration can be seen in Figure 48 which shows the complete test setup.

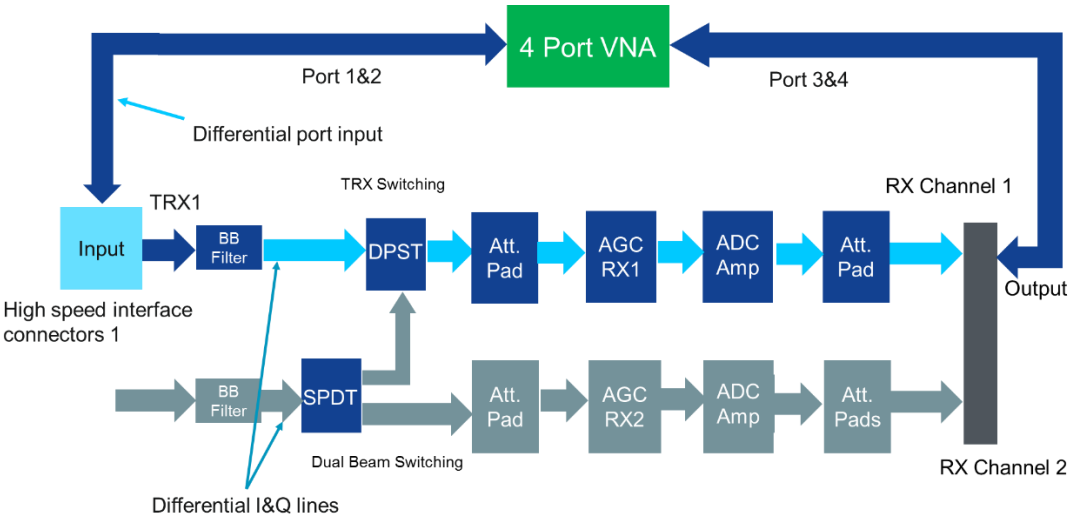

Figure 48. Test setup for RX channel 1 from TRX1.

Figure 49 shows the frequency responses of both I and Q channels of RX1. The frequency response is measured from 10 MHz to 1 GHz and it can be seen, that the 3 dB point for the RX1 channel is above 800 MHz, which satisfies the specifications. The amplitude difference between I and Q channels is also measured to be less than 0.5 dB. Maximum gain of RX 1 chain is measured to be 45 dB which is also within specifications.

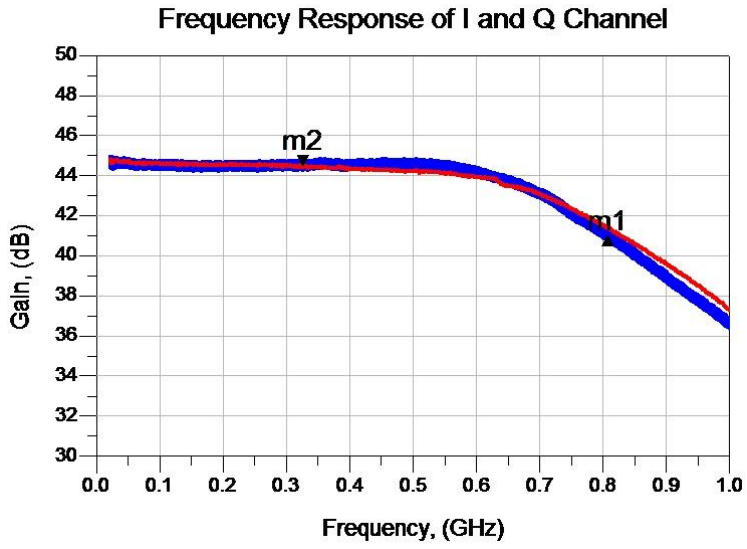

Figure 49. RX1 I and Q channel frequency responses.

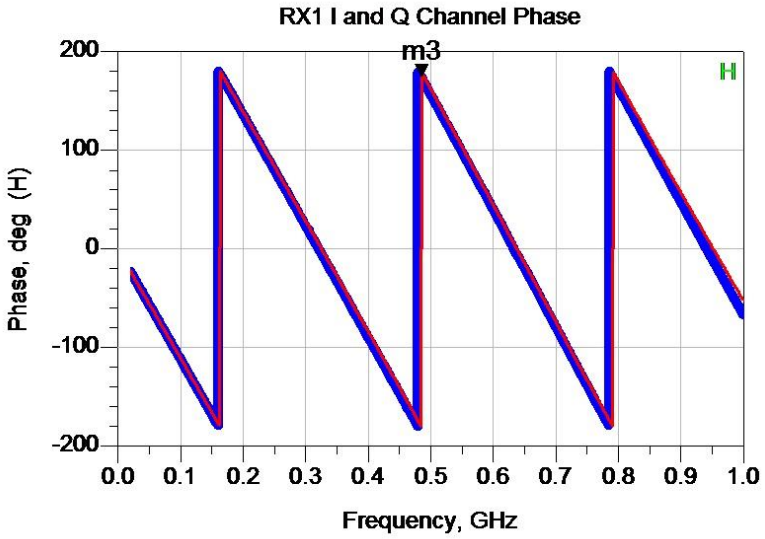

Figure 50. RX1 I and Q channel phase responses.

Figure 50 shows the phase responses of both I and Q channels. This measurement is important for the fact that I and Q channels should not have different phase delays between each other. Phase imbalance can create problems with signal detection in the modem.

6.2.2 RX Channel 2 Response

In this testing scenario the interface board is connected to high speed connector which simulates the connection from Infineon TRX2 and the output is taken from baseband RX channel 2. This testing is important in dual beam mode and the configuration can be seen in Figure 51 which shows the complete test setup.

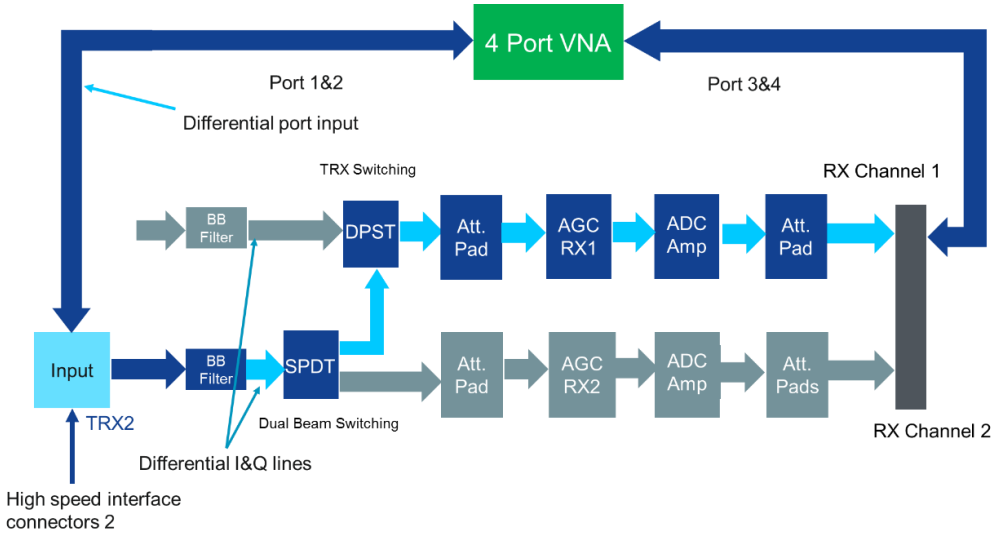

Figure 51. Test setup for RX channel 2 from TRX2.

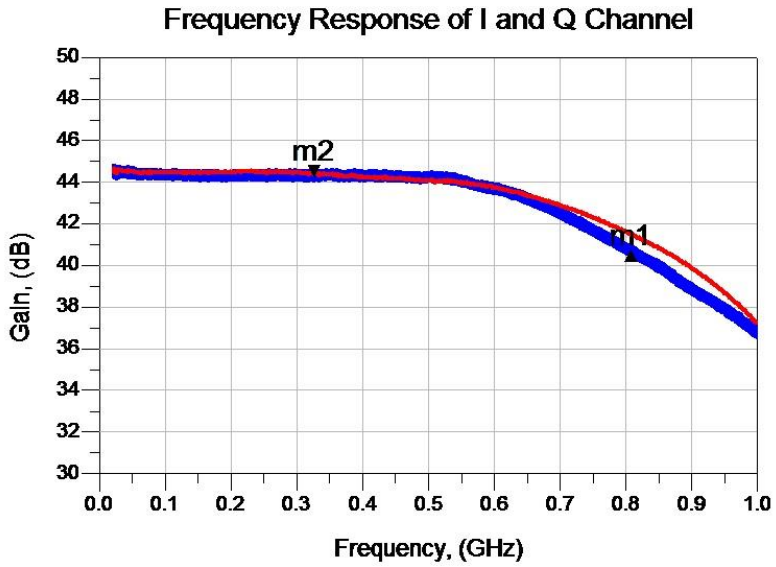

Figure 52. RX2 I and Q channel frequency responses.

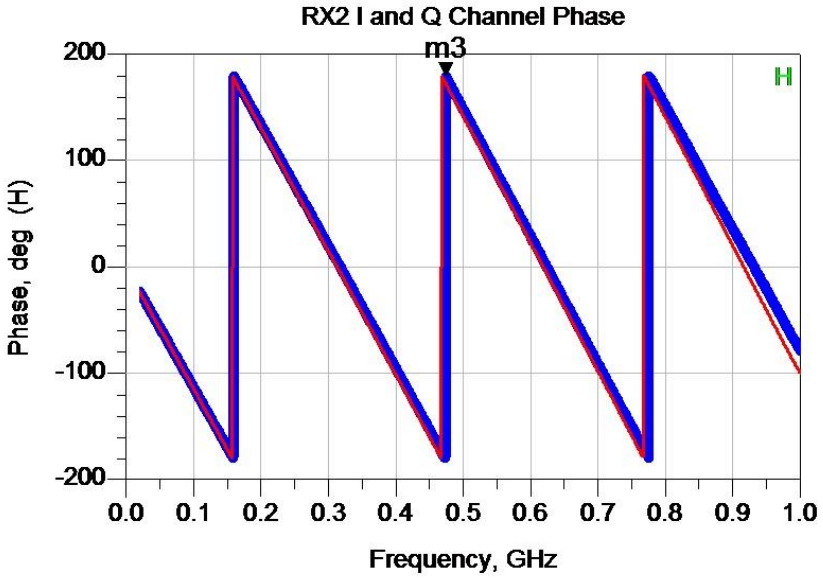

Figure 53. RX2 I and Q channel phase responses.

Figure 52 shows the frequency responses of both I and Q channels of RX2. The frequency response is measured from 10 MHz to 1 GHz and as it can be seen, that the 3 dB point for the RX2 channel is above 800 MHz, which satisfies the specifications. The amplitude difference between I and Q channels is also measured to be less than 0.5 dB.

Maximum gain of RX2 chain is measured to be 45dB which is also within specifications. Figure 53 shows the phase response of both I and Q channels. Although I and Q channels include different AGC chains, the phase difference between I and Q channels is not significant as can be seen from the measurements.

6.3 TX Channels Testing

The TX side of ABB has also two separate channels to be tested for their frequency responses and phase difference between I and Q channels separately. For testing purposes, in place of mmW module, interface boards are placed on the high speed connectors to provide proper interface for test equipment to be connected. One interface board is connected to the mmW high speed connector to act as an output to the TX chain and the TX input high speed connector is attached to another interface board to input the signal to the TX chains.

6.3.1 TX Channel 1 Response

In this testing scenario the interface board is connected to high speed connector which simulates the connection from Infineon TRX1 and it acts as the output from TX channel 1. The input is given through the interface board connected to the TX baseband high speed connector. The testing scenario can be seen in Figure 54 which represent the block diagram of TX chain testing.

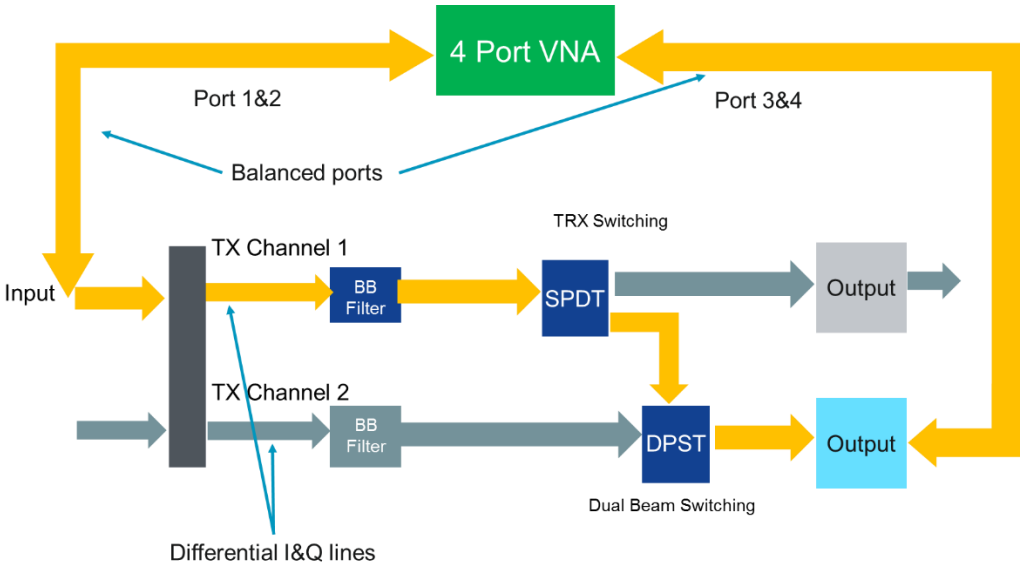

Figure 54. Test setup for TX channel 1 to TRX1.

Figure 55 shows the frequency responses of both I and Q channels of TX1. The frequency response is measured from 10 MHz to 1 GHz and as it can be seen, that the 3dB point for the TX1 channel is above 800 MHz, which satisfies the specifications. The amplitude difference between I and Q channels is also measured to be less than 0.5dB. Maximum insertion loss of TX1 chain is measured to be -5 dB which is also within specifications. Figure 56 shows the phase responses of both I and Q channels. The phase difference between I and Q channels is negligible as can be seen from the measurements.

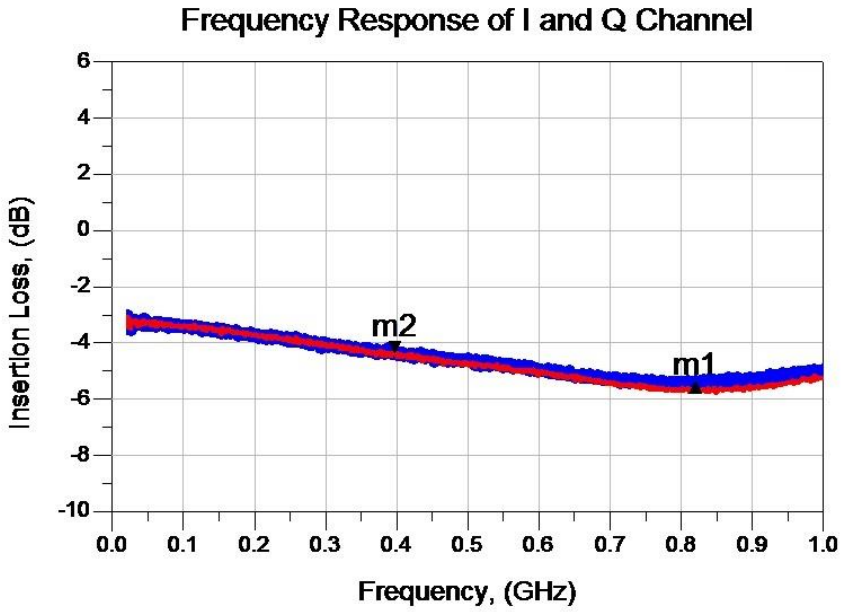

Figure 55. TX1 I and Q channel frequency responses.

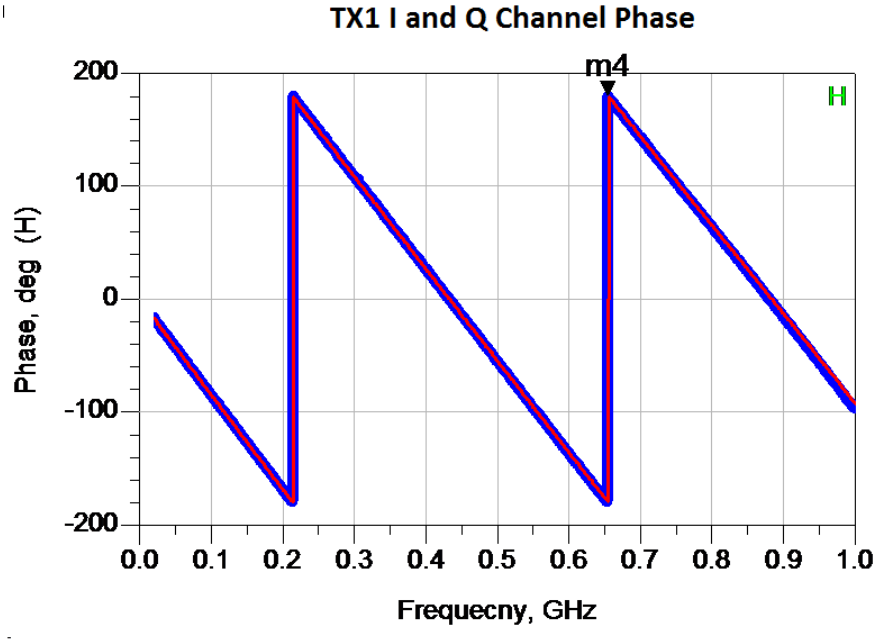

Figure 56. TX1 I and Q channel phase responses.

6.3.2 TX Channel 2 Response

In this testing scenario the interface board is connected to high speed connector which simulates the connection from Infineon TRX2 and it acts as the output from TX channel 2. The input is given through the interface board connected to the TX baseband high speed connector. The testing scenario can be seen in Figure 57 which represents the block diagram of TX chain testing.

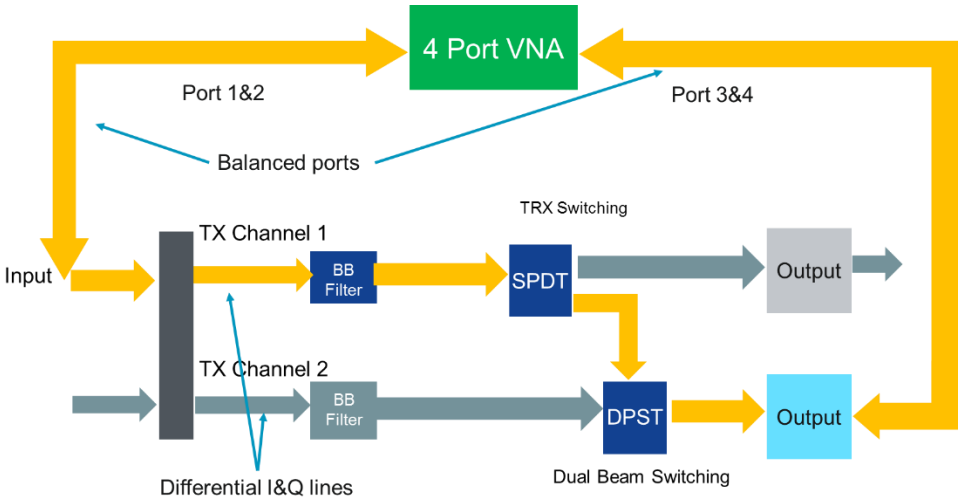

Figure 57. Test setup for TX Channel 2 to TRX2.

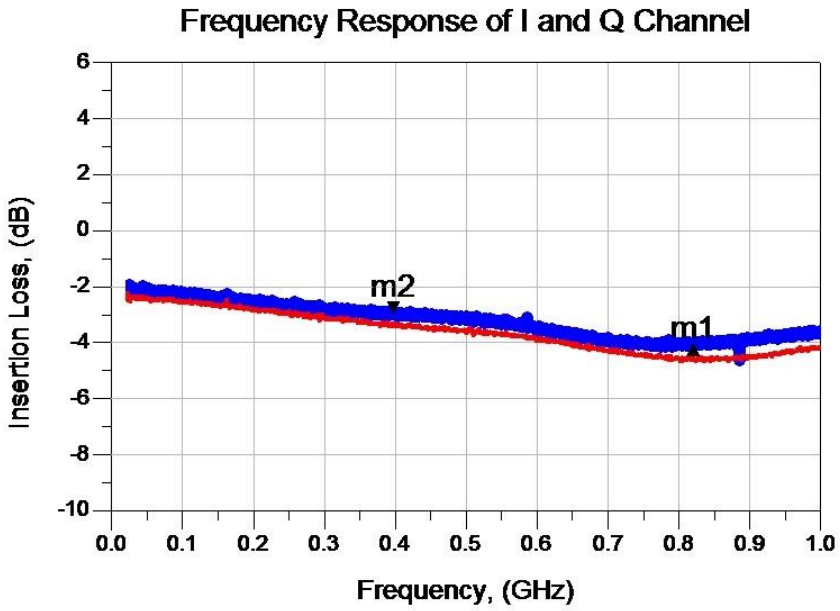

Figure 58. TX2 I and Q channel frequency responses.

Figure 58 shows the frequency responses of both I and Q channels of TX2. The frequency response is measured from 10 MHz to 1 GHz and as it can be seen, that the 3 dB point for the TX2 channel is above 800 MHz, which satisfies the specifications. The amplitude difference between I and Q channels is also measured to be less than 0.5 dB. Maximum insertion loss of TX2 chain is measured to be -4 dB which is also within specifications. Figure 59 shows the phase responses of both I and Q channels.

The phase difference between I and Q channels is a bit higher than the phase difference measured in TX channel 1 as seen in Figure 59, but is still within the specifications. In case of unequal lengths for I and Q channels, the phase difference keeps getting bigger as the frequency increases and wavelength decreases.

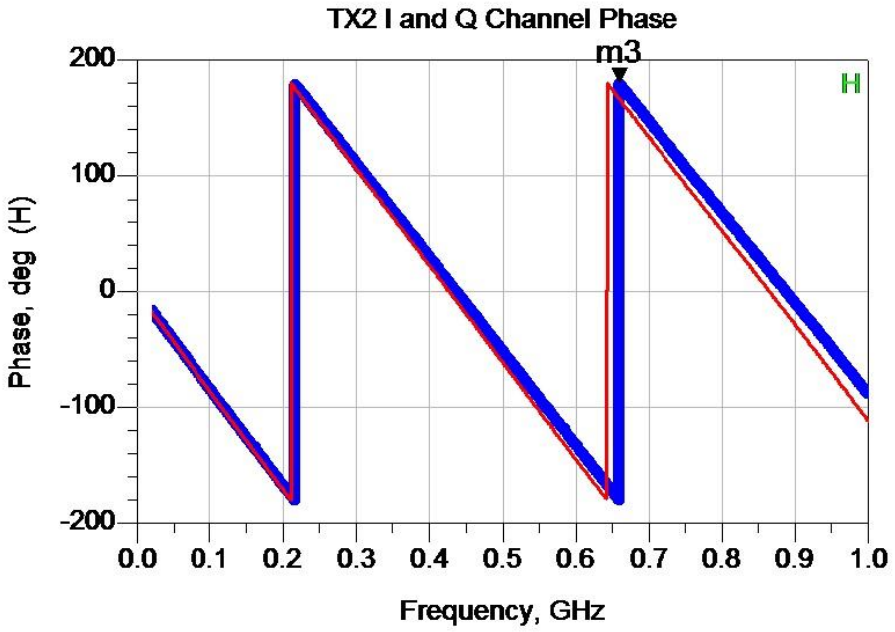

Figure 59. TX2 I and Q channel phase responses.

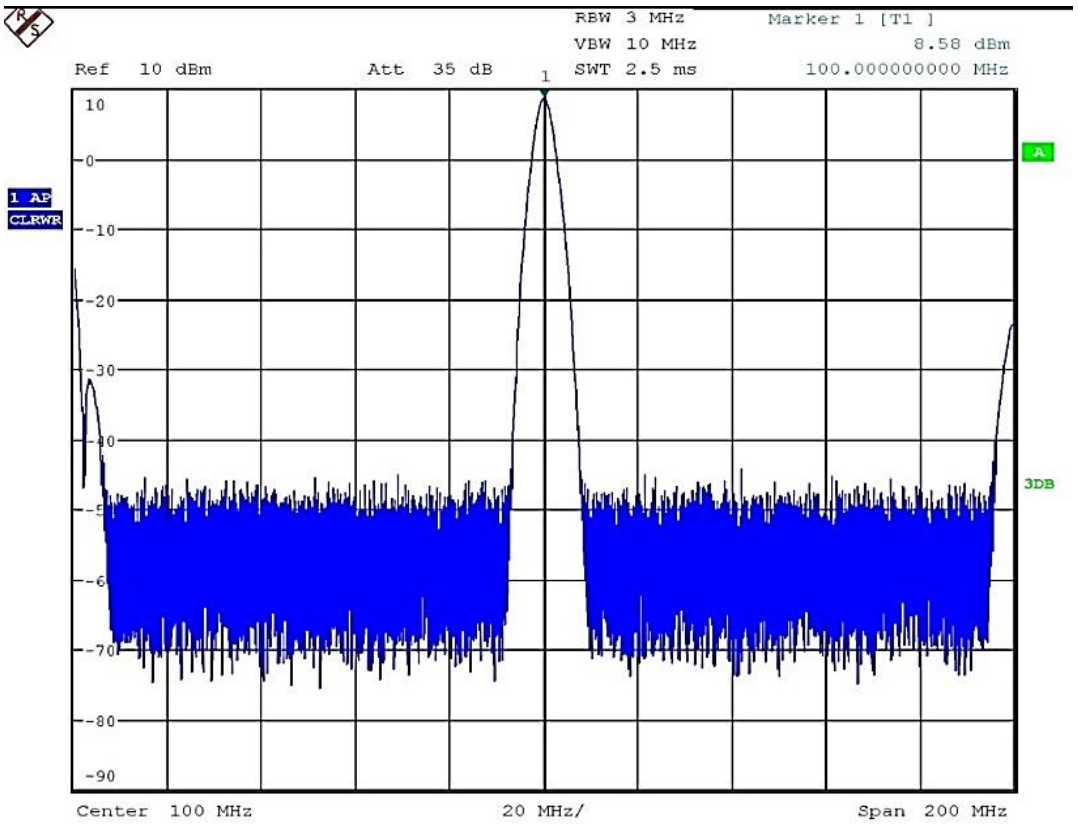

Figure 60. Reference oscillator spectrum.

6.4 Reference Oscillator Testing

The reference oscillator circuit was implemented on ABB to provide TRX PLL reference signal input on mmW module. The reference oscillator signal was given through the same high speed connector that goes to mmW module. To test the reference oscillator signal, same interface should be placed on high speed connector. The signal is analysed on spectrum analyser for magnitude and phase noise testing. The phase noise of the oscillator could not be measured directly because it was better than the phase noise of best available spectrum analyser. The performance of the reference oscillator can only be verified with the system integration testing, showing that it will not contribute significantly to transceiver own phase noise. Figure 60 shows the spectrum of oscillator on spectrum analyser. Figure 61 shows the test setup for reference oscillator.

The reference oscillator was working according to datasheet specification itself, but was causing interference with the other signals on mmW high speed connector. The high speed connector could not provide enough isolation between the oscillator pin and its neighbouring pins, so the oscillator frequency components were leaking to the baseband I/Q signal ports. The interfering signal from oscillator input on the TX2 baseband pins was about 30 dBc. Figure 62 further elaborates the interference coupling from the oscillator to other pins on the high speed connector. The interfering signal on the TX2 and RX2 ports will results in lower SNR and the system will not be able to perform up to its limits. Figure 63 shows the leakage of reference oscillator signal at TX2 signal port.

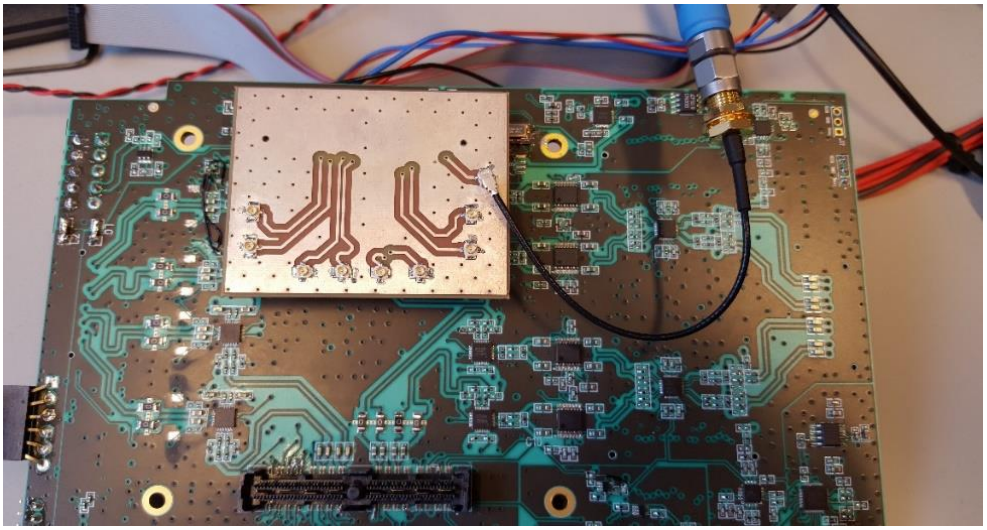

Figure 61. Test setup for reference oscillator.

Reference oscillator circuit was transferred on an independent satellite board. The satellite board was necessary to isolate the signal from the other system. The reference signal was fed into the mmW module through coaxial SMA port that was designed for external reference signal. The satellite board which has two outputs is shown in Figure 64. One for 100 MHz output for the system and 10 MHz output for possible digital baseband synchronization purposes.

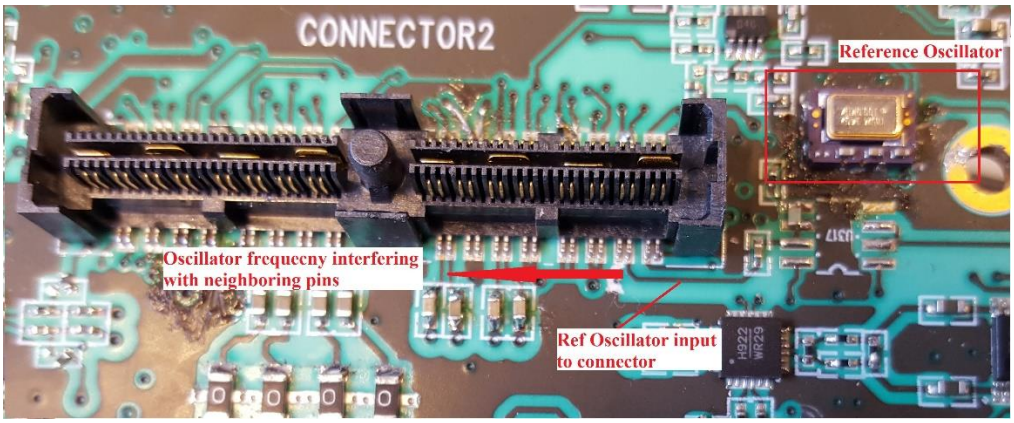

Figure 62. Oscillator interference coupling with neighbouring pin on HSC.

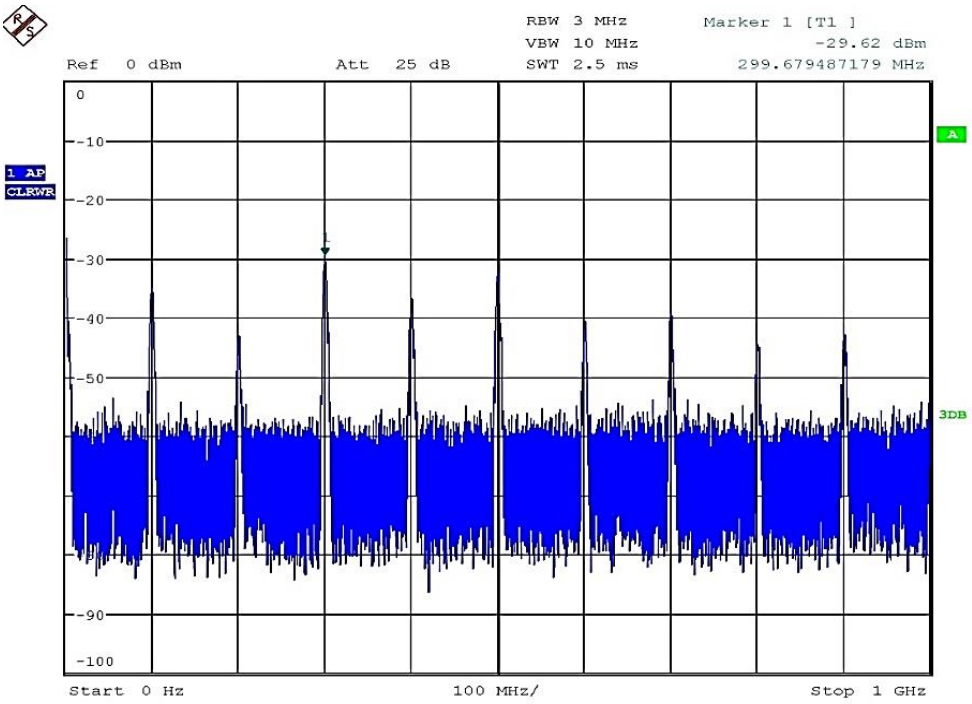

Figure 63. Reference oscillator leakage to TRX2 port.

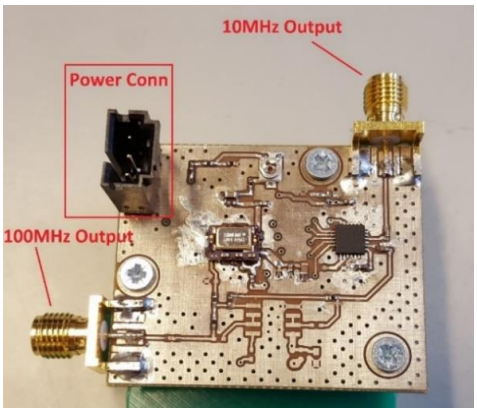

Figure 64. Reference oscillator satellite board.

6.5 ABB Test Results Summary

Beside the results mentioned above, there were some other measurements done for the analog baseband board. These test results are presented and summarized in Tables 17 and 18. These test results are also compared with the specifications tables presented in chapter 5.

Table 17. *Transmitter Chain Specifications and Results.*

Parameter	**Specifications**	**Results**
BB 3dB low pass cut-off frequency	> 800 MHz	> 1 GHz
BB 3dB high pass cut-off frequency	DC coupled	DC coupled
TX chain loss	< -6 dB	< -5 dB
TX power P1dB	> 0 dBm	> 10 dBm

Table 18. *Receiver Chain Specifications and Results.*

Parameter	**Specifications**	**Results**
BB 3dB low pass cut-off frequency	> 800 MHz	804 MHz
Frequency range of operation	1 GHz	7 dB ripple drop till 1GHz
BB 3dB high pass cut-off frequency	DC coupled	DC coupled
RX baseband gain	> 40 dB	43 dB
AGC dynamic requirement	> 45 dB of dynamic range	55 dB of dynamic range
RX power output P1dB	> 10 dBm	12 dBm

6.6 System Level Testing

The second part of the testing includes mmW radio system integration and verification testing. These measurements are mainly conducted through continuous wave (CW) testing for output power from the transmitter, frequency response measurements for 500 MHz of bandwidth and verification measurements for the phase noise of the system that was described in chapter 4. Finally, modulation quality measurements and data throughput measurements are presented by adding modem into the system level testing.

6.6.1 Transmitter Output Power

One of the common system measurements include RF transmitter output power. The RF power can be simply measured through CW signal, a pulse signal or a complex digitally modulated signal such as quadrature amplitude modulated (QAM) signal. But among them the CW testing is commonly used because of its simplicity of measuring the peak output power [35]. In this measurement setup, a signal generator is used to input 50 MHz CW signal into the baseband of the system and a spectrum analyser along with harmonic mixer with 20 dBi horn antenna is used as a receiver. The carrier frequency, 73.5 GHz is at E-band, so it cannot be fed directly into the spectrum analyser without using an external harmonic mixer which down converts the transmitted frequency to IF stage and feeds to the spectrum analyser. Figure 65 shows the test setup for the transmitter power measurements.

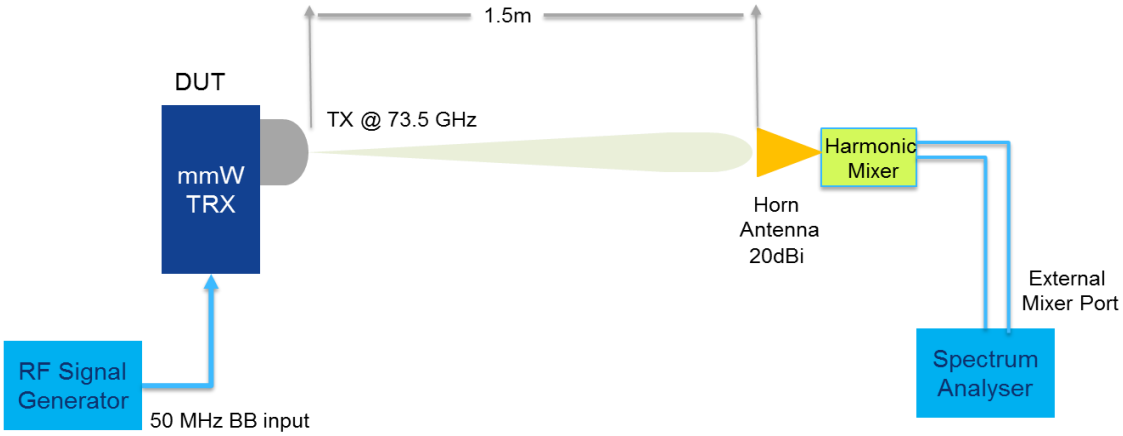

Figure 65. Test setup for TX power measurements.

The transmitter and the harmonic mixer receiver are placed at 1.5 m of distance, so the path loss at 73.5 GHz will be 73 dB. The most important testing for the transmitter is output power measurement, 1 dB compression point (P1dB) and third order intercept point (IIP3). Figure 66 shows the spectrum of the output of the transmitter with 50MHz CW input. The figure includes the main signal peak, LO leakage peak, I/Q side band with image rejection, and some spuriouse componenets. Figures 67 and Figure 68 show the TX compression graph and 3rd order intercept graph respectively. Through these measurements it can be seen that the PA output power at 1dB compression point is 21 dBm and the 3rd order intercept point is near 27 dBm. According to the link budget calculated in chapter 4 the targeted output compression point for the PA was 24 dBm which is 3 dB higher than the measured value. The EIRP for the transmitter was set to be 35 dBm including 6 dB back-off margin for PA compression at 500 MHz, but with the test results the measured EIRP is 32 dBm and if the back-off margin of 6 dB is added to these measurements then the EIRP will be 26 dBm. It can be clearly seen that the measured TX power is 8-9 dB lower than the targeted EIRP.

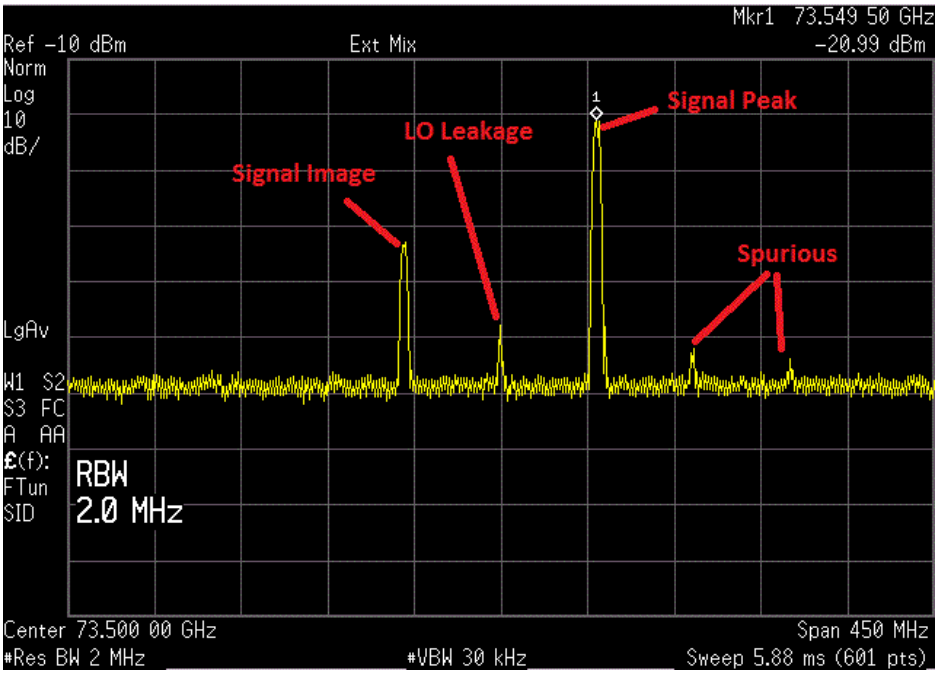

Figure 66. Transmitter output spectrum at 73GHz.

This loss of power in TX is because of higher losses in the RF switch matrix for beam-steerable antenna than in the simulated design, and because of the lower than specified performance of the TX power amplifier which has led to the loss of 8 dB in the output power. This loss in power will affect the hop length of the system, so some testing is being conducted on how to improve the signal strength and reduce the losses in the switching matrix of the beam-steering antenna.

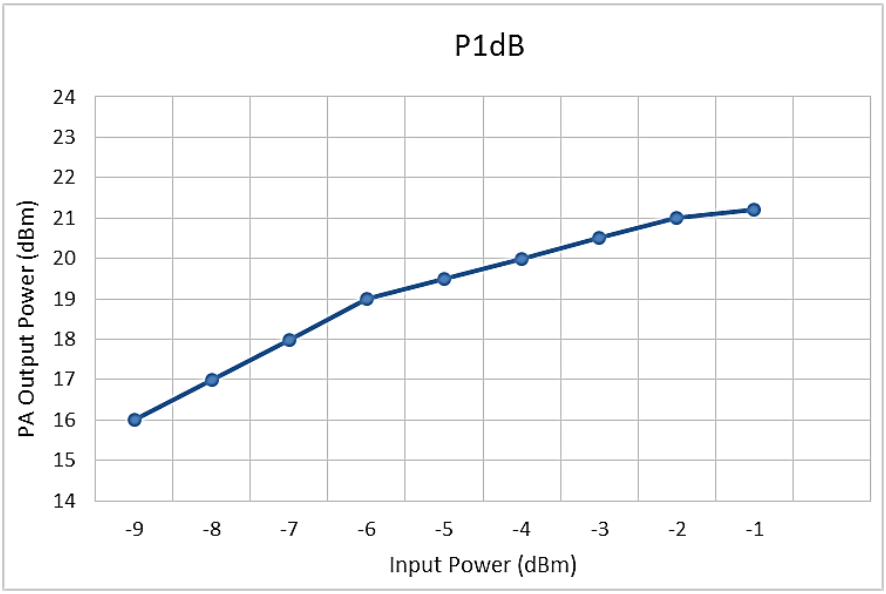

Figure 67. Compression point graph for transmitter output.

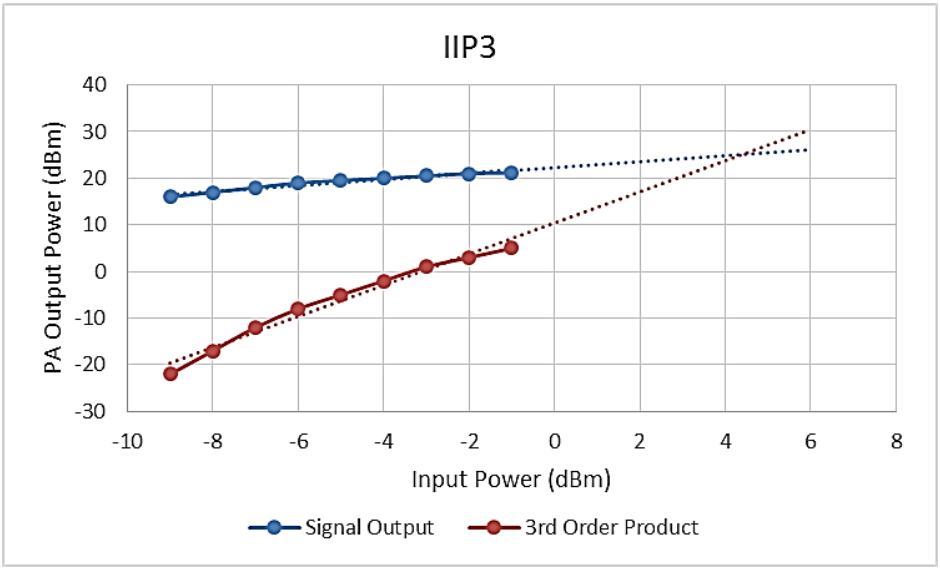

Figure 68. Third order intercept (IIP3) measurement.

6.6.2 System Frequency Response

The RF system is designed to support up to 2 GHz of bandwidth at RF, but with the current modem configuration only 500 MHz of bandwidth can be generated, which means that the 3 dB cut-off bandwidth at baseband should be at least 250 MHz. The system frequency response can be measured with the test setup defined in Figure 69. The RF system should be kept back to back with one end as TX and the other as RX. A 50 MHz signal from signal generator is provided to the transceiver configured as TX for up-conversion while the node is used to down-convert the signal again to baseband frequencies. With a sweep of frequency at TX input one can get a whole channel response of the system. Figure 70 shows the frequency response of the whole system which is flat enough till 250 MHz with the ripples being below 3 dB.

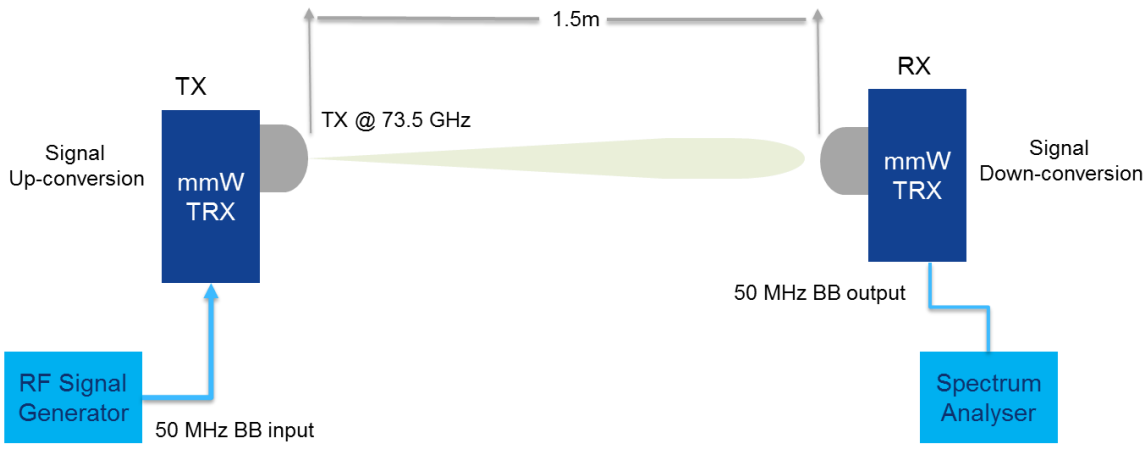

Figure 69. Test setup for system frequency response measurements.

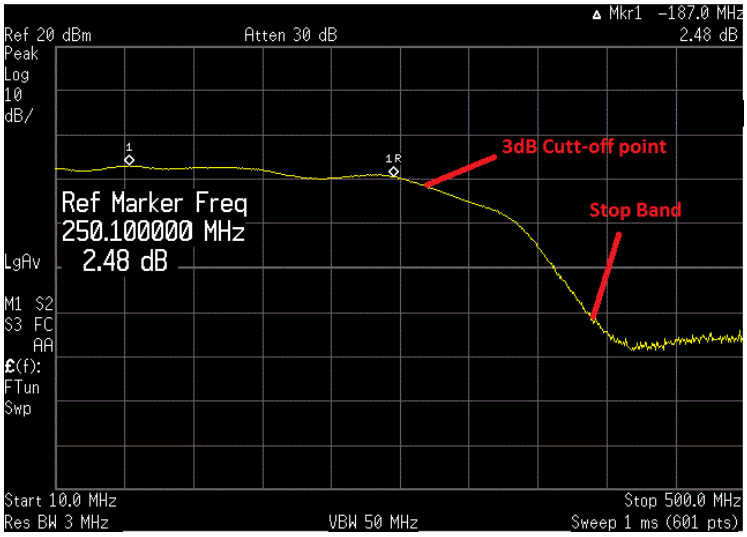

Figure 70. Measured frequency response of the mmW TRX system.

6.6.3 System Phase Noise

The frequency stability of the LO is critical in high-quality RF transmission systems. Any short-term frequency variability results in performance degradation. This short-term variability is known as phase noise, which is also known as jitter in time domain. Perhaps one of the important specifications for an RF transmitter is phase noise. RF transmitters, and receivers for that matter, typically consist of several frequency conversion stages [35].

The simplest way to test the phase noise is to up-convert the baseband signal to the final RF frequency and measure phase noise of the system at RF. But in this case the RF frequency is at E-band, so due to the unavailability of phase noise measurement equipment for this frequency range, a test setup like shown is Figure 69 is used to measure the phase noise of the system. As can be seen, the test setup contains two radio transceivers back to back one working as transmitter and other working as receiver, thus implying that the phase noise of the two LOs is included in the test results. The specifications provided by Infineon for the transceiver chip phase noise are between -77 dBc/Hz to -83 dBc/Hz at 100 kHz offset frequency. The reference oscillator design was chosen so that it does not influence the phase noise of the transceiver chip. The test results shown in Figure 71 evidence the phase noise value of -74.6 dBc/Hz at 100 kHz offset. This value gives the phase noise for two transceivers in cascade, which means that the true phase noise of the single transmitter or receiver entity is 3dBs lower. Thus to get the correct phase noise value for single transceiver system one should subtract 3 dB from the value measured. So the phase noise for single transceiver system will be -74.6 dBc/Hz-3dBc/Hz which gives -77.6 dBc/Hz at 100 kHz offset. The measured phase noise value fulfils the specifications provided by Infineon for the transceiver, which means that the designed reference oscillator is working up to the desired specifications for the system and PLL loop filter is designed correctly.

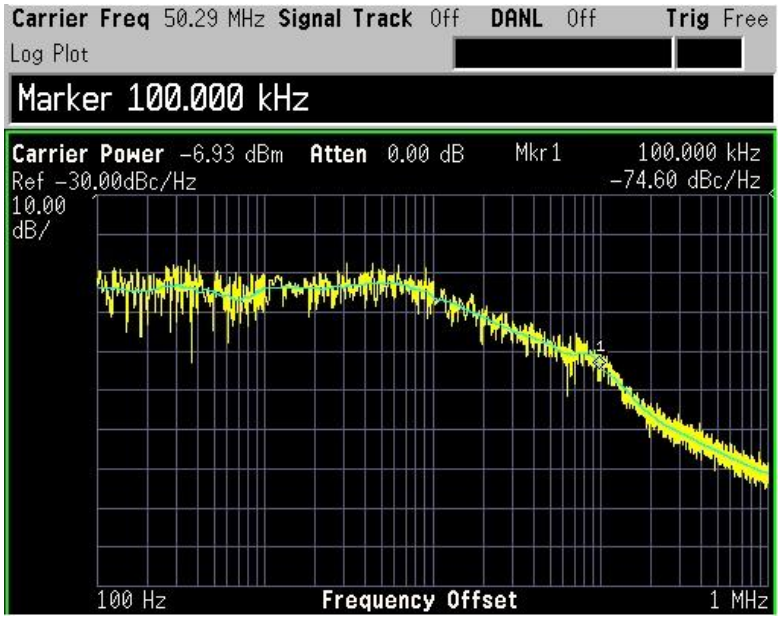

Figure 71. Measured phase noise plot for the mmW transceiver system.

6.6.4 System Integration with Modem

At this stage the RF system is integrated with the modem to perform the data throughput and modulated signal quality testing. Figure 72 provides the test setup for the RF and modem integration testing. The modem is capable to provide 500 MHz of bandwidth with symbol rate of 420 MBaud which can produce a peak data rate of 2 Gbit/s. The system is working in time division duplexing scheme and is initially tested in indoor lab environment with a fixed beam at both of the nodes.

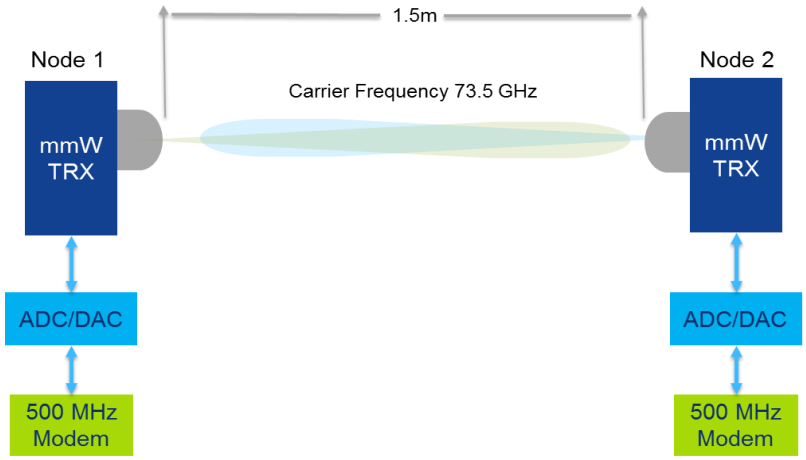

Figure 72. RF system and modem integration test setup.

Figure 73 shows the constellation diagram of 64-QAM modulation through the system. Some noise can be seen in the constellation points due to thermal noise of the receiver, but no signs of TX compression or I/Q mismatch can be seen which means the RF system is working within specifications for the modem.

In Figure 74 there are three blocks control, analysis and statistics that are taken from the modem interface GUI. The control block shows the configurations like the modem bandwidth, modulation scheme and code ratio that are set for the transmission. The analyser block shows the most important parameters as the data rate, un-coded bit-error rate (BER), coded BER and modulation error ratio (MER).

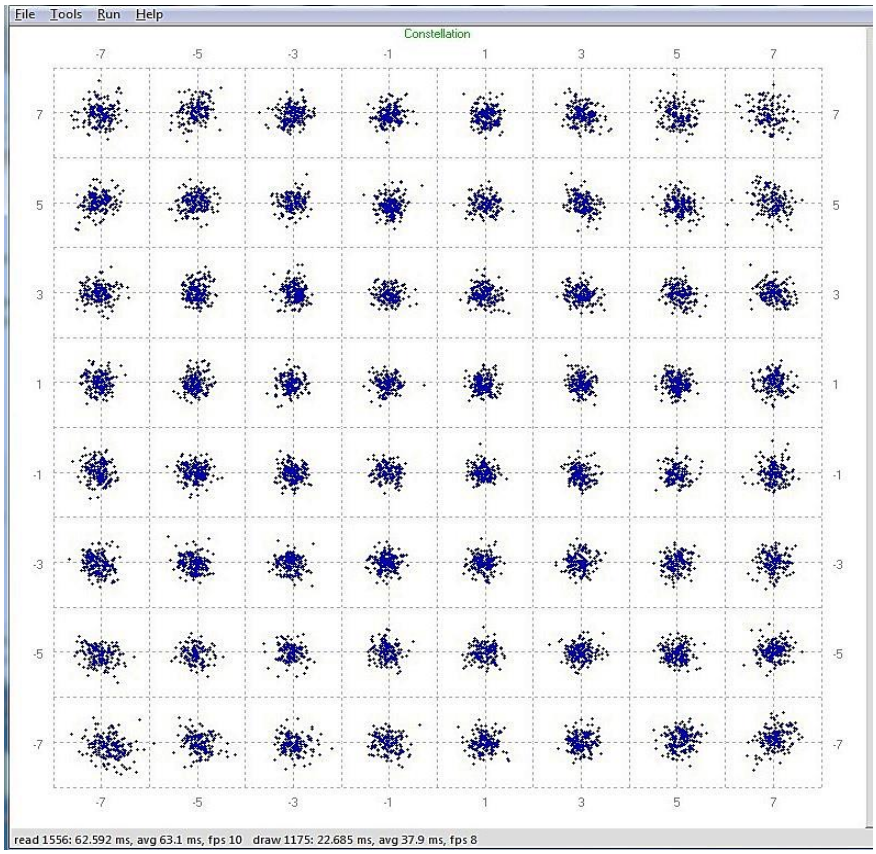

Figure 73. Constellation diagram of a 64 QAM signal through the link.

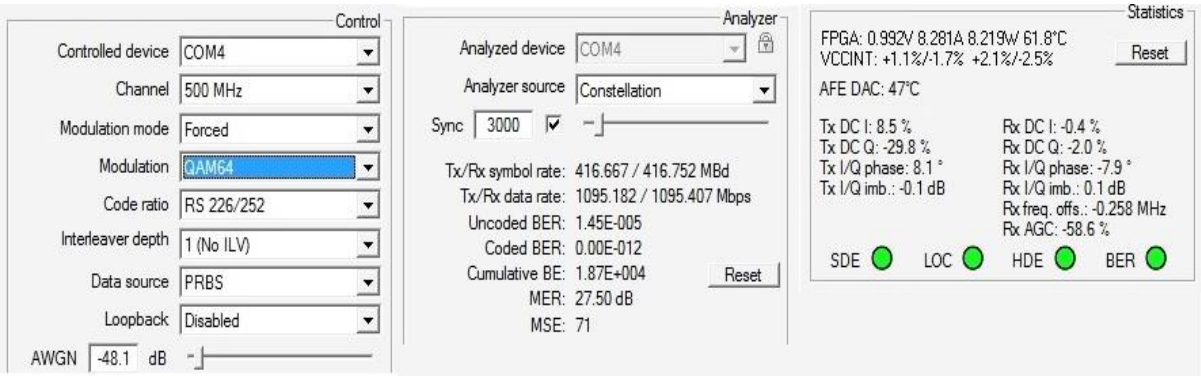

Figure 74. Modem interface GUI displaying controls, analysis and statistics.

For a digital modulation BER and MER are the most important parameters to quantify the performance of the system. MER of a system can be defined by following formula [36]:

$$MER(dB) = 10\log_{10}\frac{P_{signal}}{P_{error}}, \quad (10)$$

where P_{error} is the RMS power of the error vector, and P_{signal} is the RMS power of ideal transmitted signal [36]. BER can be defined as the ratio of number of errors to the total number of bits transmitted. These two parameters define the system performance and give the estimation for the signal to noise ratio of the system [37]. Figure 74 shows two types of BER measurements i.e. un-coded BER and coded BER shown in the analyser block. The un-coded BER gives the bit error rate before the forward error correction (FEC) module while coded BER shows bit error rate after the FEC. The third block in Figure 74 shows the statistics from the modem and AFE like I/Q phase and amplitude imbalance corrections, RX AGC range, module temperature and power consumption etc.

In general, all these test procedures have only been done in a lab environment and with shorter hop-lengths. The next steps of measurements include testing of the system with beam-steering capabilities and testing of the system in real outdoor environment for the maximum hop-length, which are part of the future work.

7. CONCLUSION AND FUTURE WORK

This thesis was started by introducing basic concepts of backhaul networks along with introduction of LTE and 5G small cell networks. After this, the mmW frequencies bands and their propagation properties were discussed. Furthermore, application and technologies that are going to be used in building the PoC system architecture were discussed. The theory also focused on the system requirements of self-aligning and self-organizing wireless mesh backhaul.

This work continued by introducing the mmW system description by explaining all the major blocks of the PoC system that was developed at Nokia Bell Labs. The system's data control flow and beam switching architecture along with link budget analysis were also presented in this section. In the further discussion, the practical part of the thesis i.e. analog baseband board design was explained. In addition, we also described the construction blocks of the analog baseband board like the PCB layer stack-up, interface design between several working modules and mechanics design of the system.

To conclude the thesis work, the testing and measurement results from the hardware design were presented. The analog baseband board design was working up to the specifications and no major design changes or layout re-runs were needed to fulfill the requirements. The required gain and linearity in the RX chain were also achieved successfully. The reference oscillator block did produce some problems for the system because its power was leaking to other ports through the high speed connector. That was then solved by putting the reference oscillator circuitry on a separate satellite board. Based on the test results from the system integration, one of the major concern was the low output power of the transmitter because of higher losses in antenna switching matrix. The other test results from the system integration such as phase noise, frequency response and modem integration were up to expectations.

For the future work, the system design can be improved by removing the reference oscillator circuitry from the analog baseband board and placing it on a satellite board so that there shouldn't be any interference from the oscillator to the system. The two stages of gain amplifiers in the RX chain can be replaced by one stage AGC. There is a new AGC chip from Texas instruments which is more wide band than the one used in the current design. The new AGC chip can also be used as the ADC driver, meaning that there is then no need for an extra ADC driver chip. The SPDT switches used in the analog baseband board are close to reaching the end of their life cycle. So they should be replaced by some other chips. The losses from the antenna switching matrix can be reduced by reducing the switching matrix and concentrating on the power amplifier layout design. The lens antenna gain should be increased from 30dBi to 38dBi so that it can meet with ETSI and FCC compliance.

REFERENCES

[1] J. G. Andrews, S. Buzzi, W. Choi, S. V. Hanly, A. Lozano, A. C. K. Soong, and J. C. Zhang, "What will 5G be?" IEEE Journal on Selected Areas in Communications, vol. 32, no. 6, pp. 1065–1082, Jun. 2014.

[2] A. Ghosh, T.A. Thomas, M.C. Cudak, R. Ratasuk, P. Moorut, F.W. Vook, T.S. Rappaport, G.R. MacCartney, Sh. Sun, Sh. Nie, "Millimeter-Wave Enhanced Local Area Systems: A High-Data-Rate Approach for Future Wireless Networks," IEEE Journal on Selected Areas in Communications, vol. 32, issue 6, Jun. 2014.

[3] Small-cell Forum, "Backhaul technologies for small-cells (5th ed.)," 2013, online. Available (accessed on 09.06.2016): http://www.scf.io/en/documents/049_Backhaul_technologies_for_small_cells.php

[4] NGMN Alliance, "Small-cell Backhaul Requirements", v1.0, 2012, online. Available (accessed on 09.06.2016): https://www.ngmn.org/uploads/media/NGMN_Whitepaper_Small_Cell_Backhaul_Requirements.pdf

[5] F. Khan and Z. Pi, ''Millimeter wave mobile broadband (MMB): Unleashing the 3–300 GHz spectrum,'' in Proc. 34th IEEE Sarnoff Symp., Mar. 2011, DOI: 10.1109/SARNOF.2011.5876482.

[6] P. Adhikari, "Understanding Millimeter Wave Wireless Communication", white, paper, Loea Corporation, San Diego, 2008, online. Available (accessed on 09.06.2016): http://www.loeacom.com/pdf%20files/L1104-WP_Understanding%20MMWCom.pdf

[7] J.Salmelin, and E.Metsälä. Mobile Backhaul. Hoboken, NJ, USA: Wiley, 2012.

[8] J.Salmelin, and E.Metsälä. LTE Backhaul. Chichester, WS, UK: Wiley, 2016

[9] Ceragon Networks, LTE/LTE-A/4G, "Wireless Backhaul Solutions for Small Cells", online. Available (accessed on 09.06.2016): https://www.ceragon.com/solutions/hetnet-hauling/lte-lte-a-4g-backhaul.

[10] E-band Communication, E-Band Technology, webpage. Available (accessed on 18.05.2016): http://www.e-band.com/index.php?id=86.

[11] Recommendation ITU-R p.837-5, "Characteristics of precipitation for propagation modelling", Available (accessed on 09.06.2016): https://www.itu.int/dms_pubrec/itu-r/rec/p/R-REC-P.837-5-200708-S!!PDF-E.pdf

[12] S. Hur, T. Kim, D. J. Love, J. V. Krogmeier, T. A. Thomas and A. Ghosh, "Millimeter Wave Beamforming for Wireless Backhaul and Access in Small-cell Networks" IEEE Transaction on Communications, Vol. 61, No. 10, no. October 2013.

[13] L. Correia, J. Reis, and P. Frances, “Analysis of the average power to distance decay rate at the 60 GHz band”, in Proc. IEEE VTC Fall, 1997.

[14] M. Marcus and B. Pattan, “Millimeter wave propagation: spectrum management implications,” IEEE Microwave Magazine, vol. 6. July, 1997

[15] S. Herle, “Topology Management for Wireless Mesh Self-Organizing Mobile Backhauls”, Master’s thesis, Aalto University, Espoo, Finland, March 2015.

[16] David T Chen, Joseph Schuler, Pekka Wainio, and Juha Salmelin, "5G Self-Optimizing Wireless Mesh Backhaul," in IEEE Conference on Computer Communications, 2015

[17] P. Wainio and K. Seppänen, “Self-optimizing last-mile backhaul network for 5G,” 2nd IEEE ICC Workshop on Next Generation Backhaul/Fronthaul Networks (BackNets’2016), accepted for publication, 2016.

[18] T. Veijalainen, “Beam steering in millimeter wave radio links for small-cell mobile backhaul”, Master’s thesis, Aalto University, Espoo, Finland, May 2014.

[19] A. Karttunen, Millimetre and submillimetre wave antenna design using ray tracing, Doctoral Dissertation, Aalto University, Espoo, Finland, 2013.

[20] J. Ala-Laurinaho, A. Karttunen, J. Säily, A. Lamminen, R. Sauleau ja A. V. Räisänen, “MM-Wave Lens Antenna with an Integrated LTCC Feed Array for Beam Steering”: Antennas and Propagation (EuCAP), April 2010.

[21] A. Artemenko, A. Mozharovskiy, A. Maltsev, R. Maslennikov, A. Sevastyanov and V. Ssorin, "2D Electronically Beam Steerable Integrated Lens Antennas for mmWave Applications": 42nd European Microwave Conference (EuMC), 2012.

[22] A. Artemenko, A. Mozharovskiy, A. Sevastyanov, V. Ssorin ja R. Maslennikov, “High Gain Lens Antennas for 71-86 GHz Point-to-Point Applications”: 43rd European Microwave Conference, 2013.

[23] B. Razavi, "Architecture and circuits for RF CMOS receivers," in Proc. IEEE 1998 Custom Integrated Circuits Conference.

[24] Intgckts, Wireless Receiver Architectures, webpage. Available (accessed on 09.06.2016): http://analog.intgckts.com/wireless-receiver-architectures.

[25] P.-I. Mak, S.-P U, and R. P. Martins, “Transceiver architecture selection: Review, State-of-the-Art Survey and Case Study”, IEEE Circuits and Systems Magazine, vol. 7, 2nd quarter 2007

[26] J. Karjalainen, M. Nekovee, H. Benn, W. Kim, J. Park, and H. Sungsoo, “Challenges and opportunities of mm-wave communication in 5g networks,” in 2014 9th International Conference on Cognitive Radio Oriented Wireless Networks and Communications (CROWNCOM), June 2014.

[27] T. Kim, J. Park, J.-Y. Seol, S. Jeong, J. Cho, and W. Roh, "Tens of Gbps support with mmWave beamforming systems for next generation communications," GLOBECOM, 2013 IEEE.

[28] Shu Sun, T. Rappapport, R. W. Heath, Jr., A. Nix, and S. Rangan, `` MIMO for Millimeter Wave Wireless Communications: Beamforming, Spatial Multiplexing, or Both?" IEEE Communications Magazine, December 2014.

[29] FCC 05-45, Allocations and Service Rules for the 71-76GHz, 81-86 GHz, and 92-95 GHz Bands, Memorandum Opinion, Federal Communications Commission, Washington D.C., 2005.

[30] FCC - Title 47, → Chapter I → Subchapter D → Part 101 → Subpart Q http://www.gpo.gov/fdsys/pkg/CFR-2013-title47-vol5/pdf/CFR-2013-title47-vol5-part101-subpartQ.pdf

[31] Application Note, Infineon, Literature number: AN377, 2014. Available (accessed on 09.06.2016): http://www.infineon.com/dgdl/Infineon--AN-v01_00-NA.pdf?fileId=5546d4624ad04ef9014aed1c0dc50a5f

[32] Radio electronics, Link Budget, webpage, Available (accessed on 09.06.2016): http://www.radio-electronics.com/info/propagation/path-loss/link-budget-calculation-formula-equation.php

[33] Electronic Tutorials, Pi-pad Attenuator, webpage. Available (accessed on 09.06.2016): http://www.electronics-tutorials.ws/attenuators/pi-pad-attenuator.html

[34] Technical Note, Samtec, QRM8/QRF8 Series, September 2012. Available (accessed on 09.06.2016): http://suddendocs.samtec.com/notesandwhitepapers/technote_qrm8-qrf8_100-gbe_25gbps_web.pdf

[35] S.Tenney, 5 RF Transmitter Measurements Every Engineer Should Know, National Instruments Newsletter. Available (accessed on 09.06.2016): http://www.ni.com/newsletter/51446/en/.

[36] Wikipedia, Modulation error ratio, 2016, webpage. Available (accessed on 09.06.2016): https://en.wikipedia.org/wiki/Modulation_error_ratio

[37] I.Poole, BER Bit Error Rate Tutorial and Definition, Radio-electronics.com, webpage. Available (accessed on 09.06.2016): http://www.radio-electronics.com/info/rf-technology-design/ber/bit-error-rate-tutorial-definition.php

[38] G.Trudgen, Phase Noise in Crystal Oscillators, Rakon UK Ltd, 2009, webpage. Available (accessed on 24.05.2016): http://www.rakon.com/products/technical-resources/application-notes?start=5

[39] K.Watermeyer, “Design of a hardware platform for narrow-band Software Defined Radio applications”, Master’s thesis, University of Cape Town, Cape Town, January 2007.